U.PORTO
FEUP FACULDADE DE ENGENHARIA
UNIVERSIDADE DO PORTO

Master Thesis in Mechanical Engineering

Development of a novel experimental tool for mechanical characterisation of adhesives

Author:
Inês Dias Costa

Supervisor:
Lucas F. M. da Silva
Co-Supervisors:
Eduardo A. S. Marques
Daniel S. Correia

Master in Mechanical Engineering

July, 2022

"And I knew exactly what to do.
But in a much more real sense,
I had no idea what to do."
— Michael Scott

Acknowledgements

First of all, I want to thank Professor Lucas da Silva for giving me the chance to work on this project and for sharing his knowledge and experience with me as a supervisor during the past few months.

I would also like to express my gratitude to my co-supervisors for the guidance and availability. My deepest appreciation goes to Daniel, with whom shared the daily challenges, pushed me to approach investigation endeavours with readiness and disruptive ideas, and for the patience to help me at all times.

To all of the AJPU members for their friendship, constant availability, and helpful advice throughout this project. A special thanks goes to my master's colleagues Bernardo, Diogo, Luís and Frederico, with whom I shared the past few months either in the laboratory or in great and long writing sessions. I am really grateful for the great companionship, solidarity, and friendship throughout the whole process. I truly enjoyed getting to know every one of you.

To all the people that I had the luck to cross paths with at Faculdade de Engenharia da Universidade do Porto (FEUP), to the ones that shaped me with their shared experiences and that significantly impacted my current approach to life, that empowered the purpose of becoming a mechanical engineer, thank you.

This project marks the end of a five-year journey where I have met the most amazing people. A special thanks goes to the ones that have joined this adventure with me, with whom I spent endless hours, grabbing each opportunity together and with whom I expect to continue to share the daily struggles and successes. I could not be happier to end this with you.

To my family, who joined this journey way long before and that supported me throughout all my education with vivacity and wise advice. To my grandparents, to my godfathers, uncles and cousins, thank you for the warm hugs and encouragement to follow my dreams, but mostly for your presence. A special thanks to my parents and brothers, who moved mountains to constantly support me on this adventure.

Abstract

Adhesives are increasingly being employed in industrial applications as a replacement for traditional mechanical joining methods, as they provide improvements in the strength to weight ratio and lower the cost of the overall structure project. As adhesives are uniformly applied on a surface, they also eliminate the need for holes, which are usually required in classical joining processes. Not only does this result in a more uniform stress distribution along the surface, avoiding stress concentrations, but it also allows for important reductions in the weight of the joint. This increased interest in adhesive bonding has led to the need for adhesive mechanical characterisation techniques that can provide the data required to build advanced numerical models that can help structural designers in adhesive selection process and allow for precise optimisation of bonded connection performance. Such characterisation techniques are currently exceedingly time-consuming and expensive, involving numerous different standards and resulting in a complex network of different specimens and data reduction methods.

This project intends to address this problem by proposing the development of a fully integrated characterisation novel experimental tool for adhesives that can greatly reduce the time required to characterise the adhesive. This novel tool will accomplish the main purpose by being designed to load novel specimens in several conditions sequentially and collect the appropriate data. Then, the resulting data will be analysed using data reduction schemes that will allow the proper and prompt extraction of mechanical properties, directly from the provided raw data. This combined experimental development of a unified apparatus for adhesive characterisation, data reduction and property extraction techniques for adhesive characterisation raw data will be used to reduce the amount of experimental testing required, lower costs, and enable the direct generation of cohesive zone laws.

Resumo

Os adesivos são cada vez mais utilizados em aplicações industriais como substitutos de métodos tradicionais de ligação, já que propiciam melhorias na resistência específica e menores custos. Os adesivos, sendo uniformemente aplicados numa superfície, não só propiciam uma distribuição de tensões uniformes, mas evitam a concentração de tensões inerentes aos processos tradicionais de ligação. Para além disso, permitem, também, a diminuição do peso das ligações.

Em função deste interesse crescente, tem aumentado também a necessidade de técnicas de caracterização mecânica de adesivos que consigam fornecer os dados necessários para construir modelos numéricos avançados, dados esses que possam ajudar engenheiros projetistas no processo de seleção de adesivos e permitir a precisa otimização da *performance* das ligações adesivas. Tais técnicas são, de momento, excessivamente morosas e caras, envolvendo diversas normas e resultando numa combinação complexa de diferentes provetes e métodos de redução de dados.

Este projeto pretende colmatar este problema ao propor o desenvolvimento de uma nova ferramenta de caracterização experimental de adesivos, completamente integrada e que possa reduzir significativamente o tempo necessário para caracterizar o adesivo. Esta nova ferramenta irá concretizar o seu principal propósito ao ser projetada para carregamento de novos provetes em várias condições, sequencialmente, e recolher os dados apropriados. Seguidamente, os dados resultantes serão analisados, usando esquemas de redução de dados que permitirão a extração correta e imediata das propriedades mecânicas dos adesivos, a partir de dados experimentais. Este estudo, que combina o desenvolvimento de um aparato unificado para caracterização de adesivos e técnicas de redução de dados e extração de propriedades mecânicas dos mesmos, será usado para reduzir o número de testes experimentais necessário, reduzir custos associados a este tipo de testes e permitir a geração direta de leis coesivas dos adesivos.

Contents

List of Figures

List of Tables

1 Introduction

In this chapter, the subject of this dissertation is introduced. As such, this chapter contains a brief background, the motivation, the goals, the methodology employed and the organisation of the present document.

1.1 Background and motivation

Adhesives are increasingly being employed in industrial applications as a replacement for traditional mechanical joining methods, as they provide improvements in the strength to weight ratio and lower the overall cost of structural designs. As adhesives are uniformly applied on a surface, they also eliminate the need for holes, which are usually required in classical joining processes. Being so, not only this results in a more uniform stress distribution along the surface, avoiding stress concentrations, but also allows decreasing weight of material connections.

This expanded use of adhesives has led to an increased need for adhesive mechanical characterisation techniques that can provide the data needed to build advanced numerical models that can help structural designers in the adhesive selection process and grant precise optimisation of the bonded connection performance. Therefore, the need for models able to replicate the mechanical behaviour of an adhesive, whether in daily use or under extreme loading conditions requires to perform tensile tests, shear tests and fracture tests in both mode I and mode II, which demands the manufacture of four different specimens, four different testing procedures and four data reduction procedures, necessary to gather the data used for the creation of a cohesive zone model (CZM).

Such techniques, however, are currently exceedingly time consuming and expensive, involving numerous different standards and resulting in a complex network of different specimens and data reduction methods.

1.2 Objectives

This project intends to address this problem by proposing the development of a novel fully integrated experimental tool for adhesives that can greatly reduce the time required to characterise the adhesive. This tool will accomplish the main purpose by being designed to load special unified specimens under several conditions sequentially and collect the appropriate data. Then, the resulting data can be analysed using custom data reduction schemes that will allow the proper and prompt extraction of mechanical properties, directly from the provided raw data. This combined experimental development of a unified apparatus for adhesive characterisation, data reduction and property extraction techniques for adhesive characterisation raw data will be used to reduce the amount of experimental testing required, lower costs, and enable the direct generation of cohesive zone laws. This versatility and simplified data extraction means that the testing tool has the potential to be a disruptive technology for many different users, including adhesive manufacturers, automotive manufacturers, the aerospace industry, the packaging industry and the electronic industry, among many others. The main focus of this thesis will be on the mode I and mode I fracture components of the unified test.

1.3 Research methodology

The goals of this thesis were met by following a series of steps, which can be divided as follows:

- A thorough study of the literature, focusing on the state of the art in adhesive bonding and quasi-static tests currently used for mechanical characterisation of adhesives;
- Numerical study of the concept, by computing behaviour changes as function of the apparatus' and specimens' geometries and addressing different adhesives;
- Experimental testing of the concept, starting by the physical models currently used, such as bulk tensile tests, thick adherend shear tests (TAST), double cantilever beam (DCB) tests, end notched flexure (ENF) tests and end loaded split tests (ELS) - focusing on the last three, i.e. the fracture tests -, and moving to isolated tests of the unified specimen;
- Implementation of data reduction schemes to the load-displacement curves resulting of both experimental and numerical tests.

1.4 Thesis outline

The work developed in this thesis is divided into four main parts. The first chapter contains an introduction to the problem to be addressed, as well as the background and motivation of the project and its objectives.

Secondly, in Chapter 2, an overview of adhesive bonds, their characteristics, their importance in the industry, their design, their classification and their failure modes is made. Since the main objective of this thesis is to develop a novel experimental tool for the characterisation of adhesives, a brief literature review of the quasi-static tests currently used for the same purpose is also given.

Chapter 3 presents the experimental test procedures used in this project, whether for standardised tests or for the newly developed test setup for the isolated tests of the end-loaded split test and the unified specimen. This chapter also explains the developed code for data treatment and properties extraction.

Chapter 4 presents the numerical model developed for the end-loaded split test (ELS), combined double cantilever beam (DCB) and also for the unified specimen.

Chapter 5 presents the summary of the appended papers, focusing on a brief description of their objectives and main conclusions.

Chapter 6 aggregates the main conclusions obtained during this research project, as well as suggestions to further improve and/or continue the work developed.

2 Literature review

2.1 Survey of adhesive joints

Adhesives have been used for thousands of years in many applications but, until around a century ago, these were mostly made from natural items such as bones, skins, fish, milk, and plants, providing very low mechanical performance and limiting usage to non-structural applications [1].

Since then, adhesives based on synthetic polymers have become available. Being initially underutilised due to their high cost and poor mechanical characteristics, since 1940, the knowledge of polymer chemistry from which structural adhesives can be manufactured has rapidly expanded, resulting in improved quality and reduced cost. Today, we find structural adhesives used in a wide range of industries, including the aerospace sector and in automotive applications. In this last case, the use of adhesive has expanded greatly, since its unique capability for multi-material joining enables a construction methodology which allows to obtain highly optimised and lightweight car bodies by combining sheets and components of different materials. Thus, adhesives made from synthetic polymers, such as epoxy resins, polyurethanes and acrylics, are now very effective alternatives to traditional connection methods including bolting, riveting, welding, and brazing [1] [2].

An adhesive is a material that can be used to join two surfaces while also resisting separation under load. The materials being bound together are called substrates before the joining process and are mentioned as adherends after it. The interface is the geometrical plane of contact between the surface and the two materials, while the interphase is the physical region between the adhesive and the adherend with differing chemical/mechanical properties from the respective components. All attraction forces between substances result from intermolecular interactions and can be referred to as an adhesion phenomenon. Cohesion, on the other hand, is defined by the intermolecular forces inside the substance itself, which prevent it from breaking apart under load [1].

Modern structural adhesives are thus extensively used to ensure the strength and stiffness of the structures they join and can withstand much higher loads than the majority of non-structural adhesives or sealants [1, 3, 4].

Their use presents some significant advantages when compared to conventional joining processes [1, 5]:

- Uniform stress distributions, resulting in higher stiffness and load transmission capabilities, that lead to cost and weight reductions - Figure 1;
- The ability to bond thin sheets of material;
- Allowing efficient plate bonding;

- Capability to easily join dissimilar materials;
- Easily automatable process;
- Flexibility in joint design;
- Allows smooth surface finishes, due to the lack of necessary discontinuities such as holes.

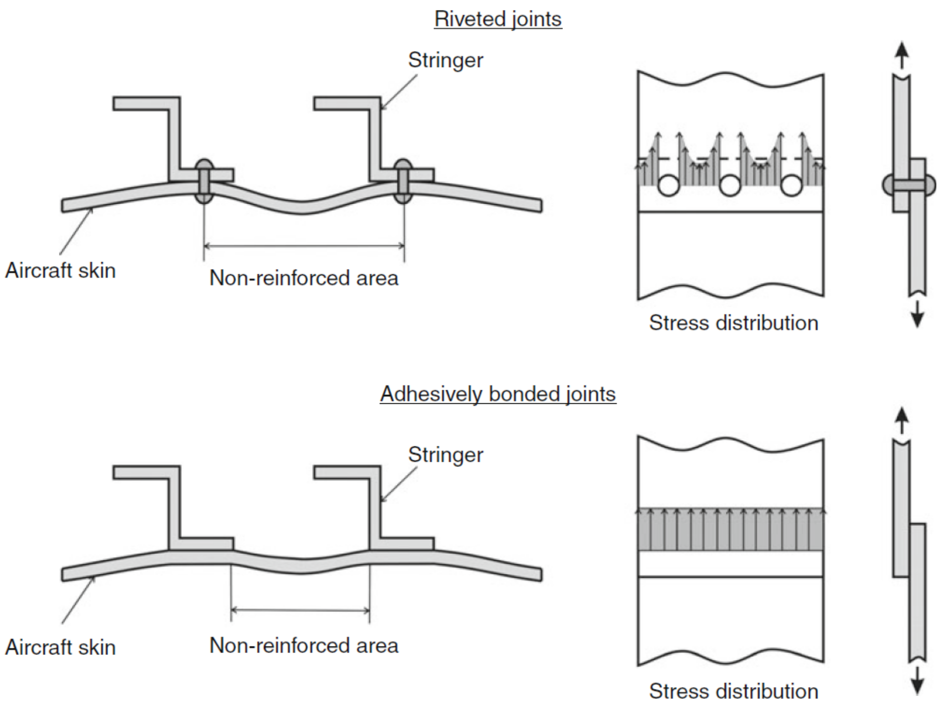

Figure 1: Stiffness improvements (left) and stress distribution (right) of adhesively bonded joints when compared to riveted joints [1].

However, as expected, adhesive bonding also exhibits some important disadvantages which must be well understood by the designers of bonded joints, for example [1, 5]:

- The need for careful surface preparation;
- If the cure process is not immediate, it typically necessitates the usage of templates to keep every component in the desired place;
- Some adhesives require particular curing conditions, such as temperature, which can occasionally represent production/economic constraints;
- Due to their polymeric composition, they have a limited ability to withstand severe temperatures and humidity conditions;

- Poor performance under peeling and cleavage pressures because these weaken joints by adding stress concentrations to the bonding process;
- Difficulties in performing quality control.

2.1.1 Adhesive classification

The majority of adhesives are polymers, which are composed of repeating chains of smaller chemical units or molecules known as monomers. These so-called polymeric chains can be arranged differently, resulting in different behaviour of the adhesives. Being so, different criteria can be used to categorise adhesives, including the polymer basis, functionality in the polymer "backbone," physical shape, functional type, chemical family, and application method [1].

The polymer base of an adhesive can be either natural or synthetic. Natural-based adhesives include vegetable or animal-based adhesives, as well as natural gums. Natural rubber, bee wax, casein-based, and protein-adhesive are examples of the aforementioned adhesive category. Synthetic base adhesives include those that are not considered to be natural, such as acrylics, epoxies, silicones, and polyesters [1,6].

A polymer can assume different functionalities, depending on the organisation of the polymeric chain, such as thermosetting, thermoplastic, elastomeric and hybrid. Thermoset adhesives are polymers that undergo an irreversible curing process caused by the chemical reactions that take place at room or high temperatures, making them permanent. They can be delivered in one-part, multiple-part systems or with dormant reactive agents. One-part adhesives are commonly stored at low temperatures since their shelf life is reduced due to often requiring high curing temperatures. Multiple-part solutions frequently have a longer shelf life and can cure at room temperature. Thermoplastic adhesives may be repeatedly melted without significantly altering their properties. They are often cured of a molten state. Elastomers often have high elongation, good toughness, and peel strength. Combining the aforementioned adhesives results in the so-called hybrid adhesives [1, 6].

Physical form, which can be classified as liquid, paste, film, or powder, typically indicates how the adhesive should be applied. With its good wettability and ability to quickly fill any gap that already exists, liquid adhesives can be applied with rolls, sprays, or brushes. Due to their high viscosity and thixotropic behaviour, paste adhesives may be applied easily on vertical surfaces. Film adhesives are ideal to restrict bondline thickness as constant and are simple to use. Powder adhesives, however, have to be heated or dissolved into a solvent to be transformed into a liquid form prior to application [1, 6].

Adhesives can be classified as structural or non-structural based on their functionality. However, in addition to other classifications, it can also be referred to as hot-melt, conductive, water-based, pressure-sensitive, and ultraviolet cured [1].

In terms of chemical family, they can be classified as epoxies, acrylics, and polyurethanes, among others. Epoxies are thermoset structural adhesives that are said to be the most versatile since they can be manufactured to be more flexible and robust without losing tensile strength despite being strong and brittle in their natural state. These adhesives are less expensive than acrylics, which, on the other hand, offer a faster cure and greater strength. Lastly, polyurethanes are tough and flexible even at low temperatures but heat and moisture sensitive [1].

In terms of application method, adhesives can be applied by coating, spraying or brushing, depending on viscosity, also indicated by their physical form [1, 6].

2.1.2 Failure modes and joint design

An adhesive joint can exhibit different possible failure modes. However, when using metal or ceramic substrates, only three are possible: cohesive failure of the adhesive, adhesive (interfacial) failure and cohesive failure in the adherend, as represented, sequentially, in Figure 2 [1].

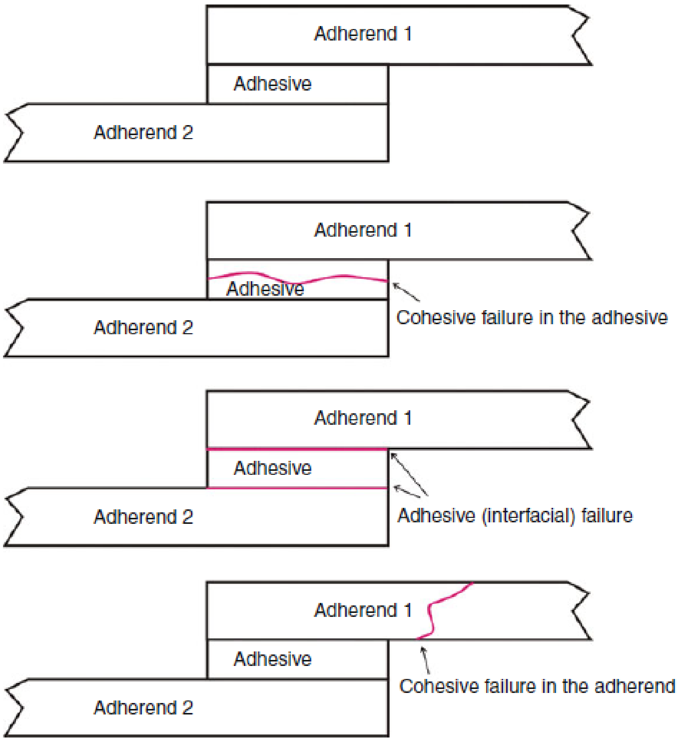

Figure 2: Schematic representation of cohesive and adhesive failure modes [1].

Cohesive failure is defined as the tear of the materials' internal connection, separating itself into two parts and when it occurs, both adherends remain coated with an adhesive layer. Thermal stresses and insufficient overlap length are a couple of the frequent causes of this mode of failure.

When the interface between the adherend and the adhesive fails, this is known as adhesive failure. This may be brought on by a lack of necessary surface treatments, a degreasing procedure done incorrectly, or poor surface preparation involving contaminants.

Additionally, in some circumstances where the adhesive connection is stronger than the substrates, a cohesive failure of the adherends is possible if the loading conditions exceed the material strength limit, failing before the adhesive bond.

As mentioned before, loading conditions play an important role in inducing different modes of failure. The most frequent mechanical loading conditions that adhesives are subjected to, like all other materials, are normal, shear, peel, and cleavage stresses, represented in Figures 3a, 3b, 3c and 3d, respectively.

(a) Normal. (b) Shear. (c) Peel. (d) Cleavage.

Figure 3: Types of stresses acting by adhesive joints. Adapted from [7].

The way the load is applied, the qualities of the substrate and adhesive, as well as the geometry of the joints themselves, all affect the sort of stress that the adhesive joint feels. Due to their simplicity, single-lap joints are the most often experimentally tested and industrially used joint configuration. Other common joint configurations include double-lap joints, scarf joints, and stepped-lap joints [8], as seen in Figure 4.

(a) Single-lap joint. (b) Double-lap joint.

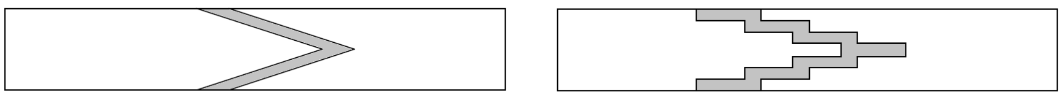

(c) Scarf joint. (d) Stepped-lap joint.

Figure 4: Most common joint configurations. Adapted from [8].

2.2 Strength prediction approaches

Joint design is a complex subject, which has been the target of intensive research during the last decades. While initial and simpler joint design methods were concerned only with analysing the stresses present within the different joint elements and ensuring that they remained below the a given level, this approach is somewhat limited for more complex applications, as complex loading conditions, crack formation and propagation, and environmental conditions can also have an important effect on joint strength. In order to allow the design of bonded structures taking these considerations into account, as opposed to just applying empirical safety factors, several methodologies have been developed throughout the years. Three primary methods can be explored for predicting the failure in adhesive joints: continuum mechanics, fracture mechanics, and damage mechanics.

2.2.1 Continuum mechanics

In continuum mechanics, continuous elements are used to describe adhesive and adherends, with the assumption that there is a perfect link between the two, allowing the prediction of the strength of adhesive joints. In such case, the interfaces are ignored and stresses and deformations are the variables to be analysed, taking their maximum values as the failure condition [9].

However, due to the presence of singularities at the joint's tip, as illustrated in Figure 1, these fracture criteria, which range from maximum stress to maximum strain, cannot accurately anticipate the adhesive joint's failure 5. When using finite element analysis, these highly mesh-sensitive zones do not allow for convergence since their stress values always increase with mesh refinement. Even though various authors have proposed solutions to this issue, none of them are useful for adhesive joint simulations because they can only be applied to continuous structures and do not allow for the description of defects or different materials [9].

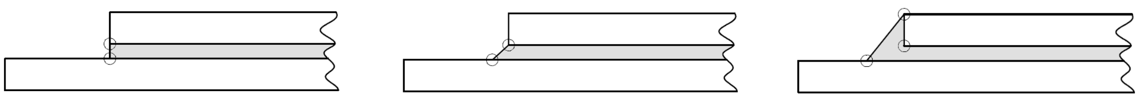

Figure 5: Singularities present at the edges of the overlap. Adapted from [9].

2.2.2 Fracture mechanics

Fracture mechanics, in contrast to continuum mechanics, assumes that there are discontinuities, allowing for the possibility of cracks, defects or other damage variables caused during manufacturing or use. This approach thereby quantifies the behaviour of structures with cracks before and throughout their propagation, determining in each case if the fracture size is greater than the critical failure size. Although several criteria can be used to describe fracture mechanics, the stress intensity factor concept and energetic considerations are the most widely used [9].

In what regards to material discontinuities, a stress concentration factor - K_t - is generally used to describe the stress distribution, representing a scaling parameter that defines the changes in the stress state in the neighbourhood of the crack tip [9].

The stress intensity factor, K, is then represented as:

$$K = Y\sigma_r\sqrt{\pi a} \tag{1}$$

where Y is a non-dimensional factor that is dependent on the geometry and loading distribution, σ_r, the remote stress which is applied perpendicular to the crack length, a. When the stress intensity factor, K, reaches a critical value known as the material fracture toughness, K, crack propagation occurs [9].

However, for sharp cracks such as the one represented in Figure 6, this factor would not be able to distinguish between similar geometries since at the crack tip the stresses would always tend to infinite.

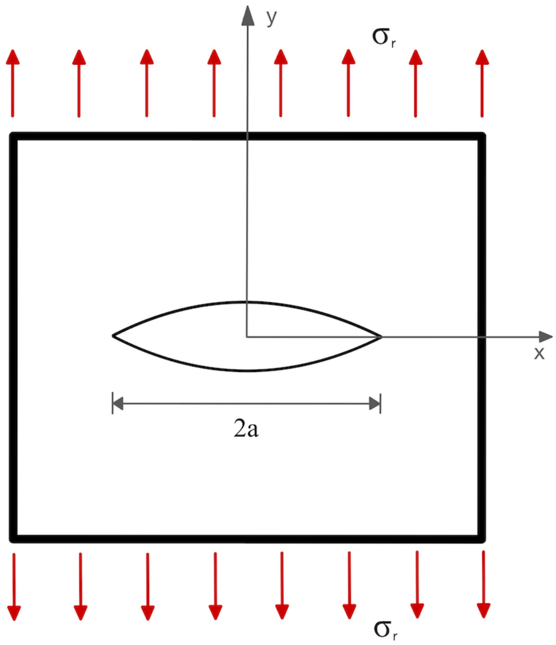

Figure 6: Schematic representation of a sharp crack.

This method considers three failure modes: mode I, for normal loading, concerning opening mode; and mode II or mode III, for different types of shear loading, as pictured in Figure 7. The most typical representation of what occurs at the crack tip under actual loading conditions is a combination of these fracture mechanisms.

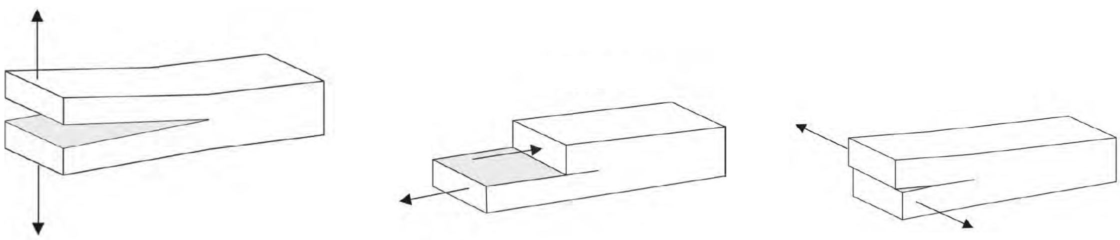

(a) Mode I. (b) Mode II. (c) Mode III.

Figure 7: Fracture modes for an adhesive joint [9].

Being so, each fracture mode has its own stress intensity factor, K_I, K_{II} and K_{III} for mode I, II and III respectively.

On the other hand, an energy based criterion considers crack propagation when the available energy, G - energy release rate -, which is function of the applied loading, is equal to a critical value where the crack propagates, G_c - critical energy release rate [9].

The presented fracture parameters (stress intensity factor, K, and energy release rate, G) in homogeneous materials are related by [10]:

$$G = \frac{K^2}{E} \tag{2}$$

being E the Young's modulus. Therefore, for plane strain conditions it can be expressed as [10]:

$$G = \frac{K^2}{E}(1 - \nu^2) \tag{3}$$

where ν is the Poisson's ratio.

Several authors have used fracture mechanics concepts to predict the toughness of adhesive joints. Most of these studies relied on the critical energy release rate criterion, which has been proven to be more reliable when it comes to difficult circumstances, such as when the crack grows near the interface [9].

Bulk materials typically propagate cracks in pure mode I or mode II loading conditions, however, in adhesive joints, cracks are forced to propagate in mixed mode I+II due to the constraints placed by the adherends. This mode mixicity can be represented by a mode ratio given by [9]:

$$\varphi = tan^{-1}\sqrt{\frac{G_{II}}{G_I}} \tag{4}$$

Using suitable criteria, the effects of both modes can be combined for mixed mode cracks to propagate, such as [9]:

$$\left(\frac{G_I}{G_{Ic}}\right)^{\alpha} + \left(\frac{G_{II}}{G_{IIc}}\right)^{\beta} = 1 \tag{5}$$

being G_{Ic} the critical energy release rate in mode I, G_{IIc} the critical energy release rate in mode II, and α and β constants.

To represent the previous behaviour it is possible to use fracture envelopes where knowing both mode I and II critical energy release rate, one can approximate the fracture behaviour using a linear or quadratic criterion, as shown in Figure 8.

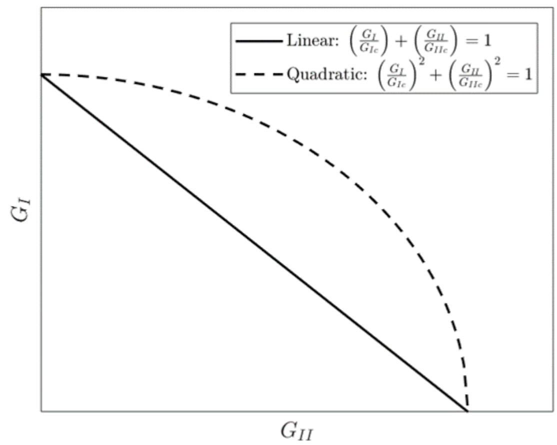

Figure 8: Schematic representation of fracture envelope approximations, using linear and quadratic criterion.

The basis for the fracture mechanics criteria is the existence of defects typically modelled as pre-cracks that are intentionally placed to simulate damage initiation. Therefore, criteria based on fracture mechanics are better suited for damage propagation than initiation, representing an inconvenience for most joint design purposes [9].

2.2.3 Damage mechanics

In order to evaluate damage initiation and propagation, a new method known as damage mechanics was developed. This method seeks to address the limitations of the previously described methodologies exhibit when modelling the typical behaviour of adhesives. A cohesive zone model (CZM), which is often built on interface elements with zero thickness that define the bonding properties between two solid surfaces, is nowadays the design technique most commonly used to to predict the mechanical performance of bonded joints. In this approach, after a stress criterion is met, each element considers a damage variable that is utilised to simulate material degradation by using a relaxation process based on a fracture energy criterion.

This method enables the modelling of non-linear processes while avoiding stress singularities and does not require the existence of pre-cracks or user interference for its propagation to occur, in contrast to continuum and fracture mechanics approaches [9].

The behaviour of the adhesives recurring to traction-separation laws is then applied using this damage mechanism. The two most frequent ones are schematically shown in Figure 9. Triangular laws are often employed since they are simple, whereas trapezoidal laws are used for very ductile adhesives.

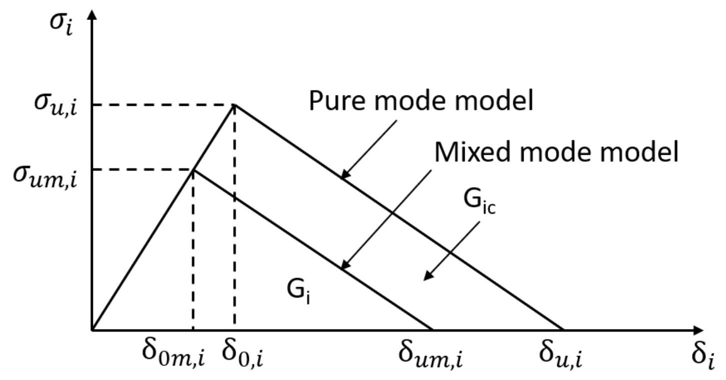

(a) Triangular traction-separation law.

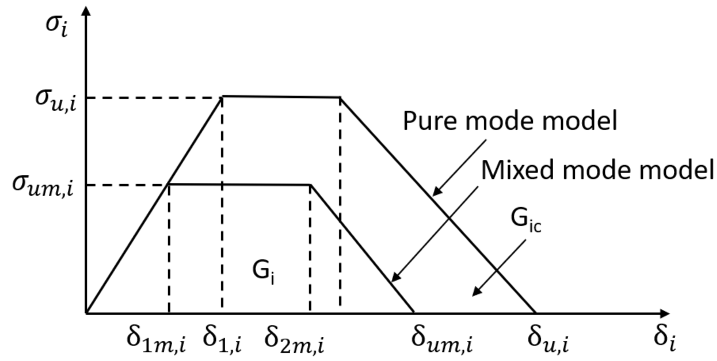

(b) Trapezoidal traction-separation law.

Figure 9: Schematic representation of traction separation laws, i=I,II.

Essentially, it is assumed that the area under the traction separation laws shown respectively, in Figure 9 represents the energy released in each mode, which is compared with the respective critical fracture energy represented by the larger element. Theses laws can exhibit multiple shapes (triangular, trapezoidal, exponential, etc...) to better match the behaviour of a specific type of adhesive. The indices o and u refer to the onset and ultimate relative displacement, respectively, and the subscript m stands for the mixed-mode case [11].

As mentioned previously, the constitutive behaviour of the cohesive element can be divided into two phases. The initial damage phase and the evolution damage phase. In the initial damage phase, the cohesive element has an elastic behaviour, up to a stress value corresponding to a critical stress above which the crack forms/propagates. The evolution damage phase represents the propagation of the crack until the complete failure of the element, which allows the element to be eliminated as it is no longer able to absorb stresses [11].

3 Experimental procedures

In the previous chapters, an overview of adhesives and of joint strength prediction approaches to the subject were presented. Building on this, this chapter discusses the experimental procedures used to characterise adhesives and develop the concept of the proposed novel experimental tool. The materials and adhesives used in this study are also presented. All tests were performed using a universal testing machine, more specifically the INSTRON® 3367 whose load cell is capable of measuring up to 30 kN.

3.1 Materials

In order to develop and validate the new experimental tool for mechanical characterisation of adhesives, two different adhesives were investigated. The selection was made to ensure two effectively different adhesive characteristics, something which is necessary to understand the geometric implications on the overall structure of the apparatus when the adhesives' mechanical properties are changed.

The first adhesive under analysis, brittle in nature, is a two-component, room temperature curing paste adhesive of high strength. According to its datasheet, when fully cured, the adhesive will have excellent performance at high temperatures and good chemical resistance. It is popular in many industrial applications where resistance to severe or warm environments is required. It is appropriate for bonding a wide range of metals, ceramics, glass, rubbers, rigid plastics, and other materials. It has been characterised in previous works [12], however, recent changes in the adhesive formula led to the need to determine the fracture toughness both in mode I and II, since the strength properties were not found to be significantly changed. This characterisation is presented in appendix B.

The other adhesive, a ductile one, that has been fully characterised by Correia et al. [13], on the other hand, is a one-part, heat-cured epoxy resin that is compatible with induction curing and can be used in place of brazing, welding, and riveting in high stress applications. Its key unique feature is improved electrical conductivity, which is a result of an aluminium filler the manufacturer added to the adhesive composition.

The properties of each adhesive studied are listed in Table 1 and 2, according to the manufacturer's datasheets.

Table 1: General characteristics of the adhesive used.

Adhesive	**Supplied as**	**Cure type**	**Cure cycle**
Brittle adhesive	Two-parts	Heat	100 °C/5 min
Ductile adhesive	One-part	Heat	150 °C/40 min

Table 2: Mechanical properties of the adhesives used.

	Brittle adhesive	**Ductile adhesive**
E [MPa]	4890	3880
σ_f [MPa]	41.00	65.60
G [MPa]	1560	1447
τ_f [MPa]	30.20	41.60
G_{I_c} [N/mm]	0.35	1.27
G_{II_c} [N/mm]	2.40	7.22

DIN 40CrMnMo7, a high strength steel, was used in the substrates and its properties are used in all subsequent numerical models. Avoiding plastic deformation during tests is the purpose of employing high strength steel, since this yielding will generate inaccuracies in the testing results. Table 3 displays the general characteristics of the substrates.

Table 3: Mechanical properties of the substrates used.

Young's modulus [GPa]	190-210
Ultimate tensile strength [MPa]	965-1030
Yield strength [MPa]	827-862
Poisson's ratio	0.27-0.3

3.2 Testing methods

The main objective of this work's experimental component is to validate the concept proposed for the novel tool that will enable adhesive mechanical properties direct extraction. In order to validate the numerical model, a prototype for combined tests setup was fitted to an existing commercial testing machine. However, to compare mode I and mode II fracture energy results, standardised tests were used, such as DCB (double cantilever beam) tests and ENF (end-notched flexure) tests, already used by the research group group and with the testing setups present in its facilities.

However, as explained in Section 1, the aim of this work was to develop a combined DCB and ELS test for mechanical characterisation of mode I and mode II of fracture energy, respectively. Before advancing to design this combined configuration, the author developed an ELS test setup. Accordingly, in this chapter, standardised setups will be first presented. After that, the designed ELS setup test will be exposed, and its construction will be described. Lastly, the combined setup for mode I and mode II characterisation will be studied.

3.2.1 Mode I fracture test

Double cantilever beam (DCB)

Figure 10 shows a DCB specimen composed by two beams with the same length and constant thickness. The pre-crack length, a_0, corresponds to an initial region without adhesive, h is the adherends thickness, and t is the adhesive thickness.

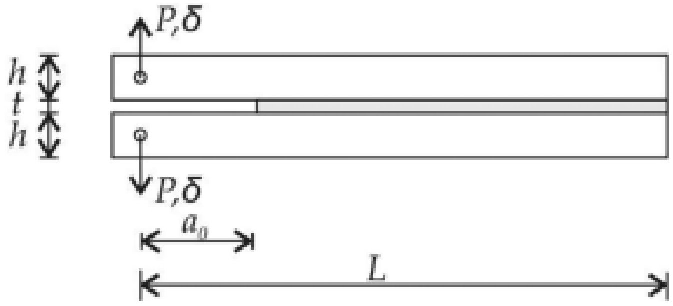

Figure 10: DCB specimen's geometry [14]. Dimensions in millimetres.

Depending on the geometry and material characteristics of the adhesive and adherends, the specimen can be loaded by opening the beams at different speeds, ranging from 0.5 to 3 mm/min. In the scope of this study, static tests were carried out with a testing speed of 0.2 mm/min using a commercial testing machine and setup, presented in Figure 11. During the test, the load - P - and displacements - δ - are recorded and, with an appropriate data reduction scheme, as discussed in subsection 3.4, the critical energy release rate in mode I, G_{I_c}, can be determined [14, 15].

In Figure 11 it is possible to observe the DCB specimen testing setup used for characterisation of mode I fracture energy in the current work.

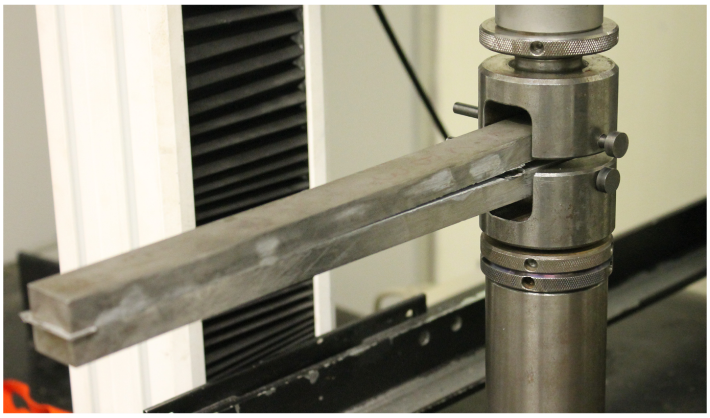

Figure 11: DCB specimen testing setup.

3.2.2 Mode II fracture tests

Due to its simplicity and extensive international standardisation, the DCB test is the most frequently employed under pure mode I (tension loading) for adhesive joints and composites. On the other hand, although being successfully modified for adhesive joints, only composites are currently eligible for standardised tests for pure mode II fracture toughness (G_{IIc}) characterisation during end-notched flexure (ENF) testing. The end-loaded split (ELS) is also proposed for the determination of mode II fracture toughness [14, 15].

Under shear loads, adhesively bonded joints have been reported to have a large fracture process zone (FPZ) compared to mode I or mixed-mode fracture tests and compared to other specimen dimensions, owing to the adhesive layer's plasticity. The large FPZ involved, along with the lack of crack opening, makes visual evaluation of the crack length difficult. To address this, approaches based on J-integral or an effective crack length (a_{eq}) that are not crack dependent have been developed. The widely used end-notched flexure (ENF) test, on the other hand, has stability issues as the crack propagation is often quite fast and the interaction between the loading supports and the crack can be significant. Multiple studies have shown encouraging results for end-loaded split (ELS) tests, which have the advantage of stable crack propagation under displacement control [11, 16]. Each of these tests and its different particularities will be discussed in greater detail in the following subsections.

End-notched flexure (ENF)

Specimens for ENF testing are constituted of two beams with constant thickness bonded together, except in the region of the pre-crack, and simply supported at the ends. As demonstrated in Figure 12, a mid-span load, causing shear in the adhesive, P, is applied on the specimen where a_0 is the initial crack length, δ the displacement of the centre of the ENF, h the height of each specimen, t the adhesive thickness and L the distance from each support, to the vertical line where the load is applied.

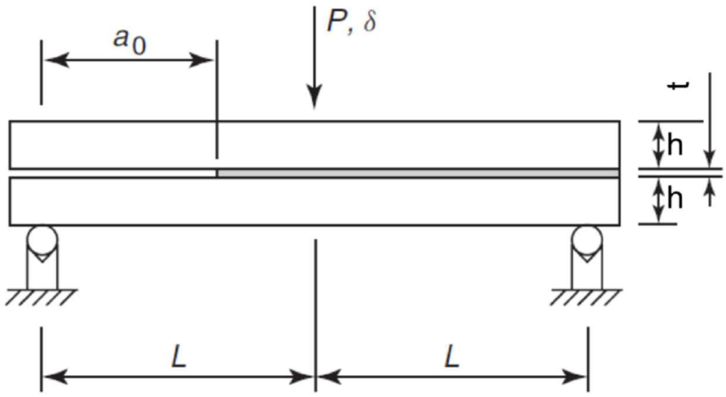

Figure 12: Schematic representation of a ENF test, dimensions in millimetres [15].

Similarly to the DCB test, both load and displacement are recorded to obtain the critical energy release rate in mode II, G_{II_c}, making use of an appropriate data reduction scheme, presented in subsection 3.4. Figure 13 shows the ENF specimen testing setup used during the experimental work of this thesis.

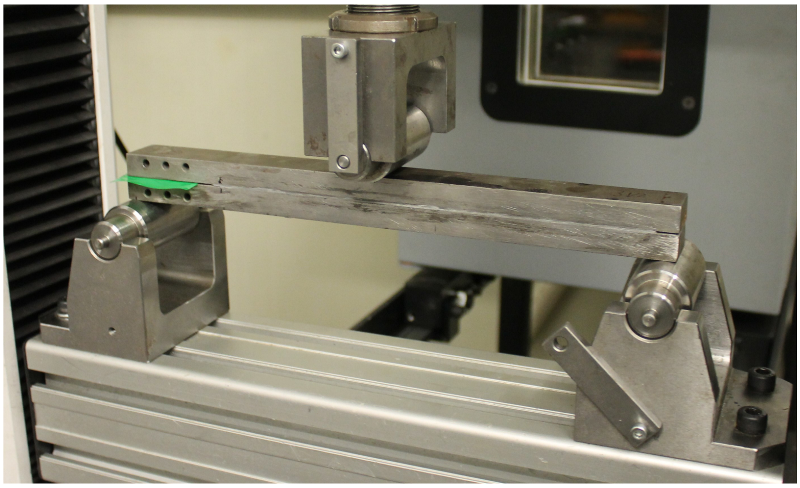

Figure 13: ENF specimen testing setup.

Although various issues related to unstable fracture propagation can arise, this is still the most popular test for G_{IIc} characterisation of bonded joints [15].

End-loaded split (ELS)

Due some of its inherent some advantages, such as a more stable crack propagation than that obtained when using the ENF testing method, the ELS test is generally seen as an effective option for describing the fracture behaviour of bonded joints under mode II loading [15].

Like ENF testing specimens, the ELS test is based on a cantilever beam geometry. Being so, the specimens are made of two beams of constant thickness that are bonded together, except for the pre-crack zone. The specimen is simply supported at one end, and a load P is applied at the other end, causing shear sliding at the pre-cracked region, a_0, between the specimen arms. As shown in Figure 14, δ is the displacement of the specimen's end where the load is applied, h the height of each specimen, t the adhesive thickness and L the distance from the point where the load is applied and the clamping tool, as also demonstrated on Figure 14.

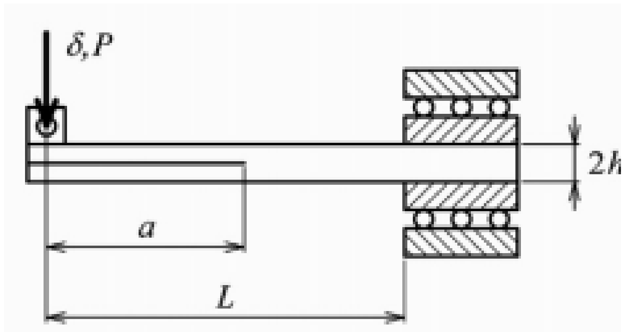

Figure 14: Schematic representation of an ELS test, dimensions in millimetres [17].

The end-loaded split tests, besides using simpler manufactured specimens, have produced encouraging results in recent studies, including the advantage of stable crack propagation under displacement control in composite joints if the initial crack to span length ratio is higher than 0.55 [18–22]. According to recent studies, a few requirements must be satisfied in order to get crack propagation during an ELS test. First, to guarantee the formation of the entire FPZ by achieving steady-state crack propagation and, consequently, the plateau of the resistance curve; second, to guarantee the stability of the test under displacement control; third, to prevent significant deflections; and fourth, to prevent adherend failure while testing. To meet these specifications, the ELS specimen geometry's span length, beginning crack length, and, if necessary, specimen total thickness must be adjusted [11, 16].

3.3 Combined test for mode I and mode II fracture characterisation

As mentioned before, a combined test for mode I and mode II adhesive characterisation was developed. The concept was numerically optimised and experimentally validated. This test, that combines a double cantilever beam with an end-loaded split test resulting in a modified DCB test, which implied the development of not only a new unified specimen, but also a new apparatus. The designed specimen is represented in Figure 15. This section will expose how the unified specimen is manufactured and how the associated testing apparatus was assembled.

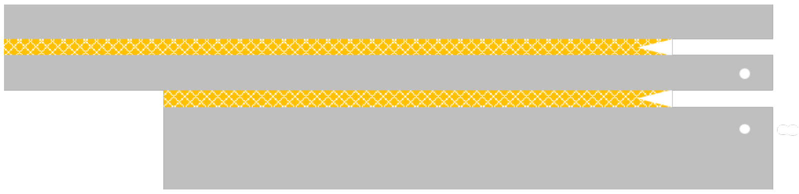

Figure 15: Schematic representation of a combined test for mode I and mode II adhesive characterisation.

Manufacturing of the new unified specimen

The substrate and mould materials, manufacturing processes, mould preparation, grit blasting, and cure cycles were employed frequently throughout the experimental part of this project for the DCB, ENF, ELS, and combined testing. All specimens were produced using the techniques described in Banea et al. [23], including the use of the appropriate moulds and pressure conditions, among other things. All of the moulds were made of construction steel and had the dimensions listed in Banea et al. [23]. These were cleaned with a thin grade of sandpaper before being manufactured. They were then degreased with acetone, and three coatings of a demoulding agent (Loctite® Frekote 770-NC) were applied to prevent adhesion of the specimens to the mould. All of the metallic substrates for standard characterisation were CNC machined from high strength steel, DIN 40CrMnMo7, to prevent plastic deformation. In all of its procedures, the CNC machining technique achieved fine general tolerances of ±0.05 mm. Every steel substrate in the standard characterisation tests was grit blasted with alumina grit at 0.6 MPa of pressure and degreased with acetone to ensure cohesive failure.

As aforementioned, the combined test merges a DCB with a ELS specimen. Since the ELS specimen is not manufactured differently than the DCB specimen, except for the fact that the blade used to induce a pre-crack must be withdrawn before testing, this unified specimen for combined testing can be understood as an adaptation of a DCB specimen. Being so, the specimen was manufactured in a proper steel mould [23] following the relevant standard ASTM D3433-99 [24], using three CNC machined high strength steel adherends, the smallest one related to the bottom substrate of the unified specimen, as can be seen in Figure 16. To guarantee strong adherence, all substrates were grit-blasted and acetone-degreased prior to the application of the two layers of adhesive. A 0.1 mm-thick, sharp razor blade placed in the middle of the bondline's thickness induced the initial crack, measured denoted as a_0, to be 45 mm long. Depending on the adhesive that was being used, the adhesive was finally cured under the temperature and pressure settings that were specified in subsection 4.1 for the hot plate press cure setup.

Figure 16: Manufactured unified specimen for mode I and mode II adhesive characterisation.

After the curing cycle related to the adhesive being studied, the excess adhesive is removed using a drilling machine with a milling head, and the upper blade of the specimen, related to the ELS part, is removed under low intensity mode I loading. The specimen is then ready to be assembled in the new testing setup.

Apparatus for mode I and mode II fracture characterisation

Since the concept of the combined test for mode I and mode II fracture characterisation merges a double cantilever beam with an end-loaded split test, the apparatus was firstly projected to work as an apparatus for ELS testing, since its boundary conditions are more complex and later could be easily adapted to work with the combined test specifications. Accordingly, an initial setup was built using an aluminium base mounted on top of two roller bearings, coupled to a guideline system and, therefore, meeting the requirement of having an horizontal degree of freedom during loading. To meet the clamping requirement, a steel bar was placed on top of the specimen in one of its ends and then fixed making use of two aluminium bars and screws distributed along the length of the aluminium base. After the fixation of the clamping tool, the setup was assemble in the universal testing machine and the specimen was loaded by a vertical displacement in an ascending movement, reproducing the prescribed loading conditions of the ELS test. On Figures 17a and 17b is represented the first developed setup.

(a) Setup layout.

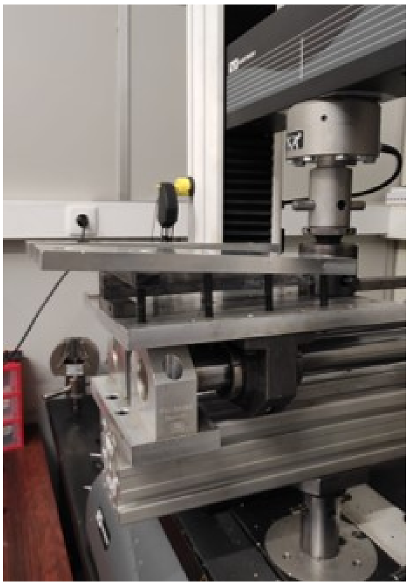

(b) Setup on the test machine.

Figure 17: First ELS setup.

It is possible to see that, in this first attempt, the aluminium bars that assure the clamping of the specimen are not fastened in a balanced manner, meaning that the fixation of the full specimen also not balanced. It is also noticeable that these bars are not stiff enough for the fastening forces involved, since they bend exaggeratedly. On Figure 18a a close up to the clamped region of the specimen is shown and on Figure 18b is presented the first load-displacement (P-δ) curve obtained.

(a) Close up on the clamped part.

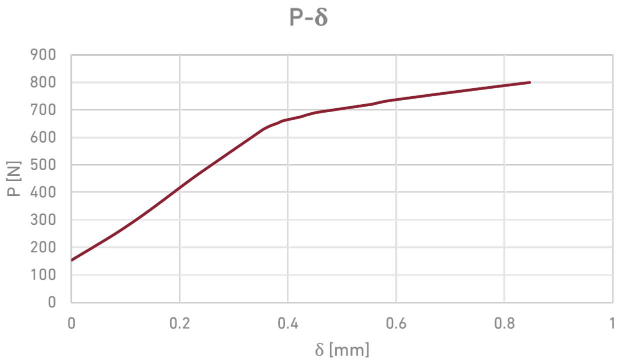

(b) First P-δ obtained.

Figure 18: First ELS test performed.

On Figure 18a it is perceptible that the lower substrate surface is not fully contacting the base, which means that the clamping force is not strong enough, the specimen slips, and no crack propagation is observed, as can also be seen in Figure 18b, where the different between the two slopes describe this slipping phenomena. Besides that, the applied force made the whole setup lean, showing a lack in stiffness. Since it was not possible to change the fixture feature of this setup to the universal testing setup, which is made in the middle of the guiding system, increasing the bending moment of the whole structure, a new setup was though, using a different material. A new base was designed using steel instead of aluminium, making it stiffer, as can be seen in Figure 19b. A new clamp tool was also designed, made of a solid block of steel that would allow a fixation to the steel based by the use of four screws, symmetrically distributed for a more even fixation force. Furthermore, the clamp block ensures better fixation since it also has a larger contact area with the specimen. Additional holes were created in the base plate for pins used to ensure the perfect alignment of the specimen. These features can be observed in Figure 19a.

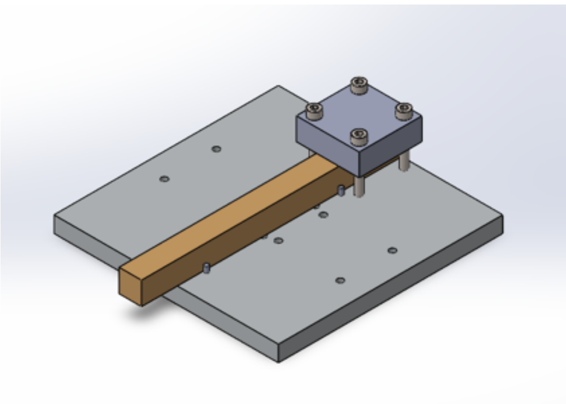

(a) Idealized setup made in steel.

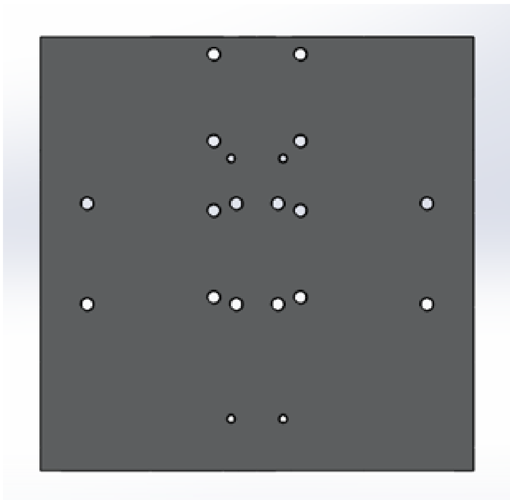

(b) Features of the new steel setup base.

Figure 19: Idealised setup made in steel using SolidWorks.

The steel base was machined in computer numerical control (CNC) milling machine and its threads were manually made. The through-holes of the block were made using a vertical column drill. The physical model is presented in Figure 20a and 20b.

(a) Steel setup top view.

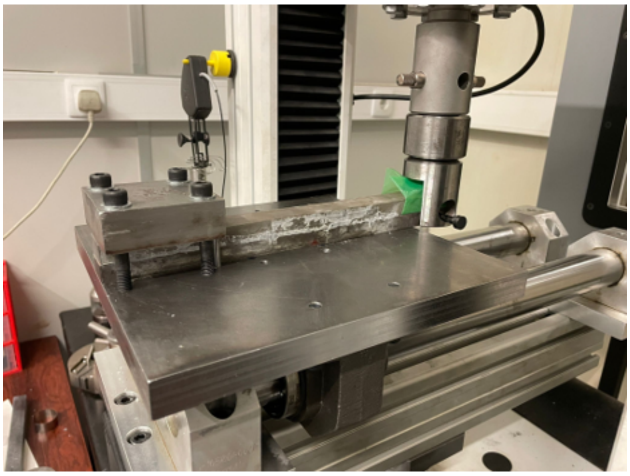

(b) Steel setup side view.

Figure 20: Produced steel setup.

However, this apparatus, although designed to be more stiff, was found to still have bending problems as the whole setup was still slightly leaning and, therefore, the displacement read by the machine was being overestimated, since the machine was reading the displacement of the whole apparatus and not that resulting from the test. This phenomena can be seen in Figure 21a. To address this issue, a DCTH1000A linear variable differential transformer (LVDT) from RDP Group was used to measure the relative displacement of the specimen against the base, allowing to remove this source of error. This LVDT, fixed to the base as shown in Figure 21b, has a measurement range of ±25 mm and, according to the manufacturer's specifications, a linearity error of ±0.5 %.

(a) Side view of the setup while leaning.

(b) LVDT to measure relative δ.

Figure 21: Leaning problems of the setup and use of a LVDT.

The use of the LVDT provided more reliable results, since it enabled good correlation with experimental results using other mode II fracture energy release rate, such as ENF. However, some leaning was still noticeable and could be leading to an overestimation of the G_{II_c} values. In an attempt to eliminate the influence of the bending moment, two more roller bearing for the same guide system were ordered and the steel base was changed for this, opening eight more threaded through-holes, as indicated in Figure 22b. However, the roller bearings did not arrive within the time limits of this project so, in another try to diminish the bending moment, the existent roller bearings were moved to opposite sides of the base, creating a wider support that better resisted bending

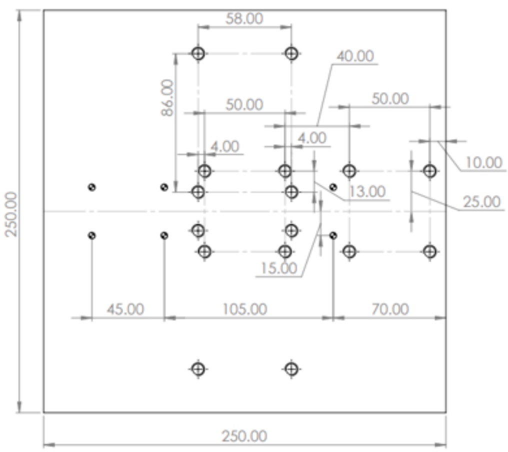

(a) Initial technical drawing.

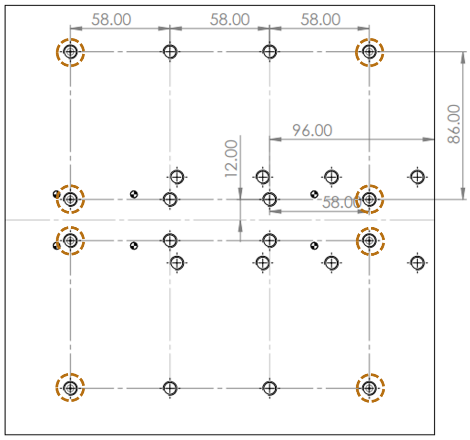

(b) New technical drawing.

Figure 22: Technical drawing of the steel base and its new features.

Considering all the possible attempts within the time range of this work, and having minimised the error as much as possible, the setup was then upgraded to being able to test the unified specimen. The only modification needed was an additional fixture for the bottom substrate to the DCB-related part of the unified specimen, preventing the movement in the horizontal and vertical direction. This modification can be observed in both Figure 23a and 23b. On the left figure, a separation between the ELS part of the unified specimen and the bottom substrate related to mode I testing is noticeable. On the left, that substrate was removed and it is possible to observe, in detail, the deflection of the ELS part of the unified specimen.

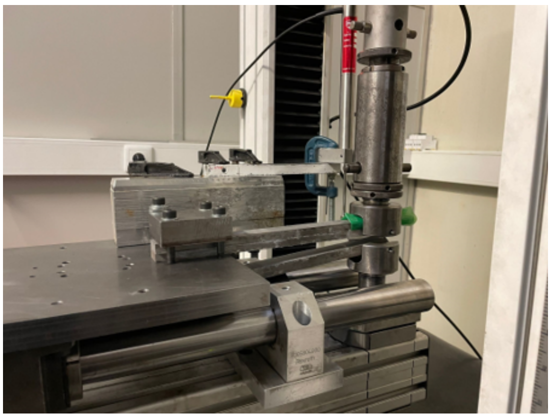

(a) Unified specimen after mode I testing.

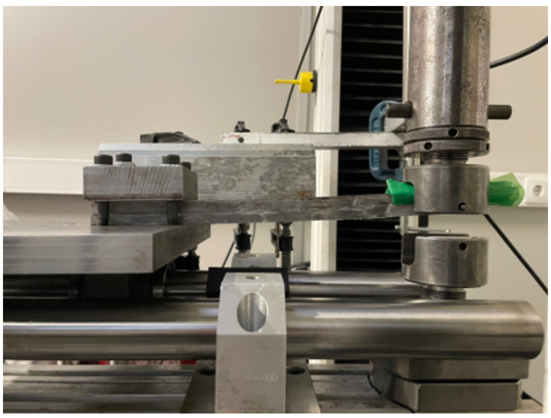

(b) Mode II testing of an unified specimen.

Figure 23: Setup for combined test for mode I and mode II fracture characterisation.

Next, two P-δ curves are presented, the first one was computed using the machine displacement, Figure 24 and the second using the LVDT displacement, in Figure 25.

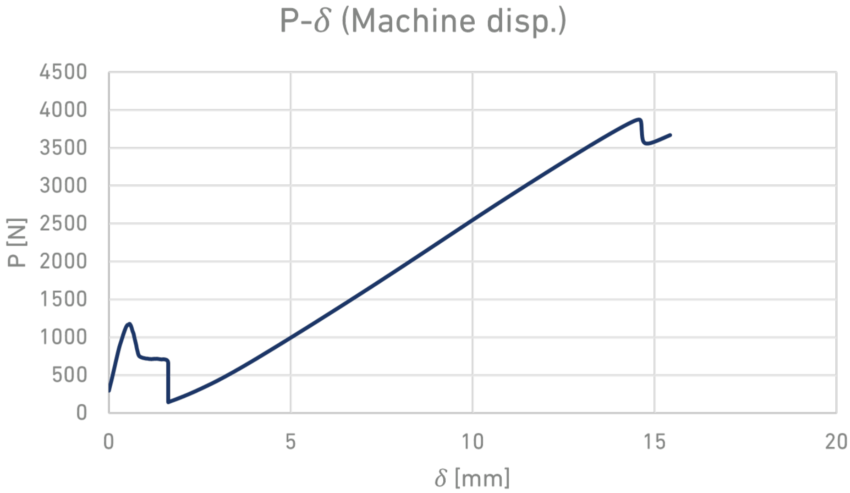

Figure 24: P-δ curve using machine displacement.

In the above figure, related to the machine displacement, a difference between the part of the curve is related to the DCB test and that concerning the ELS test, which starts around 0.3 mm of displacement. This is right after the DCB specimen breaks and, consequently, the load drops form around 700 N to 30 N. However, it is already known that the machine displacement is not a precise indicator of the specimen displacement, which is the intended measurement parameter. Being so, an LVDT was used to measure the specimen displacement. The corresponding obtained P-δ curve is represented next.

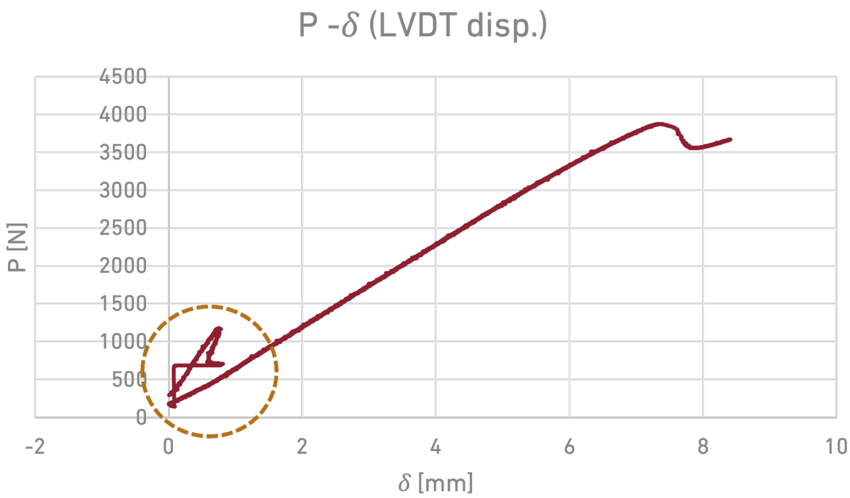

Figure 25: P-δ curve using the LVDT displacement.

It is immediately noticeable that the total displacement measured was smaller than for the machine displacement, as expected. In spite of that, some complications related to the measurement of the displacement of the DCB test still arose, as highlighted in yellow, mostly due to vibration problems. In brittle adhesives, as the one tested, the crack propagation can be sudden, the opening of the specimen, induces vibrations to the full system and in the pin where the displacement is measured, since the pin does not perfectly fit the specimen hole and thus has some freedom to oscillate. This makes analysing the DCB related part of the test difficult. Nevertheless, the ELS related part of this combined test presented accurate results (see appendix B).

For this reason, a digital image correlation (DIC) technique was used to measure the displacement of the mode I related part of the test. For this, the whole setup was flipped and the specimen top was coated with a white matte paint and speckled with black dots. To obtain the displacement field data, the recorded pictures were analysed using GOM Correlate software. A pixel in the image corresponded to 0.101 mm on the measured surface, and the facet size employed was 12 pixels. A camera and light set was also assembled, facing the region where the measurement of the displacement was intended. In Figure 26 it is possible to observe the referred setup and in Figure 27 is presented a close up to the region where displacements were measured using DIC.

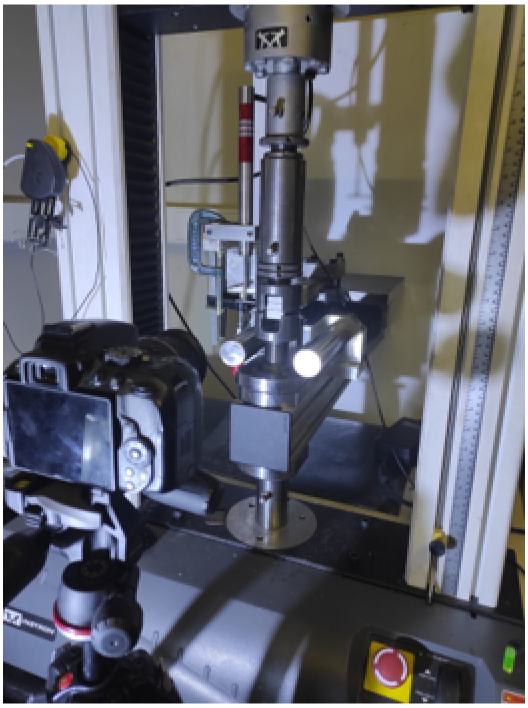

Figure 26: Set of camera and light assembled for DIC analysis.

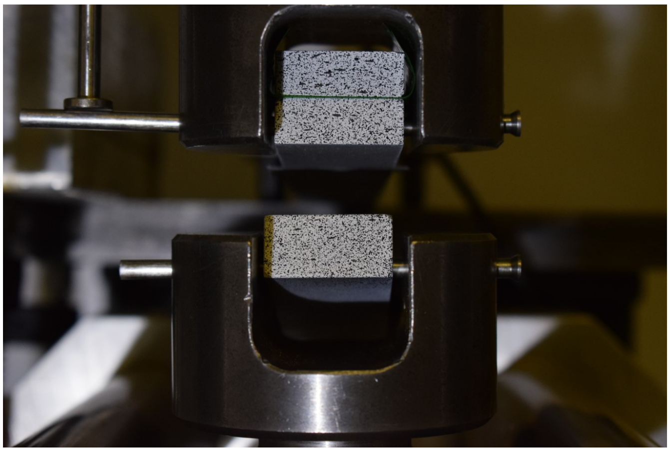

Figure 27: Close up on the targeted region for DIC analysis.

The results of measuring a relative distance between the two bottom substrates will give the displacement of a DCB test. This technique shown good correlation with numerical results.

3.4 Data reduction scheme

To determine the overall fracture energy of an adhesive, it is necessary to employ a data reduction strategy to acquire the energy release rates in modes I and II. There are classical methods such as the Compliance Calibration Method (CCM) [25, 26] and Corrected Beam Theory (CBT) [26, 27] that allow the determination of these properties. The first one is based on the the Irwin-Kies equation:

$$G_I = \frac{P^2}{2b}\frac{dC}{da} \tag{6}$$

where cubic polynomials are used to fit the compliance ($C = C_3 \cdot a^3 + C_2 \cdot a^2 + C_1 \cdot a + C_0$) as a function of the crack length (a). The Corrected Beam Theory (CBT) is also derived from the previous equation but takes into account a correction factor, Δ, that considers crack tip rotation and deflection [26–30]:

$$G_I = \frac{3P\delta}{2b(a + |\Delta|)} \tag{7}$$

The correction factor was proposed in 1992 by Wang and Williams [28] and can be determined by the following equation:

$$\Delta = h\sqrt{\frac{1}{13k}\left(\frac{E_x}{G_{xy}}\right)\left(3 - 2\left(\frac{\Gamma}{1+\Gamma}\right)^2\right)} \quad , \text{ with } \quad \Gamma = \frac{\sqrt{E_x E_y}}{kG_{xy}} \tag{8}$$

where h is the thickness of the substrate, E_x, E_y the modulus in the thickness direction and G_{xy} its longitudinal normal and shear modulus, and k the shear stress distribution constant for correcting the deflection caused by the shear forces.

After loading the specimen at three distinct load levels, an experimentally based crack length correction, Δ, can be obtained by using a linear regression. This is schematically shown in Figure 28.

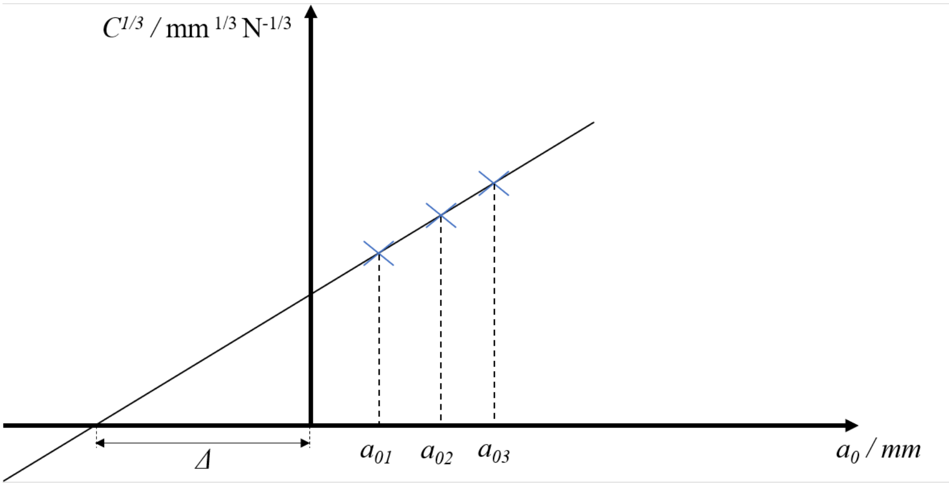

Figure 28: Graphic representation of the method used to determine the crack length correction, Δ. Adapted from [9].

Nevertheless, both CCM and CBT imply the precise determination of the crack length, which can be a challenging process, particularly in cases of sudden fracture of the adhesive. Besides that, in mode II loading, the crack opening is not pronounced since the failure occurs by sliding. A fracture process zone (FPZ), shown in Figure 29, is developed ahead of the major crack tip due to plasticization and the nucleation of many microcracks. The energy dissipated in the FPZ also rises with increased ductility, and the data reduction strategy must take this into account [25, 26, 31].

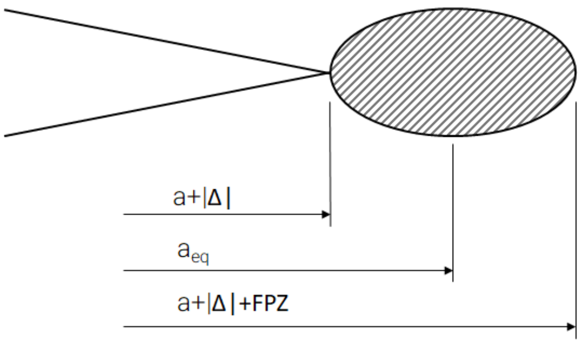

Figure 29: Schematic representation of the equivalent crack length and fracture process zone concepts. Adapted from [32].

The compliance-based beam method (CBBM), built on the basis of equivalent crack length and considers the phenomena previously described, is the one chosen to treat the fracture toughness data in light of these facts. It merely depends on the compliance of the specimen throughout the test [32, 33].

3.4.1 Mode I - Double cantilever beam

Using CBBM, the energy release rate in mode I is defined as [32]:

$$G_I = \frac{6P^2}{b^2h}\left(\frac{2a_{eq}^2}{h^2E_f} + \frac{1}{5G_{13}}\right) \tag{9}$$

being P the applied or measured load depending on the type of loading condition, b is the width of the specimen, h is the specimen height, G_{13} is the shear modulus of the substrates, a_{eq} is the equivalent crack length, whose value is derived from Timoshenko's beam theory [32]:

$$C = \frac{\delta}{P} = \frac{8a_{eq}^3}{bh^3E_f} + \frac{12a_{eq}}{5G_{13}bh} \tag{10}$$

and E_f is the corrected flexural modulus, that aims to correct the fact that the mentioned method does not take into consideration the stress concentration and substrates' rotation close to the crack tip [32]:

$$E_f = \left(C_0 - \frac{12(a_0 + |\Delta|)}{5bhG_{13}}\right)^{-1}\frac{8(a_0 + |\Delta|)^3}{bh^3} \tag{11}$$

being 0 the index set for initial values, where a_0 is the initial crack length previously defined for each method in subsection 3.2 and C_0 the initial linear compliance, and Δ a correction factor for the crack length derived from the one used in the CBT method given by the Equations 8, considering an isotropic material and 0.85 for the constant k [17].

3.4.2 Mode II - End-notched flexure

In case of mode II loading, fracture energy can be determined by [34]:

$$G_{II} = \frac{9P^2a_{eq}^2}{16b^2Eh^3} \tag{12}$$

where

$$a_{eq} = \left(\frac{a_0^3C_c}{C_{0c}} + \left[\frac{C_c}{C_{0c}} - 1\right]\frac{2L^3}{3}\right)^{1/3} \tag{13}$$

with

$$C_c = C - \frac{3L}{10bhG_{13}} \tag{14}$$

and

$$E = \frac{3a_0^3 + 2L^3}{8bh^3C_{0c}} \tag{15}$$

being L half of the ENF specimen total length and index c indicates the corrected value of a variable.

3.4.3 Mode II - End-loaded split

In this instance, G_{II_c} was obtained using four different techniques. Additionally, despite being small, substantial displacement correction factors were not insignificant. The linear regression using CCM's least squares method looked like this:

$$\frac{C}{N_2} = A + ma^3 \tag{16}$$

where N_2 is a load block (often bonded to the specimen for load transmission) and large displacement correction factor, while G_{IIC} is obtained from

$$G_{II} = \frac{3mP^2a^2}{2B}F_2 \tag{17}$$

where F_2 is a large displacements correction factor. The expressions for N_2 and F_2 can be obtained as follows:

$$F_2 = 1 - \phi_1 \left(\frac{\Delta}{L}\right)^2 \tag{18}$$

$$\phi_1 = \frac{3}{20}\frac{15 + 50\left(\frac{a_{eq}}{L}\right)^2 + 63\left(\frac{a_{eq}}{L}\right)^4}{\left(1 + 3\left(\frac{a_{eq}}{L}\right)^3\right)^2} \tag{19}$$

$$N_2 = 1 - \phi_5 \left(\frac{\Delta}{L}\right)^2 \tag{20}$$

$$\phi_5 = \frac{36}{35}\left[\frac{((1 + \frac{7}{8}(a/L)^3(35 + 182(a/L)^2 + 367(a/L)^4)}{(1 + 7(a/L)^3)^3}\right] \tag{21}$$

Now, it becomes possible to compute, from CBT:

$$G_{II_c} = \frac{9P^2(a + \Delta_{II})^2}{4B^2h^3E_1}F_2 \tag{22}$$

Following a finite element calibration procedure, $\Delta_{II} = 0.49\Delta_I$, where Δ_I is obtained from (insert citation).

On the other hand, a beam analysis of the ELS specimen with EC concept gives

$$\frac{C}{N_2} = \frac{3a_{eq}^3 + L^3}{2E_1Bh^3} + \frac{3L}{5G_{13}Bh} \tag{23}$$

Thus, for the CBTE method,

$$a_{eq} = \left(\frac{2E_1Bh^3C_c}{3} - \frac{L^3}{3} \right) \tag{24}$$

where

$$C_c = \frac{C}{N_2} - \frac{3L}{5G_{13}Bh} \tag{25}$$

and finally,

$$G_{II_c} = \frac{9P^2a_{eq}^2}{4B^2E_1h^3}F_2 \tag{26}$$

Following the procedure used for the ENF test, the CBBM now yields

$$E_{1a} = \frac{3a_0^3 + L^3}{2Bh^3C_{0c}} \tag{27}$$

and

$$G_{II_c} = \frac{9P^2C_{0c}}{2B(3a_0^3 + L^3)} \left[\frac{C_c}{C_{0c}a_0^3 + \frac{L^3}{3}\left(\frac{C_c}{C_{0c}} - 1\right)} \right]^{\frac{2}{3}} F_2 \tag{28}$$

3.5 Developed code

The first main objective of developing a supporting code was to automate the processing of the data reduction schemes. For the purpose of this work, even if the focus was in obtaining mode I and mode II energy release rate G_{I_c} and G_{II_c}, correspondingly, for the combined test, the code developed also intended to compute both the strength and shear properties. The reason for automating this process is related to the great amount of raw data generated by the data acquisition setup and the considerable amount of mathematical manipulation needed to formulate some data reduction schemes, such as the compliance based beam method (CBBM). For example, for the end-loaded split test, depending on the acquisition rate of the machine, commonly collects more than 25000 frames of load-displacement, which makes the use of conventional programs such as Excel to process this data heavy and slow. Furthermore, when linear variable differential transformer (LVDT), some noise is observed in displacement measurement, so filtering is also applied to the raw P-δ curve data. After that, the CBBM for G_{II_c} determination involves at least thirteen equations. The above mentioned reasons sustain the need for a code capable to automate this process.

For the purpose of this master dissertation, a code was developed using Python, in an attempt to meet the previously defined requirements. Next, the functionalities of the developed program will be described.

Firstly when one runs the program, the following window represented in Figure 30 opens and it is possible to chose between 'Fracture Tests' and 'Strength tests', depending on each kind of test one wants to analyse.

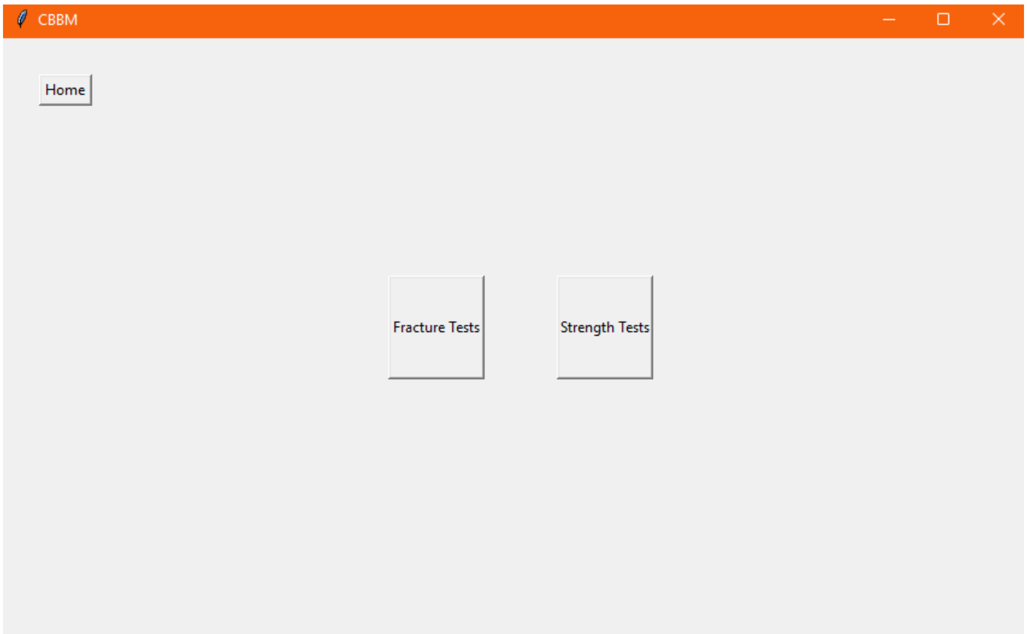

Figure 30: First interface of the program.

If 'Fracture Tests' is clicked, the initial window is close and another one opens, represented in Figure 31, related to the fracture tests.

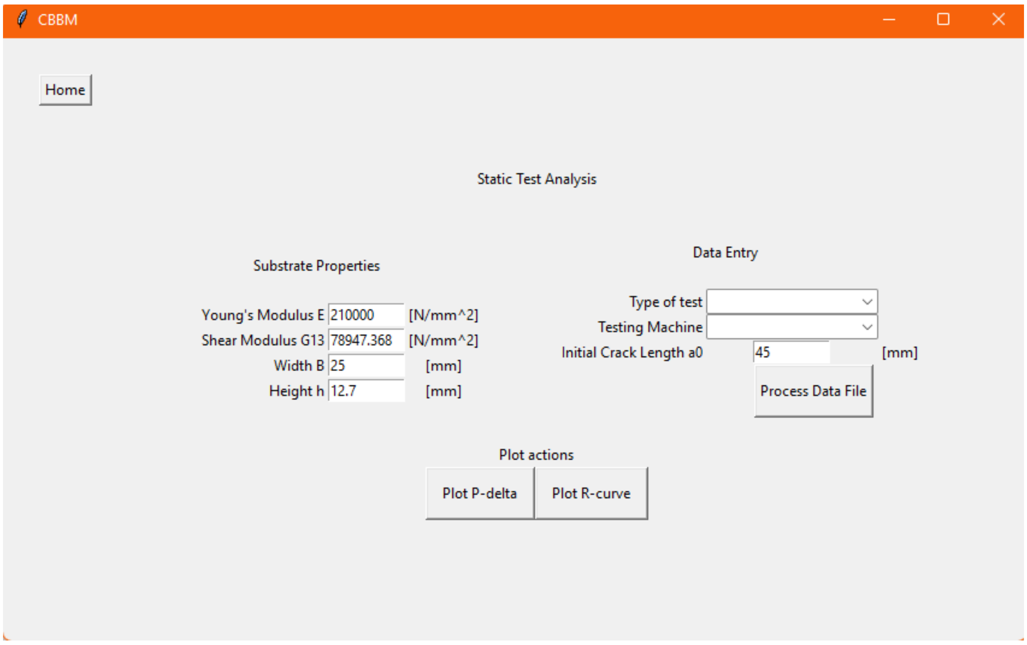

Figure 31: Fracture tests interface of the program.

The substrates properties can be input on the left textboxes and the initial crack tip, important parameter to compute CBBM, can be introduced to the program via the textbox on the right. If no parameters are inputted by the user, default values are assumed, as can be seen. In 'Type of test' a combobox lets one chose which fracture test is going to be analysed: 'DCB', 'ENF' or 'ELS'. In 'Testing Machine' it is possible to chose between 'Hydraulic' or 'Eletro-Mechanical', since the way data will be read in each case is different. The button entitled 'Home' returns to the first window of the program. The next step concerns processing the raw data file, by clicking on 'Process Data File', another window is opened like in Figure 32.

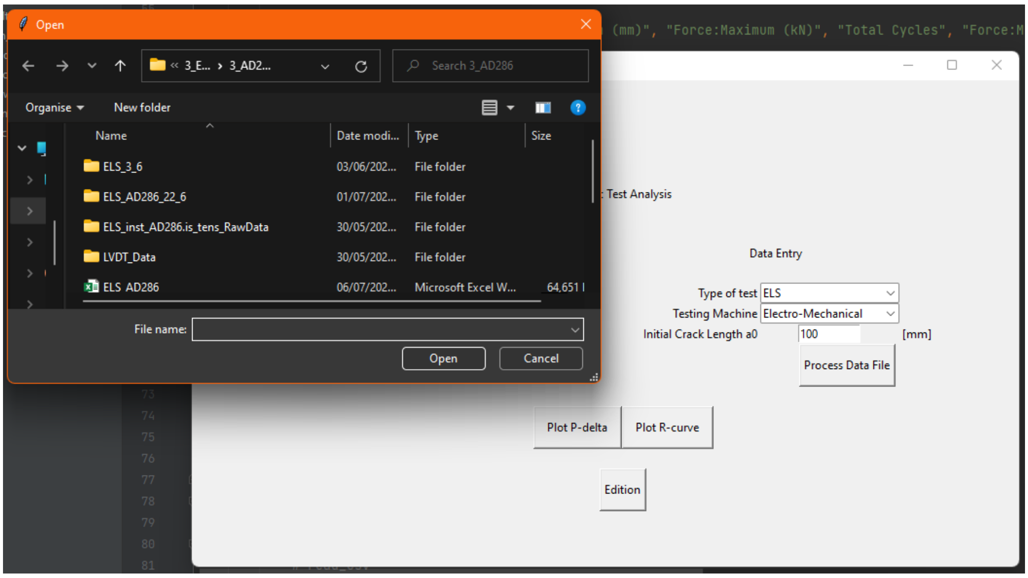

Figure 32: Window to choose the data file to be processed.

The program is prepared to read Comma-separated values, commonly denoted as 'csv' files, compatible with the type of files that the data acquisition program provides. After clicking 'Open', the file is processed and the user can choose to plot the load-displacement curve in 'Plot P-delta'. After plotting the P-δ curve, the user can choose to either plot directly the R-curve or edit the first plot, by clicking 'Plot R-curve' or 'Edition', correspondingly. Figure 33 shows an example where the provided raw data needs some further edition.

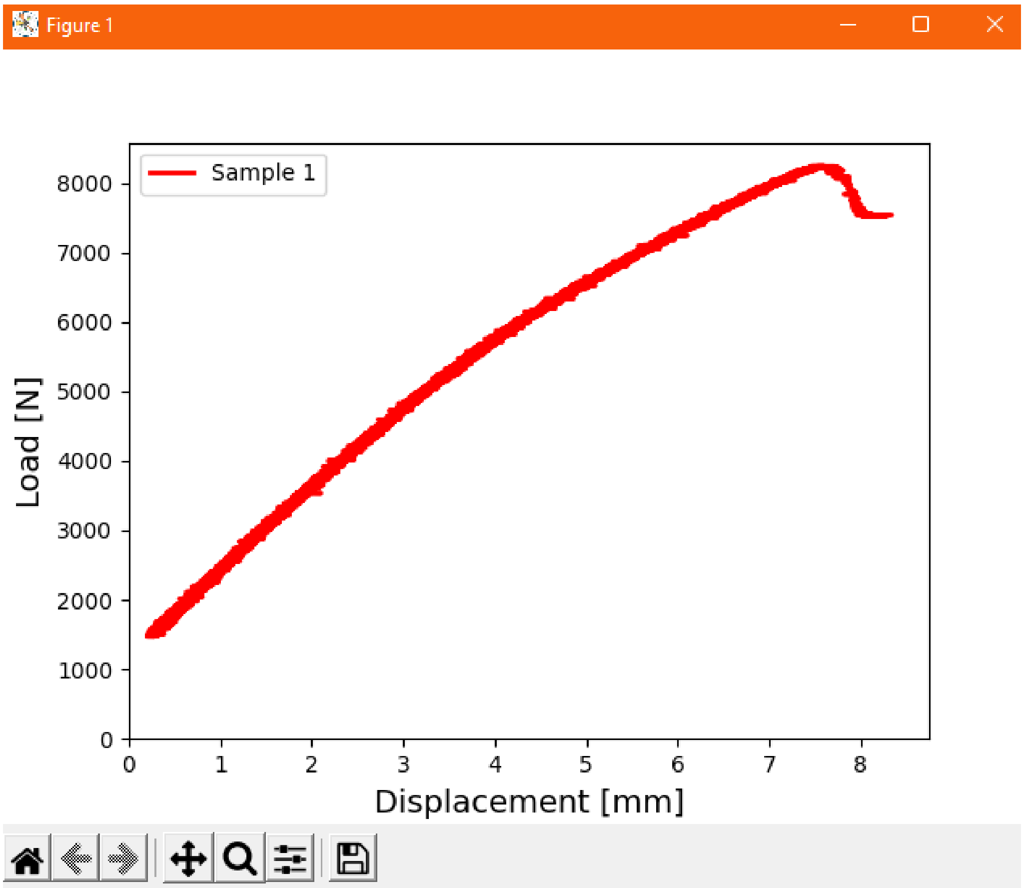

Figure 33: Raw data provided.

As it can be seen, the initial slope, related the mechanical adjustments of the machine does not fit the final slope prior crack propagation. Besides that, a linear regression and a displacement offset needs to be performed. In addition, it is noticeable that there is noise related to the measurement of displacement using a LVDT and thus filtering should be applied.

In Figure 34 the edition page is presented with the features aforementioned.

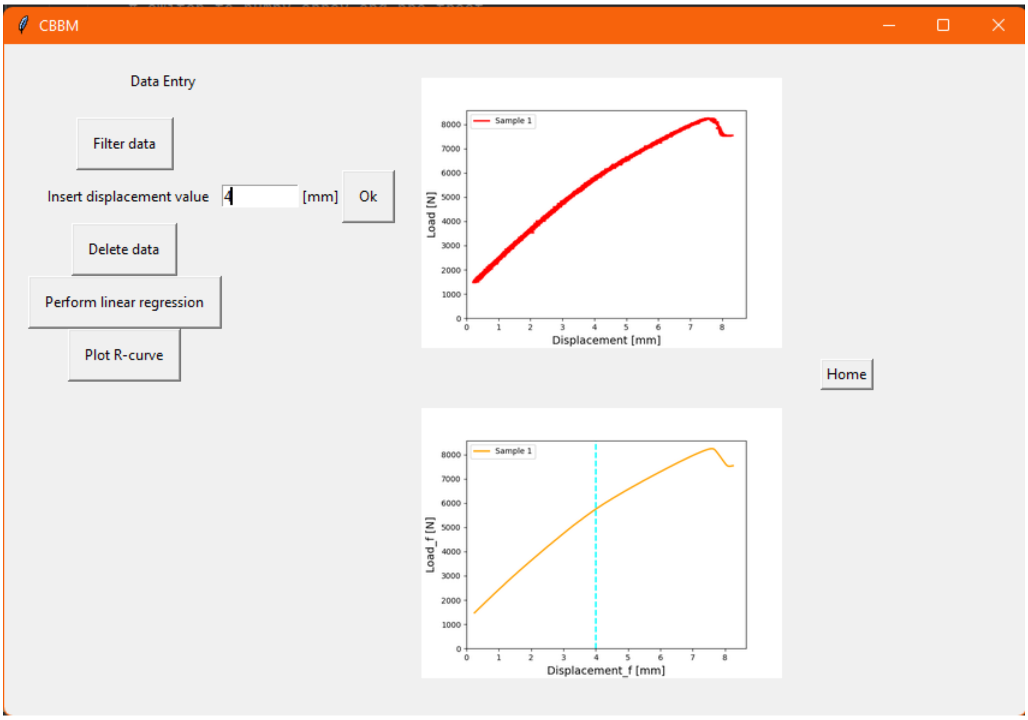

Figure 34: Edition page after applying filters to the raw data.

On the top right corner, the raw P-δ curve presented before in Figure 33 can be seen. Underneath that, the chart presented is already filtered (by clicking in 'Filter data') and a displacement value was inserted, as can be seen by the light blue line in the bottom chart, to request a deletion of the data related to displacements smaller than 4 mm. The filter used was the Savitzky-Golay Filter [35], generally indicated as the most suitable to smooth the inevitable noise present in the raw data.

Next, by clicking in 'Delete data' and 'Perform linear regression' the data related to displacements smaller than the indicated will be removed and a linear regression and positioning of the results to start in the origin of the x and y axes will be done. After that, it is possible to obtain the R-curve by clicking in 'Plot R-curve'. In Figure 35 it is possible to observe the changes aforementioned and the final R-curve on the bottom left corner.

Figure 35: Edition page after treating the raw data.

On the bottom left corner of the window the obtained R-curve is presented. Both the data related to the filtered and cleaned P-δ curve and the obtained R-curve are saved as csv files in the same folder where the raw data is located.

If, in Figure 30, the user intended to analyse strength tests, bottom 'Strength tests' should have been clicked. After that, as can be see in Figure 36, similarly to what happened for the fracture tests in 'Type of test', the user can choose between 'Tensile' or 'Shear' test and in 'Testing Machine' either choose 'Hydraulic' or 'Eletro-Mechanical'. As the data reduction schemes for these tests are much simpler than those used for fracture tests, after plotting the P-δ curve, the curves just need to be transformed to stress-strain curves with a simple math formulation.

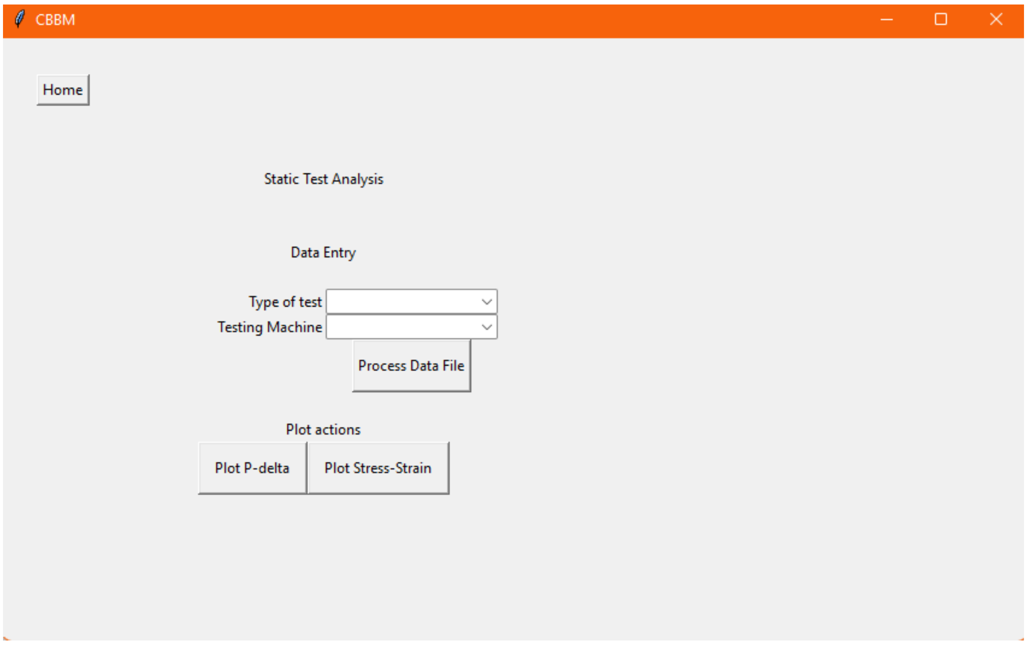

Figure 36: Strength tests interface of the program.

All of the the code developed for this work can be found in the annexes (see appendix C).

4 Numerical details

In the scope of this study, two different specimen geometries will be numerically optimised, using a commercial finite element analysis software, Abaqus®, starting from an end-loaded split test and finally moving to a combined test that intends to be used for quasi-simultaneous mode I and mode II energy release rate extraction, by merging a double cantilever beam with an end-loaded split joint, that are sequentially tested. In this chapter, the numerical model, used for both tests will be described, starting by establishing some considerations about the ELS test and moving to the combined test, which is considered an extension of this test, combined with a DCB.

4.1 Materials, geometry and general statements

As mentioned before, two different numerical models were developed, one related to the ELS test and the other one related to the combined test. The geometry of the specimens, the substrates and the adhesives used on the simulations and building of both models are the same as the ones used on the experimental work used for validation of the numerical model.

Two different adhesives were used in order to represent different ranges of adhesive's application and to understand the geometric implications in the overall specimen behaviour when each test is performed. Their properties as well as those of the substrates are presented in Section 3.

Considering both the steel and the adhesives as isotropic materials, a two-dimensional model was used for the finite element analysis of each test. In fact, shell elements were used to discretise bodies by defining the geometry at a reference surface (2D) and the thickness is defined through the section property definition. Shell elements are used to model structures in which one dimension, the thickness, or, in this case, the width of the specimen, is significantly smaller than the other dimensions, which is the case.

On Figure 37 is presented a scheme with the relevant geometric parameters used to design the end-loaded split specimen,

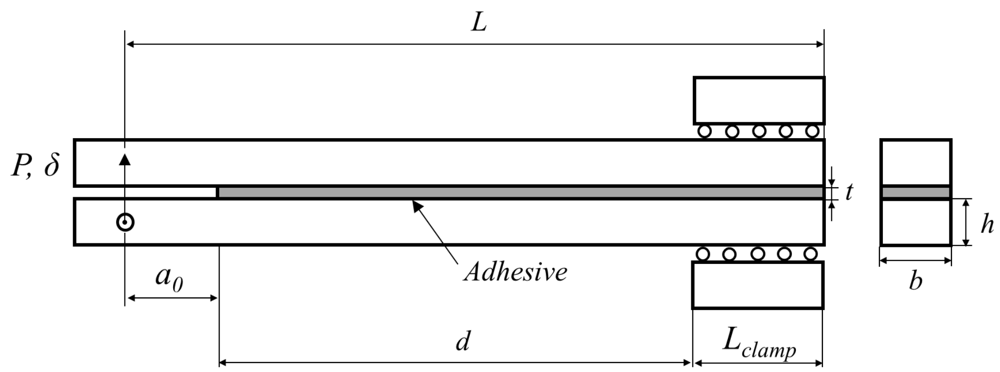

Figure 37: ELS specimen scheme, dimensions in millimetres.

where L is the length of the specimen, L_{clamp} is the specimen's length that it is clamped, d is the mid span length of the specimen, a_0 is the initial crack tip, t is the thickness of the adhesive layer, r is the radius of the hole where the load pin will fit, h is the height of the substrate and b is the width of the specimen.

In the following Table 4, the geometric properties of the ELS specimen modelled are presented, also taking into to account the specimens used on the experimental work. This will be the specimen used for numerical validation of the model and also serve as a target for numerical optimisation of its own geometry.

Table 4: Geometric properties of the ELS specimen.

L	L_{clamp}	d	a_0	h	r	t
290 mm	70 mm	260 mm	100 mm	12.7 mm	2.5 mm	0.2 mm

Concerning the combined test, in Figure 38 is presented a scheme of the geometry of the specimen and relevant variables that will be a target of study, later in the next chapter.

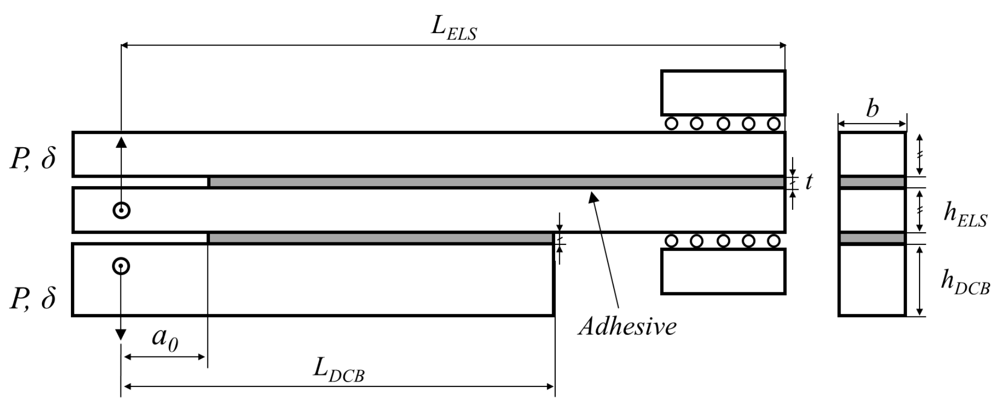

Figure 38: Combined specimen, dimensions in mm.

where, in this case, a distinction is made between the length of the ELS specimen, L_{ELS} and the length of the lower substrate of the DCB test, L_{DCB}. The same consideration is made to discriminate the height of each of the ELS substrates and the lower substrate of the combined test, h_{ELS} and h_{DCB} correspondingly.The other three variables, a_0, b and t are logically related to the initial crack tip, the width of the specimen and the thickness of both adhesive's layers as mentioned for the isolated ELS specimen geometry. The adopted geometry for the combined test specimen is described in Table 5.

Table 5: Geometric properties of the combined specimen.

L_{ELS}	L_{DCB}	a_0	h_{ELS}	h_{DCB}	t
290 mm	180 mm	45 mm	9 mm	12.7 mm	0.2 mm

As mentioned before, the new procedure was numerically validated using a two-dimensional finite element analysis but also included a cohesive damage model, which allows the simulation of crack initiation and growth. This model is based on fracture mechanics and damage theory and allows for an adequate prediction of the onset of damage evolution and crack propagation. This method consists of introducing a cohesion law in finite element modeling, which will be mentioned when the damage model is presented.

4.2 Development of the model

Boundary conditions

Computing correctly the boundary conditions of the model means being closer to a reasonable approach to a real problem, in this case, this corresponds to the real testing conditions of these two specimens. Concerning the end-loaded split test, as exemplified in Figure 37, it is recognised that there will be an imposed displacement through a pin, and the region related to the clamp tool will have only one degree of freedom on the horizontal direction. These boundary conditions are represented in Figure 39.

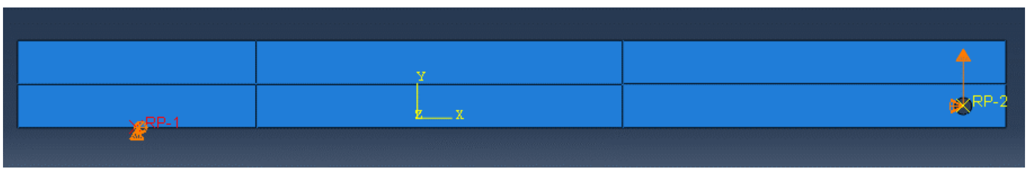

Figure 39: Boundary conditions of an ELS specimen.

In the case of the combined test, the boundary conditions applied are more complex and since the mode I and mode II tests are sequentially performed, the boundary conditions are also successively applied. In Figure 40 it is possible to observe the boundary conditions involved in this combined test.

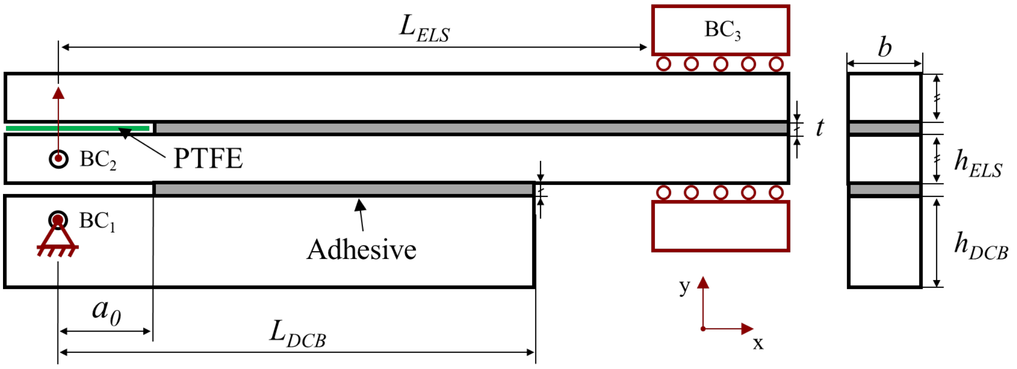

Figure 40: Scheme of the boundary conditions of a combined test specimen.

As aforementioned, the mode I test is performed in one step and, sequentially, on another step, the mode II test is also executed, implying that the boundary conditions presented in the Figure above are not all activated for the same step. In the first step, the three boundary conditions presented in Figure 40 are activated, BC_1 is related to the fixture that prevents the movement both in y and x direction, BC_2 applies the displacement to the bottom substrate of the ELS, which, for this matter is understood as the upper substrate of the DCB test. BC_3, designed to avoid movement in the y direction of the ELS specimen, is also activated in this step to avoid rotation of the whole set, which includes both the ELS and combined test specimen. In the second step, the bottom substrate and adhesive layer are eliminated from the numerical simulation. Both BC_2 and BC_3 are kept activated, meaning that the isolated ELS test can be performed. Consequently, BC_1 is deactivated, and, between the two steps, when the mode I test is fully performed, the interactions between the lower DCB substrate, including the adjacent adhesive layer, are eliminated. The ELS test is left to be performed isolated. Figure 41 shows the above mentioned boundary conditions being applied to the numerical model.

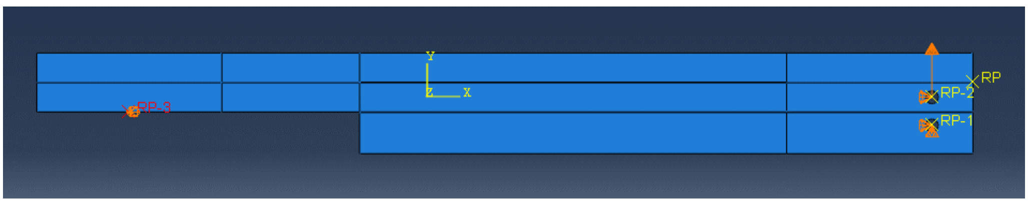

Figure 41: Boundary conditions of a combined test specimen on the numerical model.

Contact

On both ELS specimens, either the one concerning the isolated test and the one that is a part of the combined test, it is fundamental to avert interpenetration of elements in the unbounded region, between one end of the specimen and beginning of the adhesive layer. Thus, a frictionless/hard contact, standard surface to surface contact interaction was specified between the lower and upper crack faces, also called *PTFE* (Teflon®) - as in experimental tests this material presents a similar purpose.

4.3 Finite element model

The selection and pondering of the element types used in the mesh will strongly influence the result's accuracy, meaning their selection is critical in order to obtain a better model definition.

Partition

In addition to the selection of elements, attention must also be paid to the partitioning of the model, which, if done incorrectly, can be responsible for constructing a heterogeneous and unstructured mesh and, consequently, distorted elements that present convergence issues.

Partitioning is a significant step, especially if the model has some specific geometrical features, such as sharp corners and round shapes. With partitioning, it is possible to divide the model into smaller and simpler parts, which enables to run a more consistent mesh that will provide more accurate results.

As this model has a relatively simple geometry in terms of discontinuities the partitioning is only required to separate the cohesive elements from the remaining elements, dividing the model into smaller rectangular parts. However, since this work aims to perform a numerical optimisation of the specimen geometry, the partition comes as an essential component of this process. The goal is to have the partitioning be done automatically when changing the geometry on the sketch. Thus, a smooth and homogeneous mesh could be created for the model more quickly.

Mesh

Mesh creation is one of the most important steps to be made in a simulation and the computation of the mesh size plays a crucial role so that the mechanical events are replicated to the best accuracy possible. In this case, it is especially important to so as the target of this work is also to validate the model by comparing it to experimental results. Furthermore, the purpose of the ELS specimen test is to identify concentration of stresses and crack formation and propagation, which requires a properly refined mesh, so there's convergence of results.

The traditional Abaqus® shell element chosen for this project is a good example of the use of 2D elements being used to represent 3D spatial dimensionality, as explained before.

As suggested by the name, two-dimensional elements are represented geometrically in two dimensions and can be either triangular or quadrilateral. Triangular elements will be comprised of three corner nodes, while quadrilateral elements will contain four corner nodes, both of them presenting either a quadratic or a linear interpolation order. Although the element dimensionality is always planar, these elements can be used to represent either 2D or 3D space.

The Tri mesh (unstructured) is comparatively easier to generate because of its availability in the automated mesh generator. However, triangular finite elements are stiffer in bending problems because they have constant strain across the element. This makes them unsuitable for this kind of test, as Abaqus® would not be calculating the bending response correctly, which is one of the main mechanisms of the ELS test.

The quadrilateral elements usually perform better and deliver more accurate results closer to reality. Despite that, there is a possibility of the shear-locking phenomenon in this kind of element. This reason asks for more attention when analysing results to understand if they make sense for the physical problem.

A balance between performance and computational power demands must be considered to make a conscious decision about which element to use. Concerning the crack propagation simulation, cohesive elements would be used, the computational power requirements could be increased significantly, and convergence problems may appear. Even bearing that, a linear quadratic element with reduced integration was selected after realising the simulation was run within an appropriate amount of time. To avoid the emergence of the shear-locking effect, which can happen when the linear elements do not accurately model the curvature present in the actual material under bending and a shear force is applied, the reduced integration set was used.

This said, the element types chosen for the steel substrates were 4-node bilinear plane strain elements (CPE4R) with reduced integration, and 4-node two-dimensional cohesive elements (COH2D4) for the adhesive layers.

All meshes were set as structured except for the loading hole partitions, which remained free. The mesh used to simulate this specimen was generally composed of quadrilaterals of 0.5 mm by 0.5 mm side and biased meshing in the regions near the adhesive area going from 0.5 mm in the crack tip to 1mm by the clamping tool, all this in order to avoid convergence problems.

Cohesive damage model and cohesive elements

A cohesive mixed-mode damage model based on finite elements for interfaces was considered to simulate damage initiation and propagation. A constitutive relationship is established between the vectors of stresses (σ) and relative displacements (δ), as represented in Figure 9a. The method requires the local strengths (σ_{u_i}, $i = I, II$) and the critical strain energies release rates (G_{ic}) as input data parameters. Damage onset is predicted using a quadratic stress criterion.

$$\left(\frac{\sigma_I}{\sigma_{u_I}}\right)^2 + \left(\frac{\sigma_{II}}{\sigma_{u_I I}}\right)^2 = 1 \qquad if \quad \sigma_I \geq 0 \tag{29}$$

Where σ_{u_i}, $i = I, II$ represent the stresses in each mode. The crack propagation was simulated by a linear energetic criterion

$$\left(\frac{G_I}{G_{I_c}}\right) + \left(\frac{G_{II}}{G_{II_c}}\right) = 1 \tag{30}$$

The constitutive behaviour of the cohesive element can be divided into two phases, which are the initial damage phase and the evolution damage phase. In the initial damage phase, the cohesive element has an elastic behaviour, up to a stress value corresponding to a critical stress above which the crack forms/propagates. The evolution damage phase represents the propagation of the crack until the complete failure of the element, which allows the element to be eliminated as it is no longer able to absorb stresses. This criterion can also be understand an adaptation of the Power Law (PW) failure evolution where the power law coefficient used is equal to 1.

Abaqus® avails two stress based initiation criteria to chose from, the maximum nominal stress criteria (MAXS) and the quadratic nominal stress criteria (QUADS). The maximum nominal stress criteria takes into consideration the maximum stress direction and, therefore, does not make any relation between stresses from different directions. Whereas the quadratic nominal stress criteria is able to consider stresses from different directions, using quadratic ratios. Being that, it was decided to apply a quadratic nominal stress criteria (QUADS), once it is able to relate different stress directions.

Cohesive elements are often defined with null thickness, however, this model is adapted for the finite thickness case to guarantee that the elements would capture the elastic behaviour, prior to damage initiation.

To define the damage evolution associated to the cohesive material, it was possible to define its type as displacement or energy. While displacement damage evolution defines damage as a function of the total (for elastic materials in cohesive elements) or the plastic (for bulk elastic-plastic materials) displacement after damage initiation, the energy damage evolution defines damage in terms of the energy required for failure (fracture energy) after the initiation of damage. This type needs fracture energy as input which is commonly found in literature. For this reason, this type of formulation was chosen [11].

The following Figure 42 shows the resultant deformed ELS specimen after applying all the considerations aforestated. For the case of the combined specimen, the deformed shape is similar.

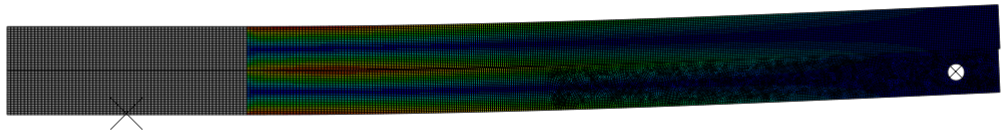

Figure 42: ELS numerical simulation, stress distribution.

4.4 Validation of the numerical model

As aforementioned, in order to perform the numerical optimisation of the concept of the end-loaded split specimen, a experimental setup was developed in order to being able to test both this type of specimens and also the combined test proposed.

Firstly, the comparison between the numerical model, performed for the brittle adhesive and experimental results will be compared, both following the same geometric features presented on Table 4, aiming to validate the ELS test model. In Figure 43 the load-displacement curves are presented, followed by the R-curves in Figure 44.

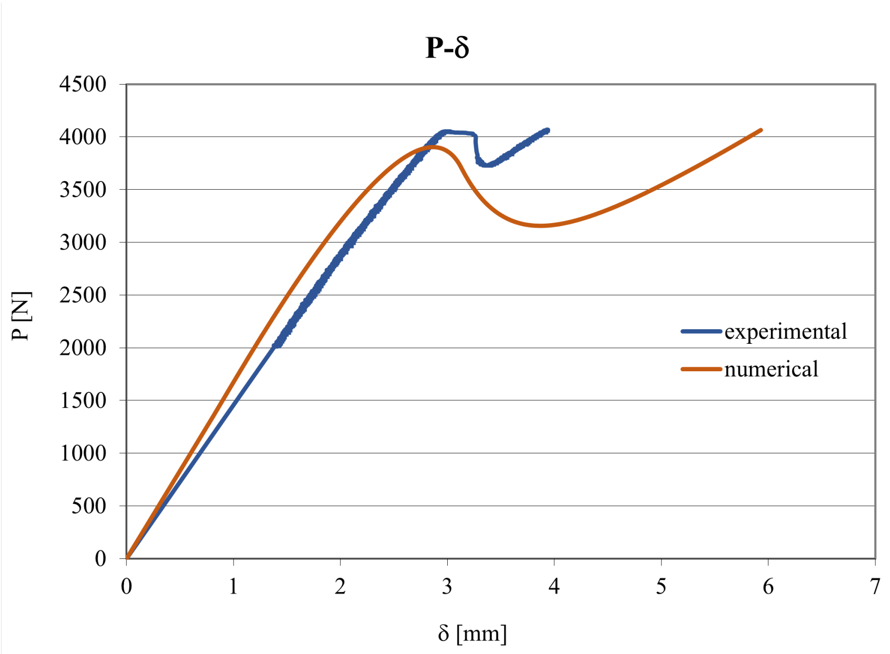

Figure 43: Numerical validation P-δ curve.

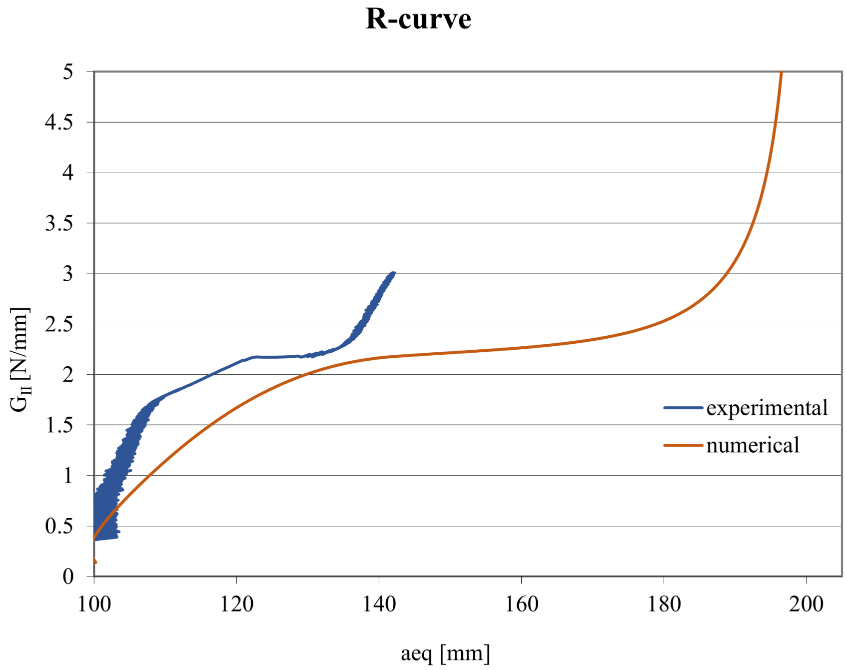

Figure 44: Numerical validation R-curve.

It is immediately found that the stiffness of the numerical simulation is higher as it is expected, and therefore displacements applied are different since, in the experimental test, this was enough for the crack to propagate fully and to compute the CBBM for G_{II_c} extraction. It was expected that the adhesive behaviour would be more brittle in the experimental test, which is also observable by the fact that the length of crack propagation through the adhesive layer was smaller than for the numerical simulation. In the numerical simulation, the test assumes perfect conditions, and the adhesive failure is smoother than in the experimental test. However, the displacement corresponding to the point where the crack starts to propagate, which is related to the peak of force, is similar for both numerical and experimental cases. The maximum load supported during the test is also quite similar.

Concerning the R-curve, the a_{eq} range for the experimental test is much shorter than for the numerical model, explained by the fact that the displacement of the experimental test is a lot shorter too and influences the compliance calculated and used to compute the CBBM. The noise observable on the experimental curves is related to the acquisition system of the machine used for performing the tests. However, both plateaus fall in the same place, providing a consistent G_{II_c} reference, leading to the validation of the numerical model for the end-loaded split test.

5 Summary of the appended papers

Paper A - Numerical optimisation of an unified specimen for adhesive characterisation

This paper presents a numerical optimisation of an end-loaded split joint, by computing specimen behaviour changes as function of the apparatus' and specimens' geometries and considering two adhesives of different nature. It also presents a combined specimen solution to characterise both mode I and mode II fracture energy release rate. This specimen geometry is also optimised by studying the influence of the different geometric parameters. Two adhesives for each of the designed specimen were tested and the most preponderant parameter, for both specimens was shown to be the mid span length. This length can be computed by changing other related parameters and its relevance is driven by the fact that this is the available length for the fracture process zone formation, significantly affecting the stability of both tests.

Paper B - Experimental study of an unified specimen for adhesive characterisation

The main aim of this paper is the experimental study of an unified specimen, designed for combined testing for characterisation of both mode I and mode II fracture energy release rate of adhesives. Since the ELS test is a preponderant part of the unified specimen, a new setup to meet the testing requirements of this kind of test was developed and validated. After that, making physical adjustments to the setup, the unified specimen was tested. It was determined that the mode I analysis's data reduction method was inaccurate because the ELS specimen introduces a different stiffness to the double cantilever beam's upper substrate. This test needs to be handled as an asymmetric double cantilever beam, which, currently, does not presented crack independent data reduction scheme, a parameter that was not monitored in the experimental work. For both tests, the ELS and combined test, the substrates of the ductile adhesive suffered plastic deformation.

6 Conclusion

6.1 Conclusions

In this work, it was possible to develop a numerical model that precisely reflected the experimental conditions of an end-loaded split test. Its geometry could be optimised by studying behaviour changes as a result of different combinations of relevant geometry parameters of this kind of specimen. By analysing the response of the various combinations on the initial crack size and total length of the specimen, a design approach that attempts to have the same mid span length finds that decreasing the total length of the specimen has a more significant impact on raising the stiffness. What must be avoided, though, is to select a smaller total length of the specimen. Once the fracture process zone is close to the clamping tool, its development is halted by significant compressive stresses. However, to have consistent fracture propagation, a minimal fracture process zone must be still be developed, and a minimal length is fundamental for that to occur. Using CBBM as data reduction scheme of the DCB related part of the unified specimen was found to have some limitations, both for the numerical and experimental work, since the behaviour is closer to that of an ADCB specimen. The data reduction scheme related to this last test enables separating the mode mixity into the contributions of mode I and mode II of the test. However, such approach is expected to bring additional complexities with regards to the crack length monitoring, since it must be precisely determined during the experimental test.

Experimentally, an apparatus for ELS testing was validated using only the brittle adhesive, since plastic deformation of the substrates was observed in the ductile adhesive test. During the unified specimen testing, it was possible to observe two phases, with two distinct behaviours corresponding to a DCB test and ELS test. Another issue arose with the ELS part of the unified specimen, where, since the substrate thickness was smaller for the brittle adhesive, the deflection imposed was significantly higher than for the isolated test (with thicker substrates). This more significant deflection not only introduced further instability to the test but also added stiffness to the specimen due to the bending force imposed, resulting in an overestimation of the G_{II_c}. For the case of the ductile adhesive, the specimen underwent plastic deformation when testing, again overestimating the fracture energy release rate in mode II for this adhesive.

The developed code allowed to process the raw data provided by the load cell, formulating the adequate reduction schemes for each test and enabling filtering features to treat the noise inherent to the displacement measurement techniques.

Finally, the three main tasks of this dissertation were mainly satisfied, providing meaningful insights about the end-loaded split test specimen design, whether from numerical or experimental points of view. Concerning the initial approach to an unified specimen for combined fracture characterisation of mode I and II, even with setbacks related to the coexistence of the three tasks and the available time window for the project, the potential of the concept was still successfully demonstrated, which will be modified to account for the aforementioned findings.

6.2 Future work

Although targeting the inclusion of a double cantilever beam in its structure, the combined test was found to be closer in behaviour to an asymmetric double cantilever beam, since the stiffness of each substrate is different. The adhesive layer of the ELS specimen plays an important role in the stiffness of the upper part of the DCB of the unified test, changing with the adhesive tested. The current data reduction scheme to treat this asymmetric double cantilever beam test (ADCB) is not crack independent and implies that the crack propagation must be measured during the experimental trial, which is very difficult and even not feasible in most cases. Future challenge concerns finding an easy way to include the contribution of the adhesive into the stiffness of the ELS specimen since, to compute the asymmetrical double cantilever beam theory, it is necessary to know the stiffness of the upper substrate. This stiffness could be considered by computing it directly from the initial slope of the ELS P-δ curve.

The plastic deformation verified in the substrates for the specimens manufactured with the ductile adhesive should be corrected by using heat treatable high strength steel substrates, with higher yield strength. The developed code could also be further developed to allow for direct extraction of the desired properties and, for the case of the combined test, being able to directly treat load-displacement curves and identify both modes of fracture, without needing to separate it in two parts. The code should also account for any future data reduction scheme modifications regarding the DCB/ADCB component of the test.

The testing apparatus should also be modified and improved to include strength tests such as the butt joint and modified TAST that make this concept whole. The vibrations generated due to sudden failure of the adhesive during the mode I portion of the test should also be solved with care. Sensitivity to these oscillations hinders the displacement measurement and, consequently, either non-contact based data extraction methods or damping systems should be provided to aid the accurate visualisation of the test behaviour.

References

[1] da Silva LFM, Öchsner A, and Adams RD. *Handbook of adhesion technology.* Springer, 2018.

[2] Petrie E. *Handbook of adhesives and sealants.* McGraw-Hill Education, 2007, 2007.

[3] Adams RD, Comyn J, and Wake WC. *Structural adhesive joints in engineering.* Springer Science & Business Media, 1997.

[4] Adams RD. *Adhesive bonding: science, technology and applications.* Elsevier, 2005.

[5] Lees WA. Adhesive selection. In *Adhesives in Engineering Design*, pages 92–123. Springer, 1984.

[6] Ebnesajjad S and Landrock AH. *Adhesives technology handbook.* William Andrew, 2014.

[7] Kinloch AJ. *Adhesion and adhesives: science and technology.* Springer Science & Business Media, 2012.

[8] Banea MD and da Silva LFM. Adhesively bonded joints in composite materials: an overview. *Proceedings of the Institution of Mechanical Engineers, Part L: Journal of Materials: Design and Applications*, 223(1):1–18, 2009.

[9] Chaves FJP, da Silva LFM, de Moura MFSF, Dillard DA, and Esteves VHC. Fracture mechanics tests in adhesively bonded joints: a literature review. *The Journal of Adhesion*, 90(12):955–992, 2014.

[10] Broek D. *Elementary engineering fracture mechanics.* Springer Science & Business Media, 2012.

[11] Toolabi M and Blackman BRK. Guidelines for selecting the dimensions of adhesively bonded en-loaded split joints: An approach based on numerical cohesive zone length. *Engineering Fracture Mechanics*, page November, June 2018.

[12] da Silva LFM, da Silva RAM, Chousal JAG, and Pinto AMG.

[13] Correia DS, Carbas RJC, Marques EAS, das Neves PJC, and da Silva LFM. Experimental study on aluminium to tungsten carbide/polycrystalline diamond (wc/pcd) adhesive bonding for milling tools. *International Journal of Adhesion and Adhesives*, 114:103121, 2022.

[14] Chaves FJP, da Silva LFM, de Moura MFSF, Dillard DA, and Esteves VHC. Fracture Mechanics Tests in Adhesively Bonded Joints: A Literature Review. *The Journal of Adhesion*, pages 1–39, June 2014.

[15] Moore DR, Pavan A, and Williams JG. *Fracture Mechanics Testing Methods for Polymers Adhesives and Composites*. ESIS Publication 28, 2006.

[16] Pérez-Galmés M, Renart J, Sarrado C, and Costa J. Suitable specimen dimensions for the determination of mode II fracture toughness of bonded joints by means of the ELS test. *Engineering Fracture Mechanics*, 202, July 2018.

[17] de Moura MFSF and de Morais AB. Equivalent crack based analyses of enf and els tests. *Engineering Fracture Mechanics*, 75(9):2584–2596, 2008.

[18] Wang H, Vu-Khanh T, and Le Van N. Effects of large deflection on mode ii fracture test of composite materials. *Journal of composite materials*, 29(6):833–849, 1995.

[19] Wang H and Vu-Khanh T. Use of end-loaded-split (els) test to study stable fracture behaviour of composites under mode ii loading. *Composite structures*, 36(1-2):71–79, 1996.

[20] Davies P, Blackman BRK, and Brunner AJ. Standard test methods for delamination resistance of composite materials: current status. *Applied composite materials*, 5(6):345–364, 1998.

[21] Blackman BRK, Brunner AJ, and Williams JG. Mode ii fracture testing of composites: a new look at an old problem. *Engineering fracture mechanics*, 73(16):2443–2455, 2006.

[22] de Morais AB and de Moura MFSF. Evaluation of initiation criteria used in interlaminar fracture tests. *Engineering fracture mechanics*, 73(16):2264–2276, 2006.

[23] Banea MD, da Silva LFM, and Campilho Raul DSG. Moulds design for adhesive bulk and joint specimens manufacturing. *Assembly Automation*, 2012.

[24] ASTM Standard. D3433-99: Standard test method for fracture strength in cleavage of adhesives in bonded metal joints, astm international, west conshohocken, pa, 2012.

[25] da Silva LFM and Öchsner A. *Modeling of adhesively bonded joints*. Springer, 2008.

[26] Saldanha DFS, Canto C, da Silva LFM, Carbas RJC, Chaves FJP, Nomura K, and Ueda T. Mechanical characterization of a high elongation and high toughness epoxy adhesive. *International journal of adhesion and adhesives*, 47:91–98, 2013.

[27] de Moura MFSF, Gonçalves JPM, Chousal JAG, and Campilho RDSG. Cohesive and continuum mixed-mode damage models applied to the simulation of the mechanical behaviour of bonded joints. *International Journal of adhesion and Adhesives*, 28(8):419–426, 2008.

[28] Wang Y and Williams JG. Corrections for mode ii fracture toughness specimens of composites materials. *Composites Science and Technology*, 43(3):251–256, 1992.

[29] Campilho RDSG and et al. Repair of composite and wood structures. 2009.

[30] Yoshihara H and Kawamura T. Mode i fracture toughness estimation of wood by dcb test. *Composites Part A: applied science and manufacturing*, 37(11):2105–2113, 2006.

[31] Chaves FJP. Fracture mechanics applied to the design of adhesively bonded joints. 2013.

[32] de Moura MFSF, Campilho RDSG, and Gonçalves JPM. Crack equivalent concept applied to the fracture characterization of bonded joints under pure mode i loading. *Composites Science and Technology*, 68(10-11):2224–2230, 2008.

[33] de Moura MFSF, Gonçalves JPM, and Magalhães AG. A straightforward method to obtain the cohesive laws of bonded joints under mode i loading. *International Journal of Adhesion and Adhesives*, 39:54–59, 2012.

[34] Costa M, Carbas RJC, Benedita M, Marques EAS, Viana G, da Silva LFM, Yokoi E, Nakada S, and Furusawa T. Static assessment of the mixed-mode behaviour of three epoxy adhesives. *Engineering Fracture Mechanics*, 182:552–565, 2017.

[35] Schafer RW. What is a savitzky-golay filter?[lecture notes]. *IEEE Signal processing magazine*, 28(4):111–117, 2011.

Appendices

A Paper A

Numerical optimisation of an unified specimen for adhesive characterisation

I.D. Costa[1], D.S. Correia[1], R.J.C. Carbas[1], E.A.S. Marques[1], L.F.M. da Silva[2]

1 Instituto de Ciência e Inovação em Engenharia Mecânica e Engenharia Industrial (INEGI), Porto, Portugal
2 Departamento de Engenharia Mecânica, Faculdade de Engenharia (FEUP), Universidade do Porto, Porto, Portugal

Abstract

Adhesives are increasingly being employed in industrial applications as a replacement for traditional mechanical joining methods, as they enable improvements in the strength to weight ratio and lower the cost of the overall structures.
This has led to a need for adhesive mechanical characterisation techniques that can provide the data needed to build advanced numerical models that can help structural designers in adhesive selection process and grant precise optimisation of bonded connection performance. Therefore, the need for simulation of the behaviour of an adhesive, whether in daily use or extreme loadings, involves numerous different standards and results in a complex network of various specimens and data reduction methods that concern techniques which are exceedingly time-consuming and expensive.
This work intends to address this problem by proposing the development of a novel fully integrated experimental characterisation tool for adhesives that can significantly reduce the time required to characterise them. The project's main focus is the numerical optimisation of the concept that computes behaviour changes as a function of the apparatus' and specimens' geometries and addresses different adhesives with a different range of applications. After studying the optimised configuration and ideal testing conditions, a prototype for combined tests setup was fitted to an existing commercial testing machine to obtain experimental validation of the concept. This combined numerical and experimental study of a unified apparatus for adhesive characterisation will be used to reduce the amount of experimental testing required, lower costs, and enable the direct generation of cohesive zone laws.

A.1 Introduction

In many industries, including those in operating in the automotive, aerospace, and aviation sectors, adhesive bonding technology is becoming a more appealing substitute for traditional mechanical joining methods. Adhesively bonded joints offer a number of significant advantages over common bonding techniques like bolting and riveting, such as a more uniform stress distribution along the bonded area which avoids stress concentrations and improves load transmission and fatigue resistance. Other important benefits include this technology's capacity to easily bond dissimilar materials together and the increased flexibility it gives the joint design [1]. As a result of these advantages, structural weight and cost reductions can be obtained with the use of well-designed bonded joints.

The growth in the use of adhesives, especially those of the structural nature, has led to a need for fast and effective adhesive mechanical characterisation techniques that can provide the data needed to help structural designers in the adhesive selection process and grant precise optimisation of bonded connection performance. Characterising the mechanical properties and knowing the limitations of each adhesive provides crucial insights for ensuring quality control, enhancing bond performance, facilitating the usually challenging adhesive selection process. [1] Currently, multiple different tests must be performed to obtain a set of the most relevant mechanical properties for joint design, such as tensile tests and shear tests (for strength and stiffness) and fracture tests in both mode I and mode II (to determine the toughness of the adhesive).

Concerning the measurement of tensile properties, bulk tensile tests and butt joints are commonly used in this sense. The ASTM D 897 and ASTM D 2095 standards describe directives related to the practical aspects and methodology of preparing and testing to perform this type of test, the first one uses short circular specimens made of metal or wood, and the second is more general and includes round and square geometries [2].

For shear properties, the thick adherend shear test (TAST) appears as a common choice, since it relies on an easy-to-make specimen and a simple testing setup. It also emerges as a great substitute for the convention single lap shear (SLS) joint, which demonstrated problems related to complex states of stress and, therefore, makes them not suitable for characterisation of the strength properties of adhesives. TAST tests can be performed using two different standards, ASTM D3983 and ISO 11003-2, where the main difference is in the size of the specimen. However, difficulties concerning the stress concentrations generated due to edge effects have been reported which directly influence the acquisition of reliable data. In order to acquire accurate experimental results, a modified TAST fixture [3] was created, but it is still not standardised. It provides a more uniform adhesive stress condition in the adhesive joint and severely restricts edge effects [2].

The most popular test specimens for determining the critical strain energy release rate in mode I (the tensile opening mode), that is, G_{I_c}, are the double cantilever beam (DCB) and the tapered double cantilever beam (TDCB) adhesive joint test specimens. In contrast to the more complicated and expensive specimens used in TDCB testing, the DCB test uses simpler, less expensive specimens. Even while the TDCB has the advantage of showing a linear change in compliance with crack length, this only makes them effective in situations where it is not practical or desirable to measure crack lengths while carrying out the test. However, when conducting these tests, it is often better to use specimens that are simple to make, as a result, DCB tests are used more commonly. Furthermore, crack independent data reduction schemes have been developed for DCB tests, which further simplifies the use of this configuration [4]. Both these tests have been studied since the 1960's and the work of different authors has led to the publication of an ASTM D3433 standard. More recently, due to the increased popularity of fiber-reinforced polymer matrix composites, a new international standard has been published, named ISO 25217 [2].

On the other hand, although being successfully modified for adhesive joints, only composites are currently eligible for standardised tests for pure mode II fracture toughness (G_{II_c}) characterisation during end-notched flexure (ENF) testing. The most common mode II tests do, however, still have certain limitations. The end-loaded split (ELS) is also proposed for the determination of mode II fracture toughness [5, 6].

Under shear loads, adhesively bonded joints have been reported to have a large fracture process zone (FPZ) compared to mode I or mixed-mode fracture tests and compared to other specimen dimensions, owing to the adhesive layer's plasticity. The large FPZ involved, along with the lack of crack opening, makes visual evaluation of the fracture length difficult. To address this, approaches based on J-integral [7] or an effective crack length (a_{eq}) that are not crack dependent have been developed [4,8–13]. On the other hand, the commonly used end-notched flexure (ENF) test has instability problems, so other tests have been developed, including the Tapered ENF (TENF) test, the Stabilized ENF (SENF) test, the Over-Notched flexure (ONF), the Four-Point ENF (4ENF), or the Inverse ELS test, among others, to achieve stable propagation. However, other issues arise from these tests, such as challenges with the production of the specimens (TENF), the complexity of the test setup (SENF), or friction-related issues (4ENF and ONF). The end-loaded split tests, in addition to have simpler manufactured specimens, based on DCB specimens, have shown encouraging results in recent studies, such as the advantage of having stable crack propagation under displacement control if the ratio between the initial crack and the span length is higher than 0.55, in composite joints [10, 14–17].

Recent research have shown that certain criteria must be met in order to obtain crack propagation during ELS test. First, to ensure the formation of the entire

FPZ by reaching steady-state crack propagation and, as a result, the resistance curve plateau; second, to ensure the test's stability under displacement control; third, to avoid significant deflections; and fourth, to avoid adherend failure during testing. The span length, initial crack length, and, if necessary, specimen total thickness of the ELS specimen geometry must be changed in order to satisfy these requirements [18, 19].

This study proposes a numerical optimisation of the ELS specimen geometry, for adhesive characterisation, computing behaviour changes as a function of the specimen's geometry while also addressing adhesives of distinct nature, with a different range of applications. A new unified specimen for a combined test for mode I and mode II fracture characterisation is then proposed based on these findings, including a study on its key geometrical parameters.

A.2 Numerical details

In the scope of this study, two different specimens geometry will be numerically optimised, starting from an end-loaded split test and moving to a combined test that intends to be used for mode I and mode II energy release rate extraction, merging a double cantilever beam with an end-loaded split joint, that are sequentially tested. In this chapter, the numerical model used for both tests will be described, starting by establishing some considerations about the ELS test and moving to the combined test, which is considered an extension of this test, combined with a DCB.

A.2.1 Materials, geometry and general statements

As mentioned before, two different numerical models were developed, one related to the ELS test and the other one related to the combined test. The geometry of the specimens, the substrates and the adhesives used on the simulations, as well as the formulation of both models are the same as the ones used on the experimental work used for validation of the numerical model and described in the latter sections of this work.

Two different adhesives were used in order to represent different ranges of adhesive's application and to understand the geometric implications in the overall specimen behaviour when each test is performed.

The first one, a brittle adhesive, is a two-component, room temperature curing paste adhesive of high strength. According to its datasheet, when fully cured, the adhesive will have excellent performance at high temperatures and good chemical resistance. It is popular in many industrial applications where the resistance to severe or warm environments is required. It is appropriate for bonding a wide range of metals, ceramics, glass, rubbers, rigid plastics, and other materials. Its strength properties were obtained by da Silva et al. [20], and as for the fracture toughness in mode I and mode II the attained value was established by Costa et al. (see appendix B).

The other adhesive, a ductile one, that has been fully characterised by Correia et al. [21], on the other hand, is a one-part, heat-cured epoxy resin that is compatible with induction curing and can be used in place of brazing, welding, and riveting in high stress applications. Its key unique feature is improved electrical conductivity and ductility, which is a result of an aluminium filler the manufacturer added to the adhesive composition.

The properties of each adhesive studied are listed in Table 1:

Table 1: Mechanical properties of the adhesives.

	Brittle adhesive	**Ductile adhesive**
E $[MPa]$	4890	3880
σ_f $[MPa]$	41.00	65.60
G [MPa]	1560	1447
τ_f $[MPa]$	30.20	41.60
G_{I_c} $[N/mm]$	0.35	1.27
G_{II_c} $[N/mm]$	2.40	7.22

DIN 40CrMnMo7, an high strength steel, was used to machine the substrates and will then be used on the numerical simulations. Avoiding plastic deformation during tests is the purpose of employing high strength steel. Table 2 displays the general characteristics of the substrates.

Table 2: Mechanical properties of the substrates used.

Young's modulus	190-210 GPa
Ultimate tensile strength	965-1030 MPa
Yield strength	827-862 MPa
Poisson's ratio	0.27-0.3

Considering both the steel and the adhesives as isotropic materials, a two-dimensional model was used for the finite element analysis of each test. In fact, shell elements were used to discretise bodies by defining the geometry at a reference surface (2D) and the thickness is defined through the section property definition. Shell elements are used to model structures in which one dimension, the thickness, or, in this case, the width of the specimen, is significantly smaller than the other dimensions, which is the case.

On Figure 1 is presented a scheme with the relevant geometric parameters used to design the end-loaded split specimen,

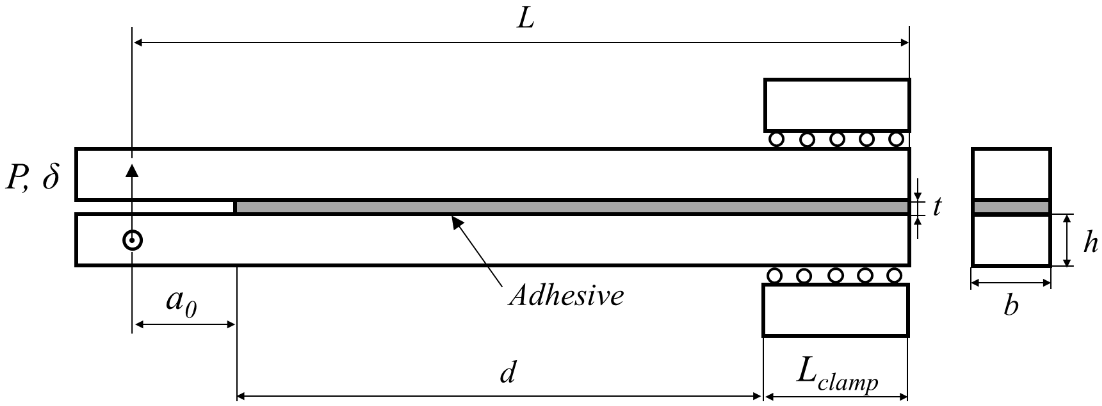

Figure 1: ELS specimen. Dimensions in mm.

where L is the length of the specimen, L_{clamp} is the specimen's length that it is clamped,d is the mid span length of the specimen, a_0 is the initial crack tip, t is the thickness of the adhesive layer, r is the radius of the hole where the load pin will fit, h is the height of the substrate and b is the width of the specimen .

In the following Table 3, the geometric properties of the ELS specimen modelled are presented, also taking into to account the specimens used on the experimental work. This will be the specimen used for numerical validation of the model and then a target for numerical optimisation of its own geometry.

Table 3: Geometric properties of the ELS specimen. Dimensions in mm.

L	L_{clamp}	d	a_0	h	r	t
290	70	260	100	12.7	2.5	0.2

Concerning the combined test, in Figure 2 is presented a scheme of the geometry of the specimen and relevant variables that will be a target of study.

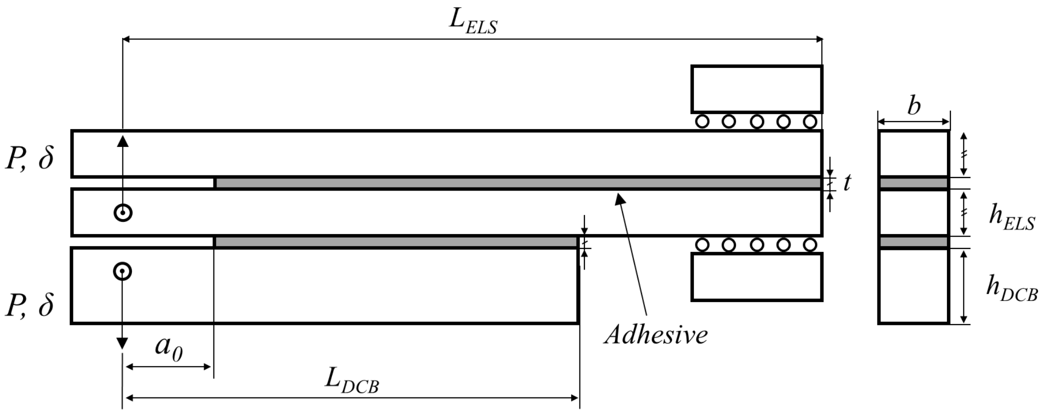

Figure 2: Combined specimen. Dimensions in mm.

where, in this case, a distinction is made between the length of the ELS specimen, L_{ELS} and the length of the lower substrate of the DCB test, L_{DCB}. The same consideration is made to discriminate the height of each of the ELS substrates and the lower substrate of the combined test, h_{ELS} and h_{DCB} correspondingly.The other three variables, a_0, b and t are logically related to the initial crack tip, the width of the specimen and the thickness of both adhesive layers as mentioned for the isolated ELS specimen geometry. The adopted geometry for the combined test specimen is describe in Table 4.

Table 4: Geometric properties of the combined specimen. Dimensions in mm.

L_{ELS}	L_{DCB}	a_0	h_{ELS}	h_{DCB}	t
290	180	45	9	12.7	0.2

As mentioned before, the new procedure was numerically validated using a two-dimensional finite element analysis but including a cohesive damage model, which allows the simulation of crack initiation and growth. This model is based on fracture mechanics and damage theory and allows for an adequate prediction of the onset damage evolution and crack propagation. This method consists of introducing a cohesion law in finite element modeling, which will be mentioned when the damage model is presented.

A.2.2 Development of the model

Boundary conditions

Computing correctly the boundary conditions of the model means being closer to a reasonable approach to a real problem, in this case, to the real testing conditions of these two specimens. Concerning the end-loaded split test, as exemplified in Figure

1, it is recognised that there will be an imposed displacement through a pin, and the region related to the clamping tool will have only one degree of freedom on the horizontal direction. These boundary conditions are represented in Figure 3.

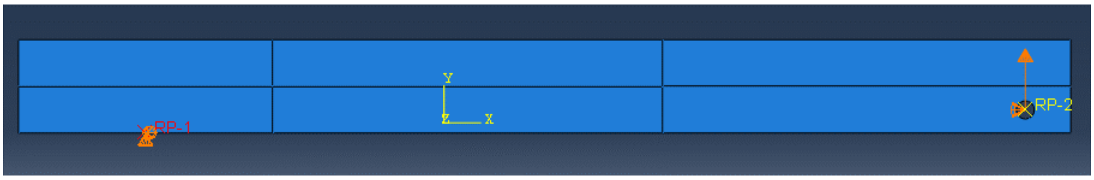

Figure 3: Boundary conditions of an ELS specimen.

In the case of the combined test, the boundary conditions applied are more complex and since the mode I and mode II tests are sequentially performed, the boundary conditions are also successively applied in different load steps. In Figure 4 it is possible to observe the boundary conditions involved in this combined test.

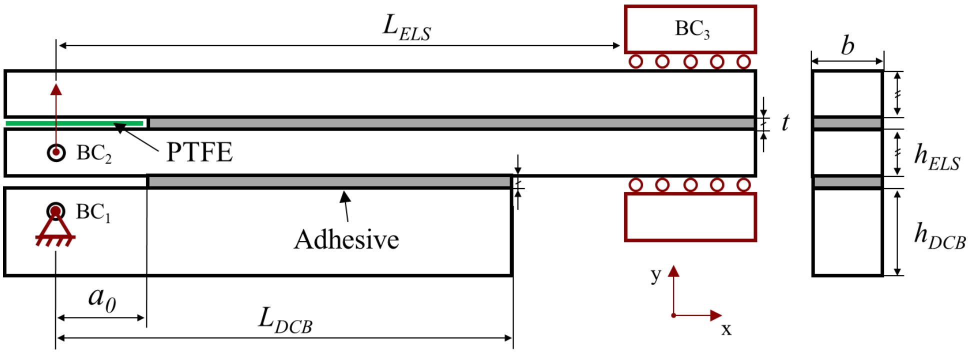

Figure 4: Scheme of the boundary conditions of a combined test specimen. Dimensions in mm.

As aforementioned, the mode I test is performed in one step and, sequentially, on another step, the mode II test is also executed, implying that the boundary conditions presented in the figure above are not all activated for the same step, as detailed in Table 5. In the first step, the three boundary conditions presented in Figure 4 are activated, BC_1 is related to the fixture that prevents the movement both in y and x direction, BC_2 applies the displacement, u_y, to the bottom substrate of the ELS, which, for this matter is understood as part of the upper substrate of the DCB test. BC_3, designed to block movement in the y direction of the ELS specimen, is also activated in this step to avoid rotation of the whole set, which includes both the ELS and combined DCB test specimen. In the second step, the bottom substrate and adhesive layer are eliminated from the numerical simulation. Both BC_2 and BC_3 are kept activated, meaning that the isolated ELS test can be performed. Consequently, BC_1 is deactivated, and, between the two steps, when the mode I test is fully performed, the interactions between the lower DCB substrate, including the adjacent adhesive layer, are eliminated. The ELS test is then left to be performed in an isolated manner.

Table 5: Boundary conditions used in the numerical study.

Boundary conditions	**Mode I step**	**Mode II step**
BC_1	{ 0 , 0 , - }	Deactivated
BC_2	{ 0 , $u_{y,I}$, - }	{ 0 , $u_{y,II}$, - }
BC_3	{ - , - , 0 }	{ - , 0 , 0 }
Interactions	**Mode I step**	**Mode II step**
$PTFE$	Surf. to surf. contact	Surf. to surf. contac

Figure 5 shows the above mentioned boundary conditions being applied to the numerical model.

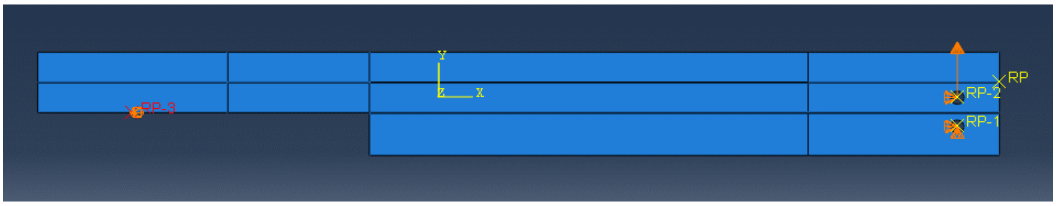

Figure 5: Boundary conditions of a combined test specimen on the numerical model.

Contact

On both ELS specimens, either the one concerning to the isolated test and the one that is a part of the combined test, there is the risk of interpenetration of elements in the unbounded region, between one end of the specimen and beginning of the adhesive layer. To avoid this, a frictionless/hard contact, standard surface to surface contact interaction was specified between the lower and upper crack faces, also called $PTFE$ (Teflon®) - as in experimental tests the use of this material presents a similar purpose.

A.2.3 Finite element model

The selection and pondering of the element types used in the mesh will strongly influence the result's accuracy, meaning their selection must be thought about and studied to lead to a better model definition. A geometrically non-linear analysis considering auto adjustable small increment values was performed to obtain smooth crack propagation, considering a maximum increment of 0.5% of the applied displacement. Non-linear geometry was also taken into consideration in the cohesive element formulation.

Partition

In complex simulation the definition of small partitions of the model is commonly done dividing it into smaller rectangular areas, to whom each element type and size could be attributed, thus that a smooth and homogeneous mesh could be created for the model. Such areas can be seen in Figure 5.

Mesh

Concerning the mesh elements, since this was a 2D simulation, the elements considered for the steel substrates were 4-node bilinear plane strain elements (CPE4R) with reduced integration was selected after realising the simulation was run within an appropriate amount of time. To avoid the emergence of the shear-locking effect, which can happen when the linear elements do not accurately model the curvature present in the actual material under bending and a shear force is applied, the reduced integration set was used.

Additionally, taking into account the fact that cohesive zone models were used to simulate the adhesive, 4-node two-dimensional cohesive elements (COH2D4) were used.

All meshes were set as structured except for the loading hole, which remained free. The mesh used to simulate this specimen was generally composed of quadrilaterals of 0.5 mm by 0.5 mm side and biased meshing in the regions near the adhesive area going from 0.5 mm in the crack tip to 1mm by the clamping tool, all this in order to avoid convergence problems.

Cohesive damage model and cohesive elements

A cohesive mixed-mode damage model based on finite elements for interfaces was considered to simulate damage initiation and propagation. A constitutive relationship is established between the vectors of stresses (σ) and relative displacements (δ), as represented in Figure 6.

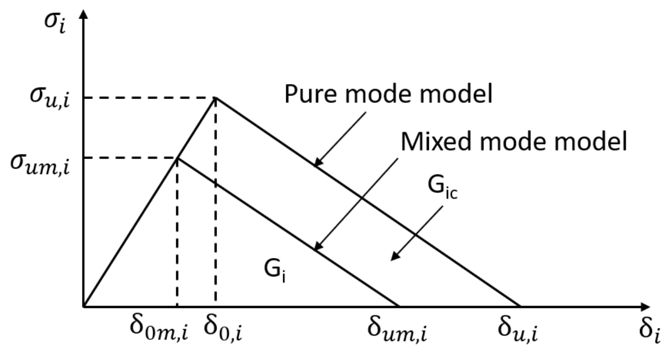

Figure 6: Triangular traction-separation law.

The method requires the local strengths (σ_{u_i}, $i = I, II$) and the critical strain energies release rates (G_{ic}) as input data parameters. Damage onset is predicted using a quadratic stress criterion:

$$\left(\frac{\sigma_I}{\sigma_{u_I}}\right)^2 + \left(\frac{\sigma_{II}}{\sigma_{u_I I}}\right)^2 = 1 \qquad if \sigma_I \geq 0 \tag{1}$$

Where σ_{u_i}, $i = I, II$ represent the stresses in each mode. The crack propagation was simulated by a linear energetic criterion,

$$\left(\frac{G_I}{G_{I_c}}\right) + \left(\frac{G_{II}}{G_{II_c}}\right) = 1 \tag{2}$$

This criterion can also be understand an adaptation of the Power Law (PW) failure evolution where the power law coefficient used is equal to 1. Essentially, it is assumed that the area under the small triangle in Figure 6 represents the energy released in each mode, which is compared with the respective critical fracture energy represented by the larger triangle. The indices o and u refer to the onset and ultimate relative displacement, respectively, and the subscript m stands for the mixed-mode case.

The constitutive behaviour of the cohesive element can be divided into two phases. The initial damage phase and the evolution damage phase. In the initial damage phase, the cohesive element has an elastic behaviour, up to a stress value corresponding to a critical stress above which the crack forms/propagates. The evolution damage phase represents the propagation of the crack until the complete failure of the element, which allows the element to be eliminated as it is no longer able to absorb stresses.

Abaqus avails two stress based initiation criteria to chose from, the maximum nominal stress criteria (MAXS) and the quadratic nominal stress criteria (QUADS). The maximum nominal stress criteria takes into consideration the maximum stress direction and, therefore, does not make any relation between stresses from different directions. Whereas the quadratic nominal stress criteria is able to consider stresses from different directions, using quadratic ratios. Being that, it was decided to apply a quadratic nominal stress criteria (QUADS), once it is able to relate different stress directions.

Cohesive elements are often defined with null thickness, however, this model is adapted for the finite thickness case to guarantee that the elements would capture the elastic behaviour, prior to damage initiation.

To define the damage evolution associated to the cohesive material, it was possible to define its type as displacement or energy. While displacement damage evolution defines damage as a function of the total (for elastic materials in cohesive elements) or the plastic (for bulk elastic-plastic materials) displacement after damage initiation, the energy damage evolution defines damage in terms of the energy required for failure (fracture energy) after the initiation of damage. This type needs fracture energy as input which is commonly found in literature. For this reason, this type was choosen [22].

The following Figure 7 shows the resultant deformed ELS specimen after applying all the considerations aforestated. For the case of the combined specimen, the deformed shape is similar.

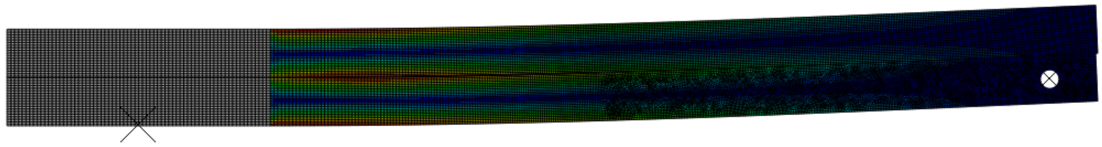

Figure 7: Numerical simulation of an ELS test.

A.2.4 Validation of the numerical model

As aforementioned, in order to perform the numerical optimisation of the concept of the end-loaded split specimen, an experimental setup was developed in order to being able to test both this type of specimens and also the combined test proposed.

Firstly, the comparison between the numerical model, performed for the brittle adhesive and experimental results will be compared, both following the same geometric features presented on Table 3, aiming to validate the ELS test model. In Figure 8 the load-displacement curves are presented, followed by the R-curves in Figure 9.

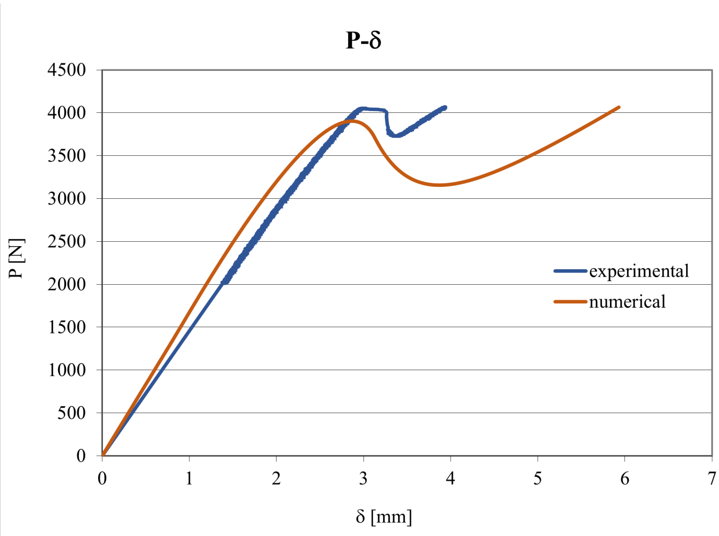

Figure 8: P-δ curve for numerical validation of the ELS model.

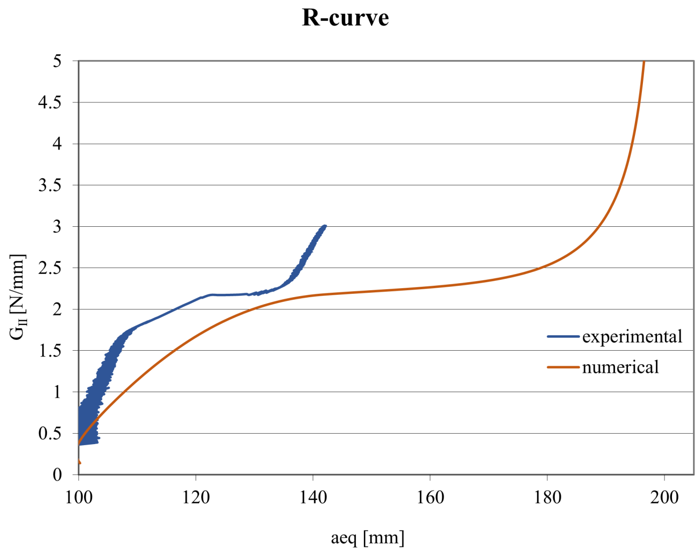

Figure 9: R-curve for numerical validation of the ELS model.

It is immediately found that the stiffness of the numerical simulation is higher as it is expected, and therefore displacements applied are different since, in the experimental test, this displacement was enough for the crack to propagate fully and to compute the CBBM for G_{II_c} extraction. It was expected that the adhesive behaviour would be more brittle in the experimental test, which is also observable by the fact that the length of crack propagation through the adhesive layer was smaller than for the numerical simulation. In the numerical simulation, the test assumes perfect conditions, and the adhesive failure is smoother than in the experimental test. However, the displacement corresponding to the point where the crack starts to propagate, which is related to the peak of force, is similar for both numerical and experimental cases. The maximum load supported during the test is also similar.

Concerning the R-curve, the a_{eq} range for the experimental test is much shorter than for the numerical model, explained by the fact that the displacement of the experimental test is a lot shorter too and influences the compliance calculated and used to compute the CBBM. The noise observable on the experimental curves is related to the acquisition system of the machine used for performing the tests. However, both plateaus fall in the same place, providing a consistent G_{II_c} reference, leading to the validation of the numerical model for the end-loaded split test.

A.3 Numerical results and discussion

A parametric research on how the changes in the specimen's geometry affect the specimen performance and the extracted data was firstly done. Some relevant dimensions for the end-loaded split and unified specimen were studied in order to compute behaviour changes of this test, whether by analysing the load - displacement curves (P - δ curves) or the resultant R-curves, computed using the compliance based beam method (CBBM) for each test. The DCB test was treated as in [4] and the ELS as in [9].

A.3.1 End-loaded split test specimen

The dimensions considered for the study regarding the ELS were the initial crack tip size a_0, the total length of the specimen, L, and the substrates' thickness, h. Besides that, a study about the development of the fracture process zone in this type of specimens was carried on. Some other considerations about other parameters directly related to this main parameters were made.

In order to be able to approve this work for a different range of adhesive applications, two different adhesives were considered. Firstly the study mentioned above was carried on for a more brittle adhesive, and then the same approach was applied to a more ductile adhesive, employing cohesive zone laws based on the mechanical properties mentioned on subsection A.2.1.

End-loaded split test design - brittle adhesive

Firstly, a study about the influence of changing the initial crack tip size was carried on for the model presented in subsection A.2.1. Using L =290 mm and setting the clamped part length of the specimen as 70 mm the obtained Load-displacement curve is shown in Figure 10.

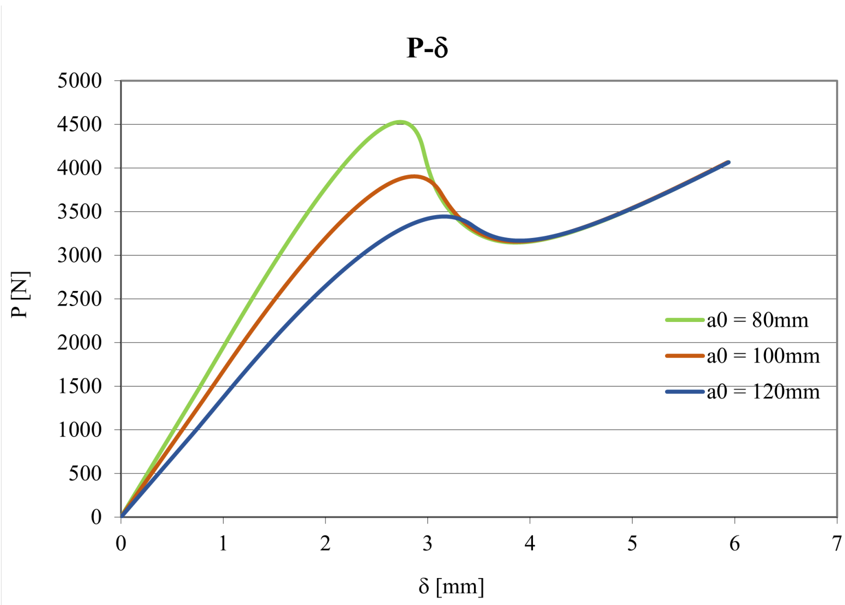

Figure 10: P-δ curve related to a_0 study for a brittle adhesive.

The corresponding G_{II_c}, computed using the CBBM, is presented in Figure 11.

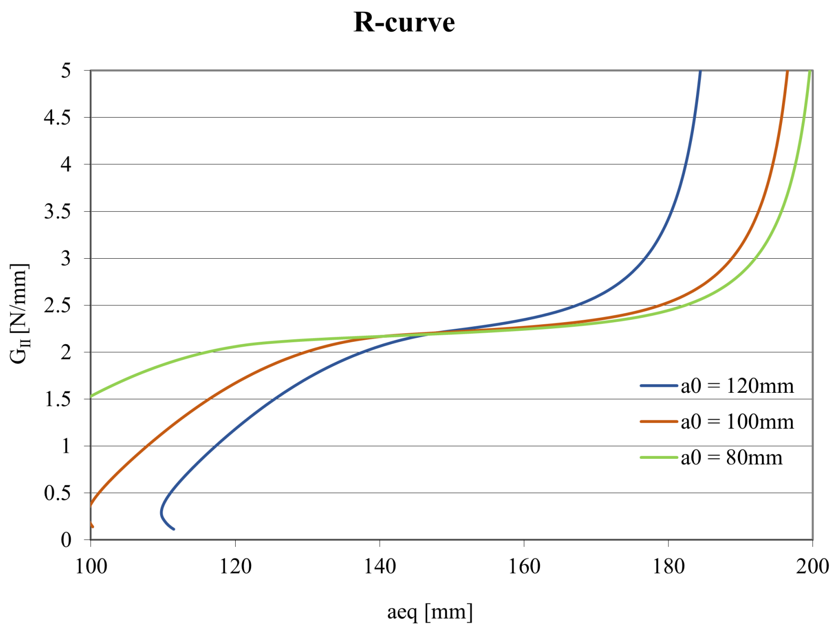

Figure 11: R-curve related to a_0 study for a brittle adhesive.

It is possible to understand that, by decreasing a_0, a more pronounced plateau is obtained, providing a more useful and direct upper limit for mode II fracture energy release rate to be extracted. However, when decreasing the initial crack tip for the same specimen's length and clamping conditions, the failure process, given by the combination of a steeper slope and smaller displacement between the highest and lowest peak of the P-δ curve after reaching its maximum, is more brittle. This might represent problems of stable crack propagation when this study is carried out experimentally. Depending on the data acquisition systems, it could be challenging to gather enough points to compute a reliable R-curves when sudden failures occur. In order to provide a geometric guide for designing these specimens, stability criteria that relates the ratio between the initial crack tip and the total length of the specimen have been developed for composite materials.

On the other hand, it is feasible to conclude that, by increasing the initial crack tip size, the specimen's stiffness is influenced, decreasing its value, since the crack tip introduces a weakness in the specimen. Bearing that, increasing a_0 means diminishing the total stiffness of the specimen.

Taking into account the aforementioned considerations, for the following study of the influence of changing the total length of the ELS specimen, a middle value of $a_0 = 100\,\text{mm}$ was chosen.

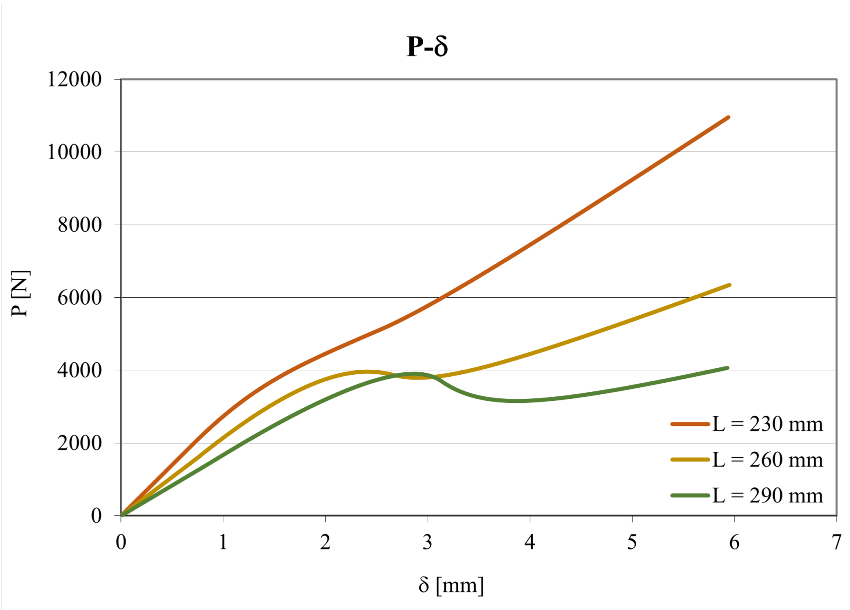

Figure 12: P-δ curve related to L study for a brittle adhesive.

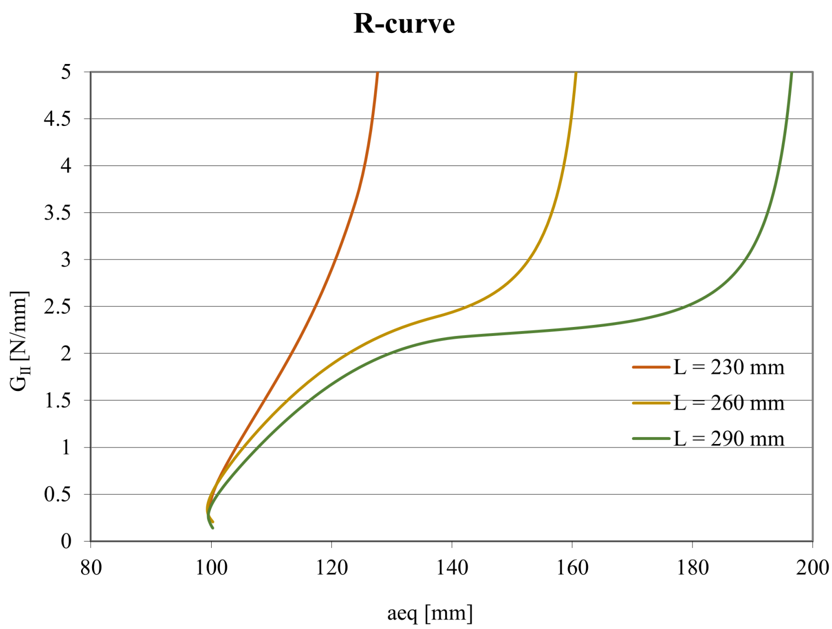

Figure 13: R-curve related to L study for a brittle adhesive.

From Figures 12 and 13 it is recognisable the influence of 30 mm decrements, considering $L = 290$ mm as reference, in the load-displacement curves and consequently, on the R-curve obtained.

Taking as example a double cantilever beam loaded with P on the free end, the displacement is given by

$$\delta = \frac{PL^3}{3EI} \tag{3}$$

where E is the Young's modulus of the beam's material and I the second moment of inertia. The stiffness of the beam is then given by

$$K = \frac{P}{\delta} \Leftrightarrow K = \frac{3EI}{L^3} \tag{4}$$

Being the overall stiffness of the beam influenced by the power of 3 of its total length, by decreasing L, there is a substantial decrease in K. Not only there is less space for the crack to fully propagate, but the beam itself becomes too stiff, making it impossible to attain a stable propagation, controlling the displacement.

Given that, a general conclusion is that the larger the total length of the specimen, the better stable propagation conditions arise. However, this might not be feasible in many practical cases since it means that exceedingly large specimens might need to be manufactured, causing possible constraints with not only the manufacturing process but also with the preparation of adequate testing setups and load cell capacity.

Figure 14 and 15 present a study of the substrate's thickness influence in both the load-displacement curves and R-curves, respectively.

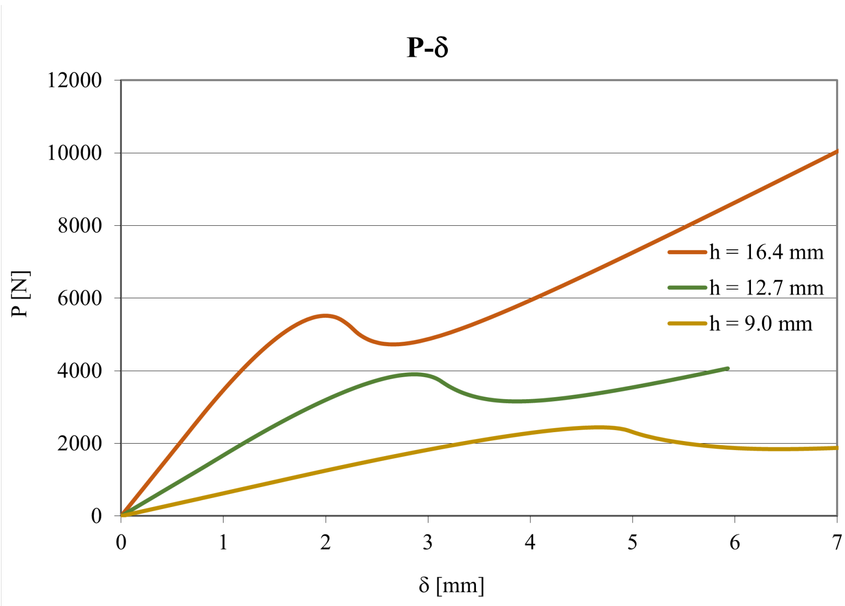

Figure 14: P-δ curve related to h study for a brittle adhesive.

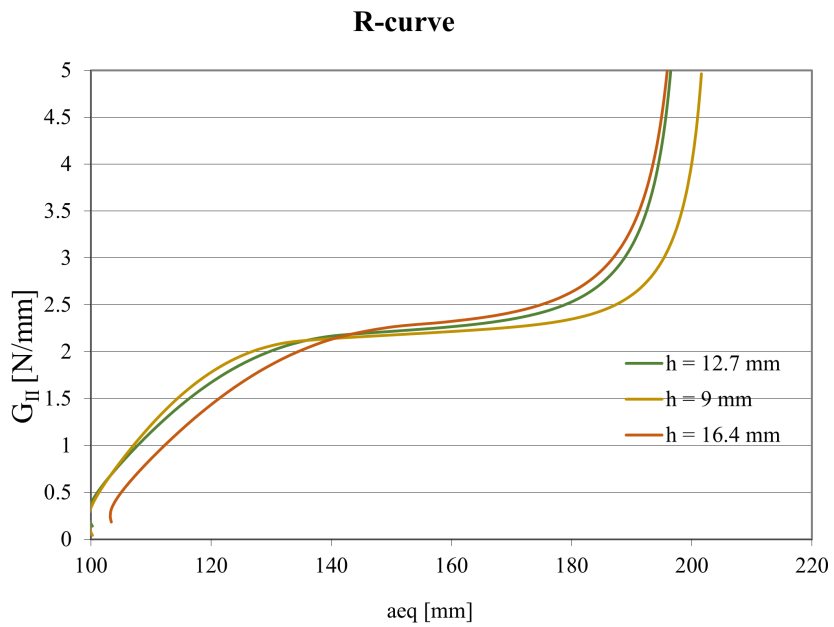

Figure 15: R-curve related to a_0 study for a brittle adhesive.

Similarly to what was observed during the analysis of the total length of the specimen, there is a direct relation between the increase of the substrate thickness and the increase of the stiffness of the specimen, which is also explained using the cantilever beam example. In this case, h directly influences the second moment of inertia, considering the rectangular shape of the cross section area of the specimens, as it follows,

$$I = \frac{bh^3}{12} \tag{5}$$

which, in terms of stiffness, K, reflects like:

$$K = \frac{3Ebh^3}{12PL^3} \tag{6}$$

Having a weight of power 3 on the stiffness of the substrate, the substrate thickness can be considered as a relevant parameter when designing ELS specimens. When analysing the corresponding R-curves, it is possible to observe that there are not significant changes in their shape, since the CBBM formulation presupposes a small influence of this variable for the computation of the fracture energy release rate in mode II, G_{II_c}. However, increasing the specimen stiffness, as it happens when decreasing the initial crack tip, a_0, may introduce stability problems when performing theses tests experimentally. Being so, a middle value was chosen and kept constant to continue this study, $h = 12.7\,\text{mm}$.

The following plots compare different combinations of the total length of the specimen and the initial crack tip, for the same mid span length, denoted as d. The same mid span length is understood as the distance between the crack tip and the clamping tool, which can be obtained by different combinations of L and a_0, as mentioned.

Firstly, on Figure 16 are presented the load-displacement curves for $d = 90$ mm, obtained by different combinations of a_0 and L. Sequentially, the corresponding R-curves, for the same case are presented on Figure 17.

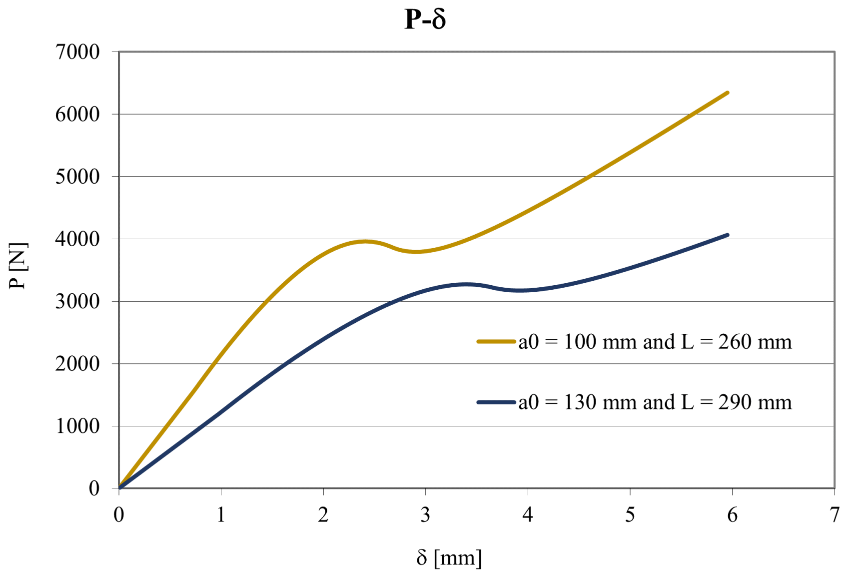

Figure 16: P-δ curve related to different combinations of a_0 and L that can compute $d = 90$ mm.

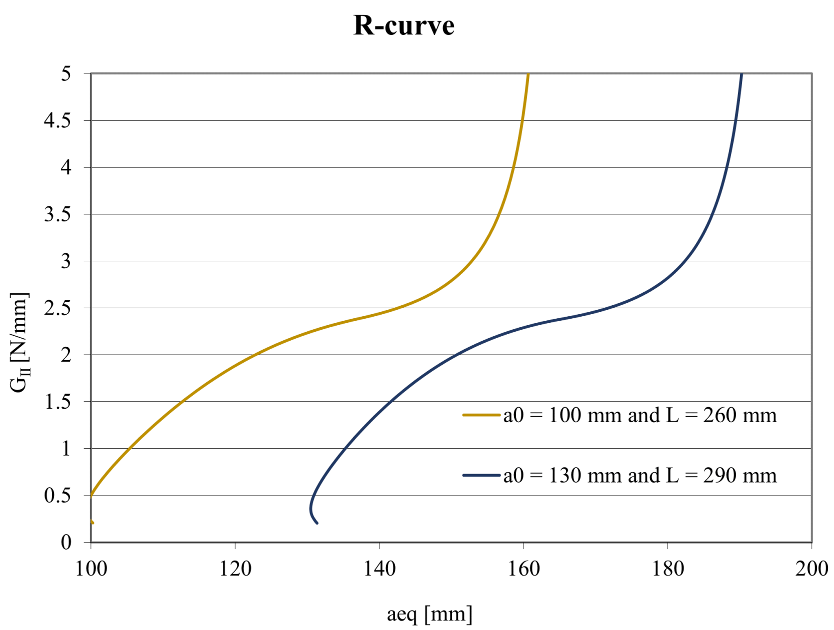

Figure 17: R-curve related to different combinations of a_0 and L that can compute d =90 mm.

When analysing the P-δ curve, it is evident that there is a significant variation in stiffness, yet there is no apparent change when analysing the R-curve, where both curves have exactly the same shape, but different a_{eq}, given by the CBBM formulation. The first affirmation is supported by the fact that decreasing the total length of the specimen, immediately increases the stiffness by the power of 3, as demonstrated in Equation 4. The second affirmation is true due to the fact that both variables, a_0 and L have the same weight in the G_{II_c} formulation, they both have the same exponent.

When selecting the mid span length, it is important to understand that this is the length available for crack propagation, which can be potentially more or less stable, depending on the geometry of the specimen. It was shown that having a bigger L propitiates a more stable crack propagation and, consequently, in this case, where the mid span length is kept constant, it is preferable to choose having a bigger initial crack tip, even that meaning that a more brittle failure might occur in experimental practising, since decreasing the total length of the specimen has a more significant influence.

As mentioned before, a fracture process zone (FPZ) is developed ahead of the major crack tip due to plasticization and the nucleation of many microcracks. The stability of the end-loaded split test thus depends on the complete formation of the fracture process zone, implying that the aforementioned mid-span length must be large enough for this phenomenon to occur. Since this test has the particularity of having a clamping tool, a study was made to understand if the FPZ could be affected by the clamped region, affecting the stability of the test, as some studies have already shown.

To better acknowledge the relation of this mid span length and the formation of the FPZ, this study compares the development of this FPZ with the evolution of the equivalent crack and the effective growth of the crack in the specimen. This analysis makes use of damage features of Abaqus, where the damage evolution capability for ductile metals presupposes that damage manifests as a progressive degradation in material stiffness that ultimately results in material collapse. A damage initiation criterion for ductile metals must be utilised in conjunction with the damage evolution. After damage initiation, this criterion uses mesh-independent measurements, either plastic displacement or physical energy dissipation, to control damage evolution. It also considers the combined role of different damage mechanisms acting simultaneously on the same material, offers options for describing how each mechanism contributes to the overall degradation of the material and provides options for what happens in the event of failure, such as the removal of elements from the mesh [23].

The length and development of the fracture process zone was then computed using the Abaqus' damage parameter SDEG, studied along a path created through the adhesive layer, measuring the state of damage, as an overall scalar stiffness degradation, of each element that it crosses. When this parameter reaches its maximum value, 1, the element is deleted, meaning that the crack starts to propagate. In Figure 18a it is possible to observe the crack tip of the ELS specimen and the correspondent damage region ahead is coloured, following a different distribution of damage, as shown in Figure 18b. This parameter is related to other parameter, STATUS, which provides, as indicated by its name, the status of the element, being 1 if the element is active and 0 if the element is not. Once the SDEG parameter reaches 1, the STATUS parameter starts to identify elements that become active and eliminates them from the adhesive layer elements.

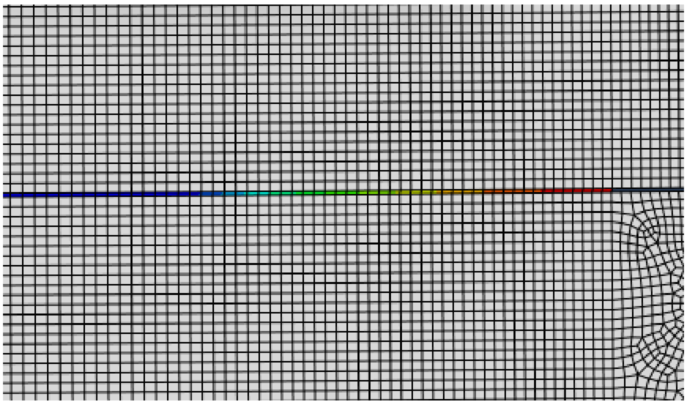

(a) SDEG.

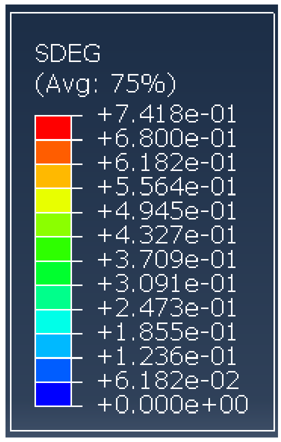

(b) SDEG.

As aforementioned, the SDEG damage parameter was used to estimate the fracture process zone development and, consequently, its length along with the adhesive layer. In terms of the crack propagation, a, was computed using the STATUS parameter since it reveals when an element has reached its maximum damage state and is deleted from the adhesive layer. Both these parameters were measured in terms of true distance from the beginning of the chosen path, which means that the vertical axes of the following charts exhibit the distance along the adhesive layer, starting from the crack tip. The equivalent crack evolution was also determined using CBBM, and it is also represented in terms of true distance from the initial crack tip.

In Figure 19, the study comparing the evolution of these three variables: fracture process zone length, equivalent crack and actual crack propagation, is presented, relating these developments with the applied displacement on the specimen. It is also presented the clamp tool distance, in order to easily study some of the variables reaches this point, possibly introducing problems with attaining stable crack propagation. The first case is for a 290 mm long specimen, with an initial crack tip of 100 mm.

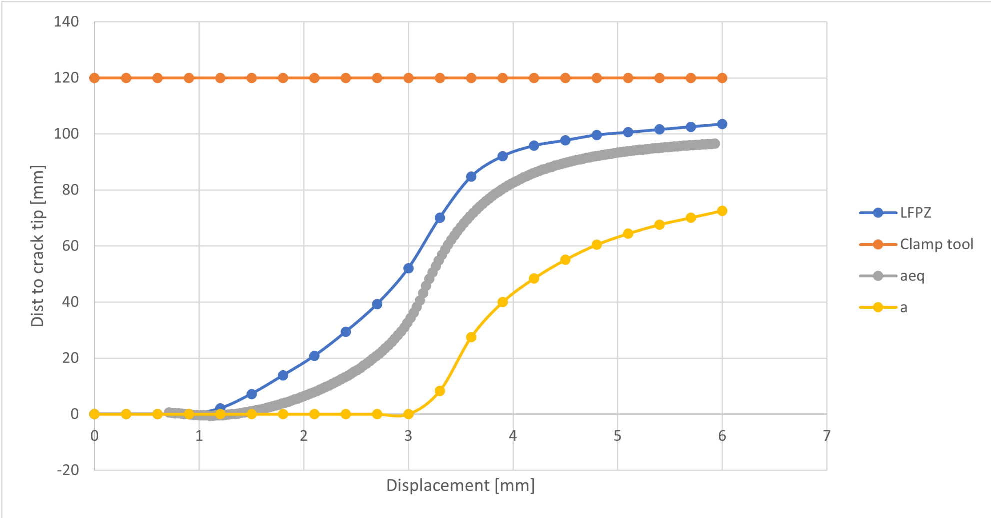

Figure 19: Study of L_{FPZ}, a_{eq} and a for $L = 290\,\mathrm{mm}$ for the brittle adhesive.

It is possible to observe that none of these parameters reached the clamped area, which was expected since for this specimen design, it was shown in Figure 12 and 13 that it is possible to attain a secure plateau for the G_{II_c} extraction before any interaction with this boundary condition. As mentioned in Section A.1 CBBM accounts for the effect of the formation of the fracture process zone, so the evolution of the equivalent crack, a_{eq} should be sufficient to determine a sufficient mid-span length, d, to have stable propagation. However, the fracture process zone length is more significant than a_{eq}, which means that this length should be considered in the specimen's design. On the other hand, it is possible to see that the FPZ starts growing before the others, which is also expected since the FPZ is a representation of the damage being accumulated ahead of the crack tip. In comparison, the real crack, a, only starts propagating later because this happens when the damage variable SDEG first reaches 1, which is around at 3.2 mm of displacement. The difference between the starting point of the fracture process zone length and the equivalent crack has to do, as previously mentioned, with the fact that the length of the FPZ considers damage differently, using the SDEG parameter whilst the a_{eq} is formulated following the naturally indirect CBBM propositions.

Identifying a set of larger displacements where the evolution of these three parameters remains constant and stops developing is also feasible. This is due to compressive stresses induced by the clamp tool, which represents a final barrier for plastic deformation of the adhesive and therefore completely hinders the crack propagation. In order to illustrate this in a much more clear sense, a study of the evolution of these parameters was done for a different specimen's geometry, where the $L = 230\,\mathrm{mm}$ and the other dimensions are kept the same. This design was shown to be unsuitable since it does not provide stable crack propagation in both Figure 12 and 13, so it is a good example to understand what is the influence of the clamp tool and this analysis is presented in Figure 20.

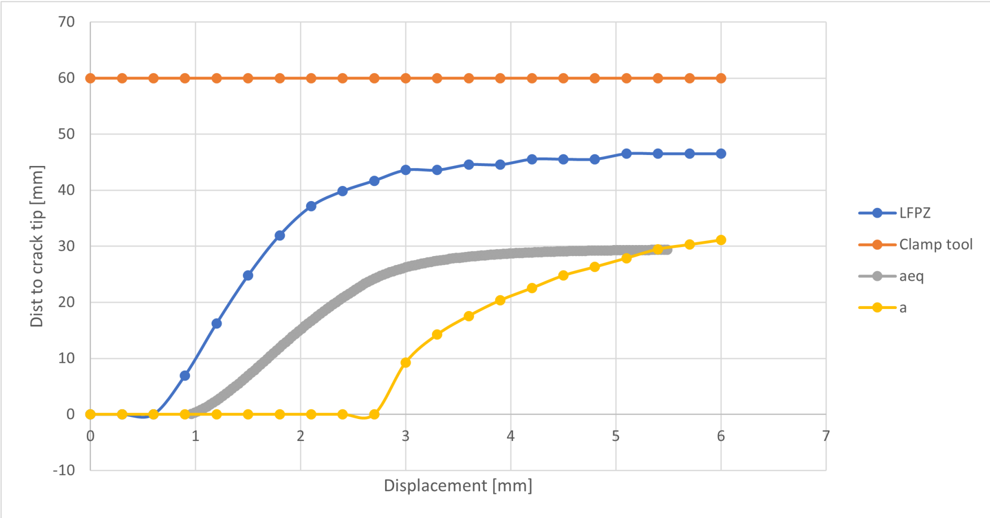

Figure 20: Study of L_{FPZ}, a_{eq} and a for $L = 230$ mm for the brittle adhesive.

It is right away noticeable that none of the parameters develops further through the clamped region, which could be unexpected, since the specimen's length is shorter and the displacement applied is the same. However, as mentioned before, the clamping tool induces compressive stresses on the adhesive that restrains the plastic deformation and avoids the damage evolution until failure of the adhesive. For the case of this model, where compressive stresses take a significant influence in determining the end of the development of FPZ, the instability of the test is related to the fact that the FPZ is not long enough for stable crack propagation, meaning that even if the clamped region is not reached, the specimen's geometry is still not propitious for the crack to fully propagate and to attain a plateau in the R-curve.

This means that the length of the fracture process zone is a relevant parameter in designing these specimens, meaning that the mid span length, d, must be long enough to fully develop the FPZ. Some authors have proposed an analytical formula to determine this length:

End-loaded split test design - ductile adhesive

As mentioned before, the same parametric study of the influence of changing dimensional parameters such as the initial crack tip, a_0, the total length of the specimen, L and the substrates' thickness, h on the overall behaviour of the specimen under testing conditions of an end-loaded split joint will now be made for a ductile adhesive.

Firstly, using the same geometrical configuration set on chapter A.2.1 and following the adapted geometry for experimental testing of these specimens a study about the influence of changing the initial crack tip size was done. Using $L = 290$ mm and the clamped length as 70 mm, the obtained load-displacement curve and R-curve are presented in Figure 21 and 22.

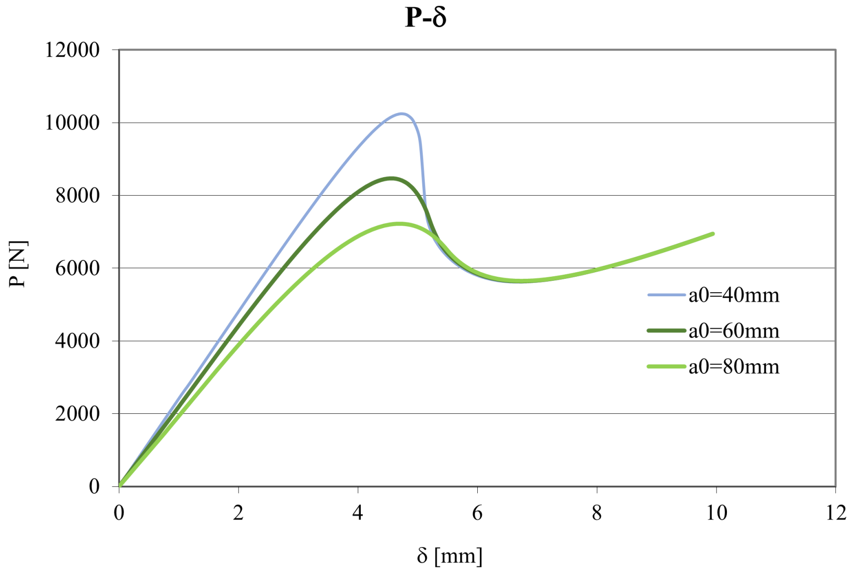

Figure 21: P-δ curve related to a_0 study for a ductile adhesive.

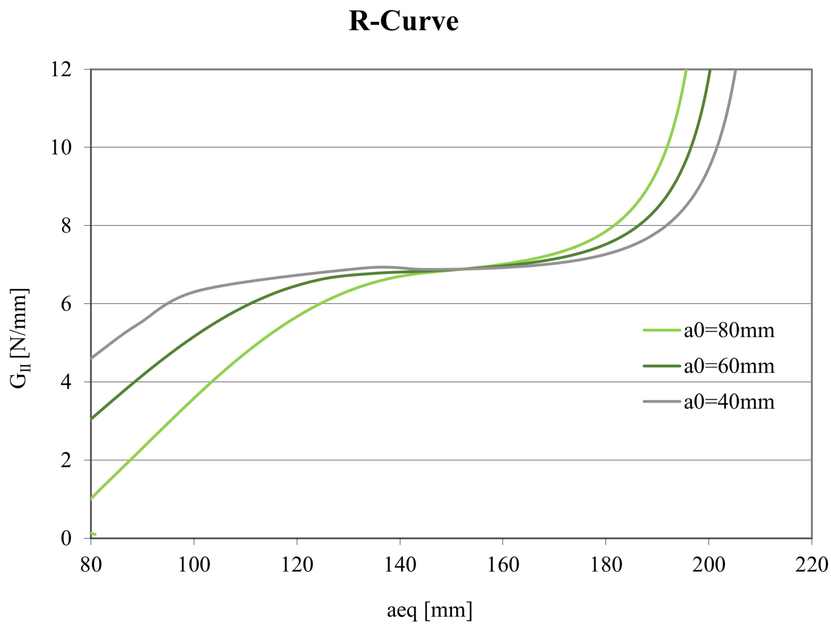

Figure 22: R-curve related to a_0 study for a ductile adhesive.

It is possible to immediately conclude that both adhesives have similar behaviours in terms of P-δ and R-curves, even considering different a_0. The fact that the study concerning the initial crack tip influence considers different lengths of a_0 has to do with the stability criterion mentioned in A.1. For larger initial crack tips, a stable crack propagation could not be achieved and, therefore, no plateau on the R-curve could be identified. However, the same increments are considered. As expected, since this is a more ductile adhesive, the energy absorption during testing would naturally be larger and the supported loads would also be increased. In fact, the maximum supported load for the case of the ductile adhesive is more than twice than for the case of the brittle adhesive.

The initial slope of the P-δ curve, can be understood as the stiffness of the specimen prior to being damaged, as it has been before compared with the case of a cantilever beam. As expected, this initial slope would not be the same for both adhesives, as the stiffness of the specimen is a function not only of the substrates but also the adhesive, meaning that the slope of the ductile adhesive and, consequently, its correspondent specimen stiffness is higher than that for the brittle adhesive.

Additionally, the considerations made for this kind of study in the case of the brittle adhesive are also observable for this case. Looking at the R-curves, by decreasing a_0, a more pronounced plateau is achieved, which allows to extract G_{II_c} with more certainty. However, decreasing a_0 brings the same disadvantage in changing the failure mode into a more sudden process, which will then result in the reduction of datapoints available for the determination of the desired fracture toughness values.

It is also conceivable to draw the conclusion that, because the presence of the crack corresponds to an important discontinuity in the specimen, by increasing the initial crack tip size the specimen's stiffness is lowered . Given this, raising a_0 implies decreasing the specimen's overall stiffness.

In order to explore the effects of altering the overall length of the ELS specimen, a midway value of $a_0 = 60$ mm was selected, taking into account the aforementioned factors.

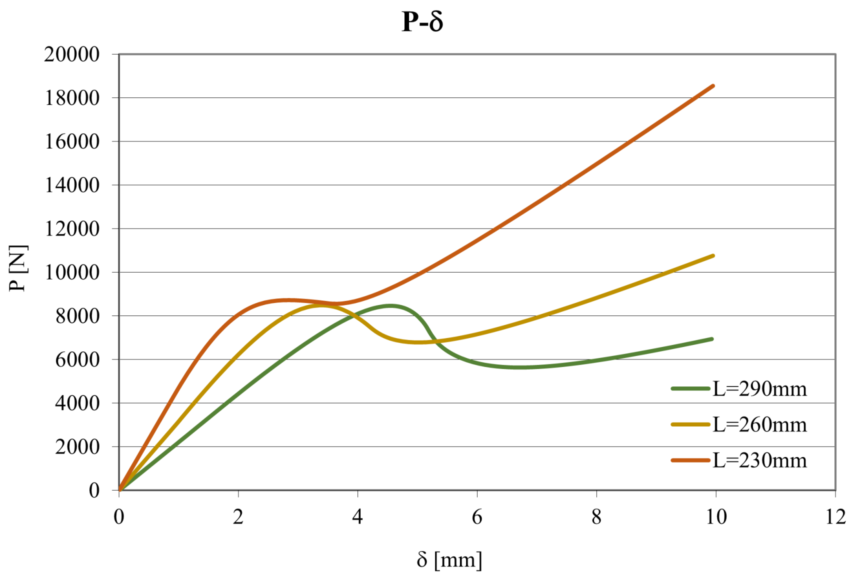

Figure 23: P-δ curve related to L study for a ductile adhesive.

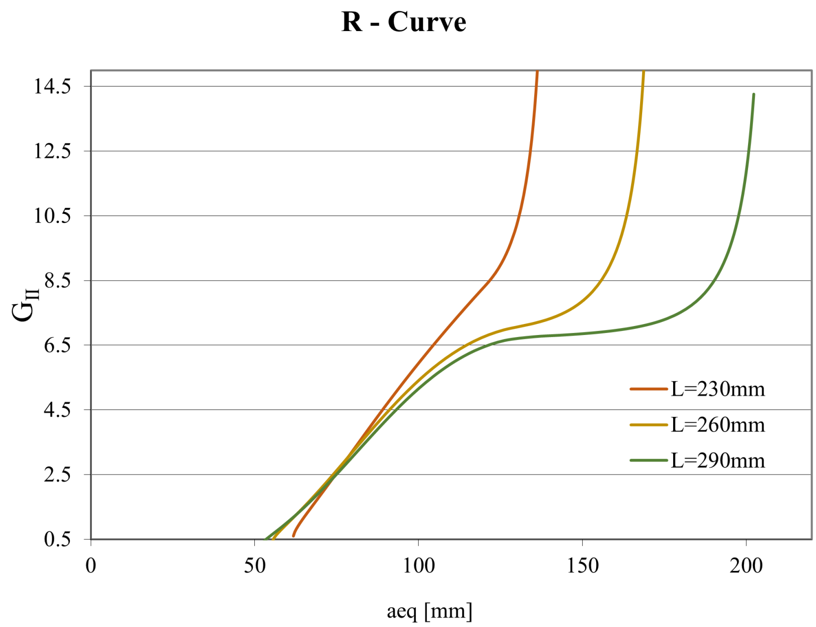

Figure 24: R-curve related to L study for a ductile adhesive.

From Figure 23 and 24 it is possible to observe the same trend identified for the brittle adhesive, in spite of the fact that in this case, the supported loads are larger. Using $L = 290\,\text{mm}$ as a reference and studying the influence of decrements of 30 mm it is recognizable the increase of stiffness of the specimen. Being so, the increase of L means having a more stable crack propagation, also seen by the enhanced formation of a plateau on the R-curves. However, as also mentioned before, manufacturing exceedingly long specimens is sometimes unfeasible, considering its process but also the size of the testing machine. Then, the same L was kept constant and equal to 290 mm for studying the substrate's thickness influence in P-δ curves and R-curves, as can be seen in Figure 25 and 26.

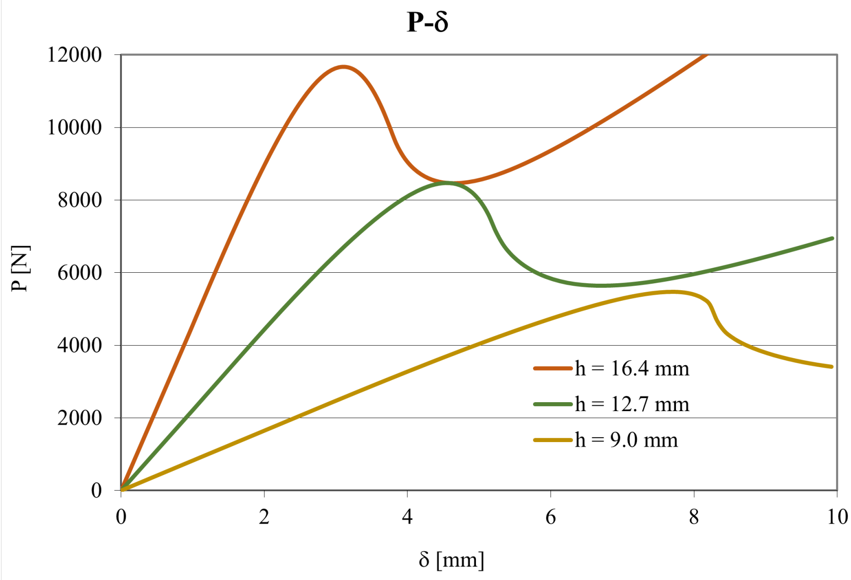

Figure 25: P-δ curve related to h study for a ductile adhesive.

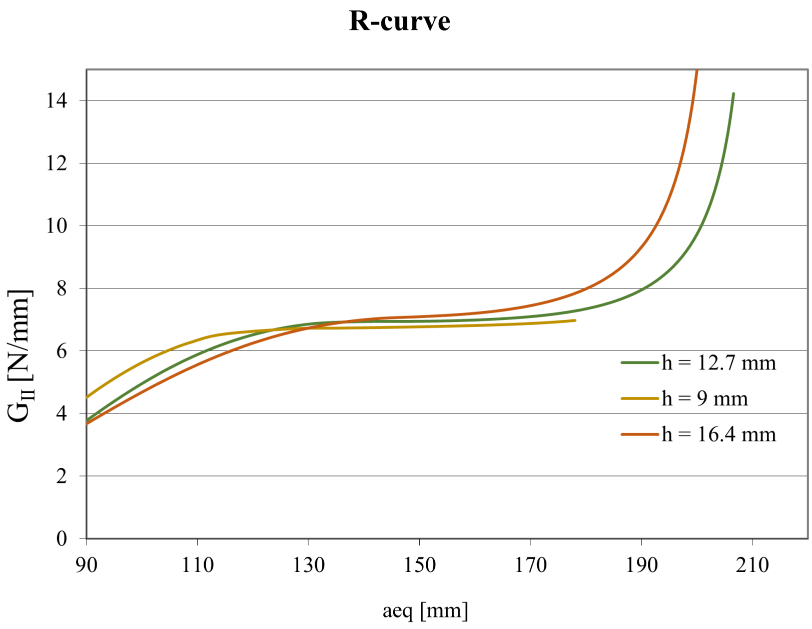

Figure 26: R-curve related to L study for a ductile adhesive.

Similarly to what was observed in the brittle adhesive behaviour and also for the case of the study of the length of the specimen influence in this ductile adhesive, the thickness of the substrate plays a relevant role on the stiffness of the specimen. As foreseen, the slope of the elastic part of the P-δ curve that indicates the stiffness of the specimen prior adhesive failure, is different for the ductile adhesive, even using the same increments of substrate's thickness in the study. This has to do with the fact that the adhesive, itself, introduces stiffness to the specimen, in this case with the stiffness of the ductile adhesive being larger than that of the brittle one.

However, the influence of increasing the thickness of the substrate is generally the same for both adhesives, where, using the analogy of the cantilever beam, there is an increase in the second moment of inertia of the substrates, consequently increasing the the stiffness of the specimen. However, as already shown for the brittle adhesive, the resulting changes on the R-curves are minimal, since the CBBM formulation considers the thickness influence as small compared to other parameters, such as the length of the specimen. However, when conducting these tests experimentally, increasing the specimen stiffness, as occurs when reducing the initial crack tip, a_0, may cause stability issues. Due to this, a midway value of $h = 12.7$ mm was chosen and maintained constant for the rest of the study.

Following the same path of study as for the brittle adhesive, the following Figures 27 and 28 compare different combinations of the total length of the specimen and the initial crack tip, for the same mid span length, $d = 130$ mm.

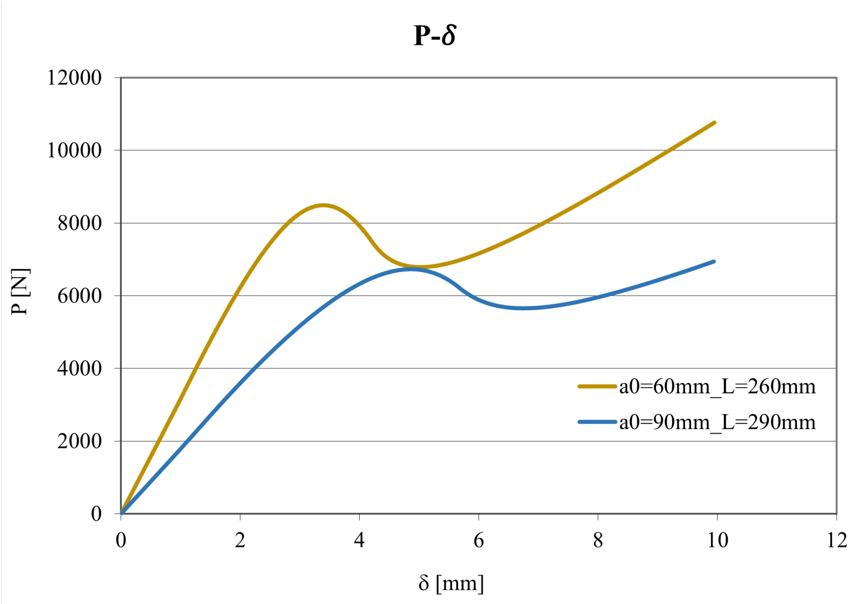

Figure 27: P-δ curve related to different combinations of a_0 and L that can compute $d = 130$ mm.

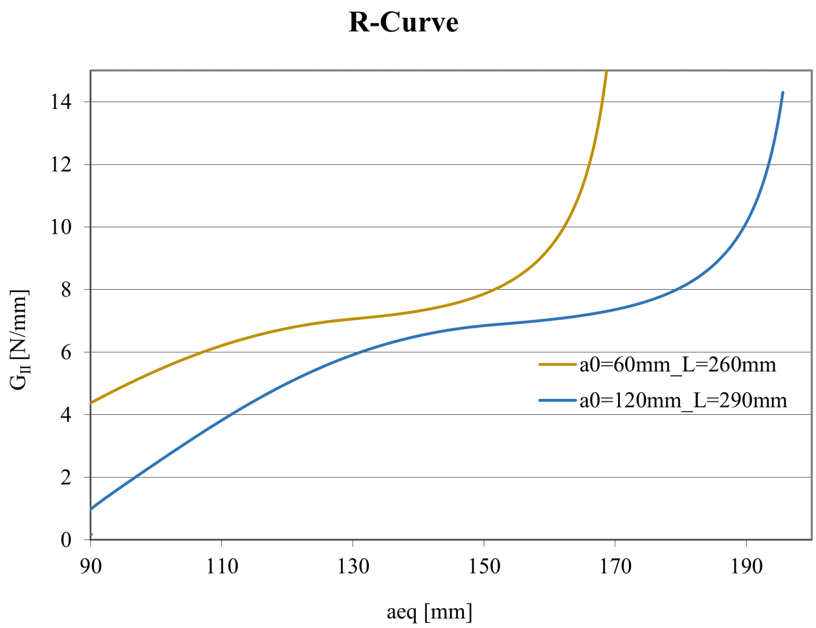

Figure 28: P-δ curve related to different combinations of a_0 and L that can compute $d = 130$ mm.

When analysing the P-δ curve, it is clear that there is a considerable variation in stiffness; yet, when analysing the R-curve, both curves have the exact same shape but have different a_{eq} as determined by the CBBM formulation, there does not appear to be an important change. The first claim is corroborated by the fact that, as shown in equation 4, calculating adjustments that result in a reduction in the specimen's overall length immediately increase stiffness by a factor of 3. The second statement is accurate because both variables, a_0 and L, have the same exponent and are equally weighted in the G_{II_c} formulation.

The study relating the mid span length and the evolution and growth of the fracture process zone to the equivalent crack and the actual crack was also repeated for the ductile adhesive. Using the same damage criterion and feature of Abaqus as described for the brittle adhesive but using the properties of the ductile adhesive, both the fracture process zone length and the crack length were computed, whilst the equivalent crack length evolution was determined using the CBBM formulation. These three parameters were presented in terms of true distance from the initial crack tip.

In Figure 19 the study carried out for these parameters is represented for 290 mm long specimen with an initial crack tip of 60 mm. This combination of L and a_0 was already shown to be a proper fit for the specimen's geometry.

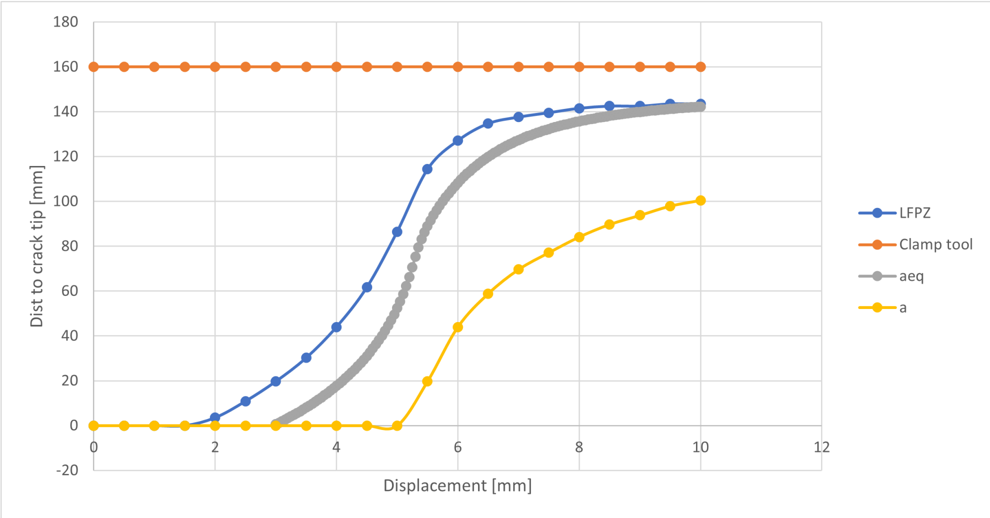

Figure 29: Study of L_{FPZ}, a_{eq} and a for $L = 290\,\mathrm{mm}$ for the ductile adhesive.

As expected, none of the parameters under analysis reached the clamped area and in Figure 22 can be seen that, for this configuration a plateau is achieved. The process zone length is more significant than the equivalent crack length evolution. It is also possible to identify a set of larger displacements where the evolution of these three parameters stops and remains constant. Again, this is because the clamping tool's compressive stresses act as a barrier to the adhesive's plastic deformation and significantly restrict the crack's ability to propagate. Similarly to what was done for the brittle adhesive, a study of the evolution of these parameters was conducted for a different specimen's geometry, keeping the $L = 230\,\mathrm{mm}$ and other dimensions constant, in order to demonstrate this in a much more understandable way. This is represented in the following Figure 30.

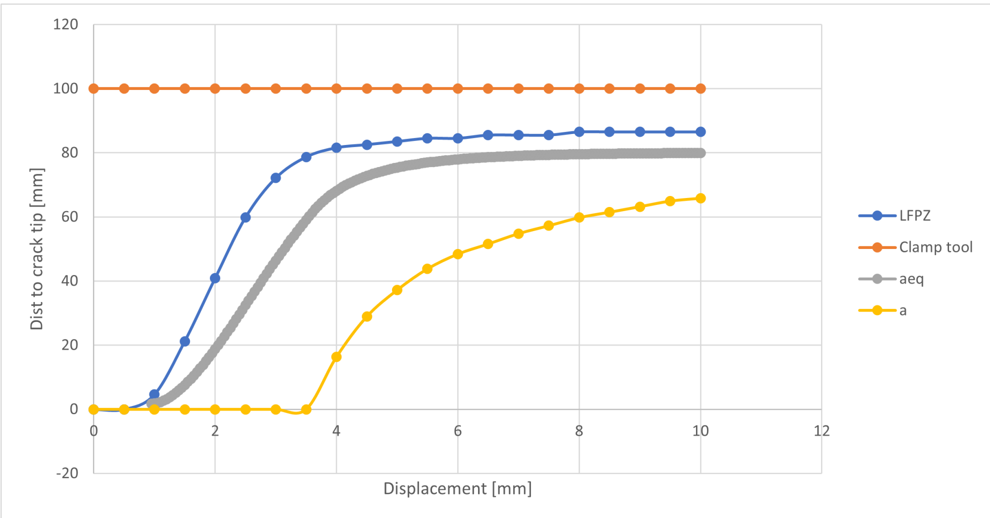

Figure 30: Study of L_{FPZ}, a_{eq} and a for $L = 230$ mm for the ductile adhesive.

As it happened for the first adhesive, although it was expected that some of the parameters under analysis could progress and reach the clamping tool, since the specimen is shorter and the mid span length is consequently shorter, this situation was not verified. Although the effective space for crack propagation is indeed shorter this did not imply that any of the parameters developed under the clamp tool affecting the stability of the tests and prevented attaining a reasonable plateau for G_{II_c}. In fact, the reason behind this difficulty in attaining the plateau is related to a lack of a minimum length for proper crack propagation, hindered by the compressive stresses induced by the clamp tool.

A.3.2 Combined mode I and mode II test specimen

As mentioned before, a new unified specimen for combined mode I and mode II fracture characterisation was developed. This specimen is to be sequentially loaded, performing firstly a mode I fracture test, a double cantilever beam (DCB) test, and, after that, the same load cell would solicited the upper part of the specimen, performing a mode II fracture test, an end-loaded split (ELS) test. Since the ELS specimen geometry was optimised for both adhesives, for the purpose of this study, the only part of the test being analysed will be the DCB.

Firstly, to understand the influence that the upper substrate, corresponding to the ELS specimen, would have on the P-δ curves of the DCB test, different configurations for the upper substrate were considered. The adhesive being tested, in this case, is the brittle one and the three upper configurations were studied, taking into account the parameters mentioned in Figure 2, one solid DCB, and the other two making use of different adhesives:

Table 6: Geometric properties of the combined specimen. Dimensions in mm

	Solid DCB	**DCB (brittle adhesive)**	**DCB (ductile adhesive)**
L_{ELS} [mm]	290	290	290
L_{DCB} [mm]	160	160	160
a_0 [mm]	45	45	45
h_{ELS} [mm]	12.7*	9	9
h_{DCB} [mm]	12.7	12.7	12.7
t [mm]	0.2	0.2	0.2

* in this case, as a solid DCB is considered, h_{ELS} is considered as the total ELS height, which, in this case, is 12.7 mm.

Assuming the geometries aforementioned in table 6, the P-δ curves obtained by numerical simulation are presented in Figure 31.

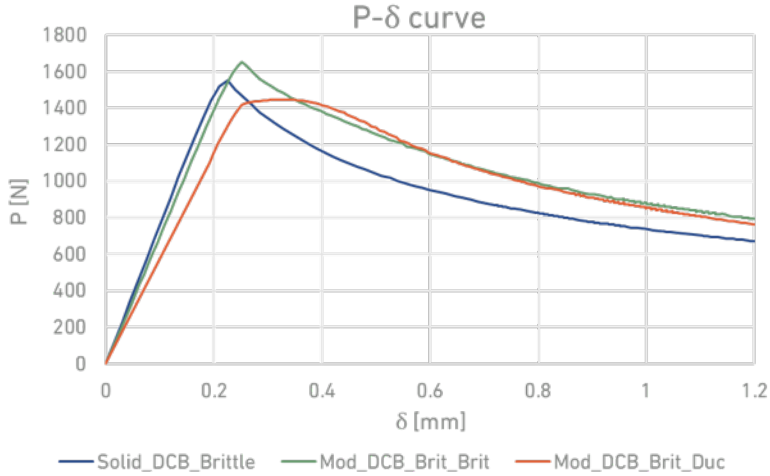

Figure 31: Behaviour changes on the P-δ curves of the DCB related part of the unified specimen.

As it can be observed, computed changes in the upper substrate related to the ELS part of the unified specimen have a major influence on the P-δ curves concerning the DCB test. The solid DCB can be considered a reference, since it is carried out using standard specimen dimensions. As expected, the P-δ curve related to the brittle adhesive shows a smaller initial slope, followed by the P-δ curve related to the ductile adhesive. This is justified by the the fact that these combinations of upper substrates: solid DCB, DCB (brittle adhesive) and DCB (ductile adhesive) have descending rigidity properties. Furthermore, the configuration where the brittle adhesive is used supports a larger load than the solid DCB, whilst being the configuration where the ductile adhesive reaches the smallest maximum load. In Figure 32 are also represented the R-curves concerning the aforementioned configurations.

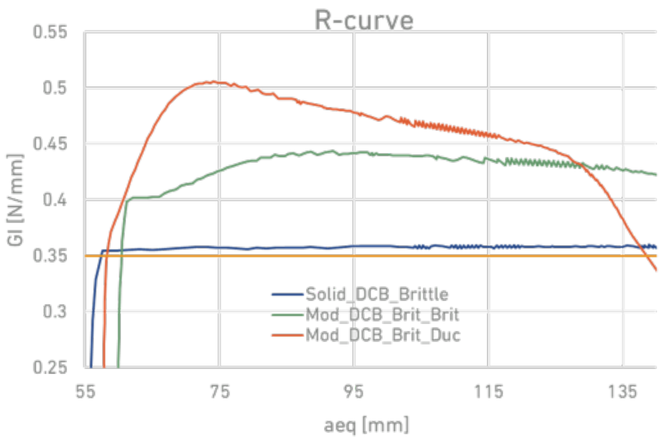

Figure 32: Behaviour changes on the R-curves of the DCB related part of the unified specimen.

Since the stiffness of the ELS specimen introduces changes in the P-δ curves related to the DCB test, it was expected that the corresponding R-curves would suffer some changes too. The brittle adhesive configuration, being the one that presents the largest maximum load supported, presents a R-curve that overestimates the value of G_{II_c}, followed by the ductile adhesive configuration that, due to its smaller initial stiffness leads to the largest overestimation of the fracture energy release rate in mode I. These computed changes represent a limitation of the reduction scheme used to analyse the energy release rate in mode I, since the CBBM formulation does not take into account the influence that the upper substrate, which, in this case, is the ELS specimen. In fact, the behaviour of the DCB specimen was found to be closer to an asymmetric double cantilever beam (ADCB), since the substrates stiffness are different. The adhesive layer of the ELS test plays an important role on the upper substrate thickness of the DCB related part of the unified specimen. The existing data reduction method for the asymmetric double cantilever beam testing (ADCB) assumes that the crack propagation must be measured during the experimental work, which was not feasible for the current work. Since knowing the stiffness of the top substrate is required to calculate the asymmetrical double cantilever beam theory, a future challenge lies in the development of a simple approach to add the contribution of the adhesive into the stiffness of the ELS specimen and, consequently, to the DCB related part of this unified specimen, increasing the accuracy of such test procedure.

A.4 Conclusions

In this work, it was possible to develop a numerical model that precisely reflected the experimental conditions of an end-loaded split test and its geometry could be optimised by studying behaviour changes by computing different combinations of relevant geometry parameters of this kind of specimen. By analysing the response of the various combinations of the initial crack size and total length of the specimen, a design approach that attempts to have the same mid span length, finds that decreasing the total length of the specimen has a more significant impact on raising the stiffness. However, due to the use of the CBBM formulation, neither affects the R-curves. What must be avoided, though, is to select a smaller total length of the specimen. Once the fracture process zone is close to the clamping tool, the zone's development is halted by large compressive stresses. However, in order to have consistent fracture propagation, a minimal fracture process zone must be developed and a minimal length is fundamental for that to take place. Using CBBM as data reduction scheme of the DCB related part of the unified specimen was found to be imprecise, since the ELS specimen introduces different levels of stiffness to the upper substrate of the double cantilever beam. Ideally, this test needs to be handled as an asymmetric double cantilever beam, for which there is currently no crack independent data reduction scheme.

References

[1] da Silva LFM, Öchsner A, and Adams RD. *Handbook of adhesion technology*. Springer, 2018.

[2] da Silva LFM, Dillard DA, Blackman BRK, and Adams RD. *Testing adhesive joints: best practices*. John Wiley & Sons, 2012.

[3] Cognard JY and Créac'Hcadec R. Analysis of the non-linear behavior of an adhesive in bonded assemblies under shear loadings. proposal of an improved tast. *Journal of adhesion science and technology*, 23(10-11):1333–1355, 2009.

[4] de Moura MFSF, Campilho RDSG, and Gonçalves JPM. Crack equivalent concept applied to the fracture characterization of bonded joints under pure mode i loading. *Composites Science and Technology*, 68(10-11):2224–2230, 2008.

[5] Moore DR, Pavan A, and Williams JG. *Fracture Mechanics Testing Methods for Polymers Adhesives and Composites*. ESIS Publication 28, 2006.

[6] Chaves FJP, da Silva LFM, de Moura MFSF, Dillard DA, and Esteves VHC. Fracture Mechanics Tests in Adhesively Bonded Joints: A Literature Review. *The Journal of Adhesion*, pages 1–39, June 2014.

[7] Pérez-Galmés M, Renart J, Sarrado C, Rodríguez-Bellido A, and Costa J. A data reduction method based on the j-integral to obtain the interlaminar fracture toughness in a mode ii end-loaded split (els) test. *Composites Part A: Applied Science and Manufacturing*, 90:670–677, 2016.

[8] Silva MAL, Morais JJL, de Moura MFSF, and Lousada JL. Mode ii wood fracture characterization using the els test. *Engineering fracture mechanics*, 74(14):2133–2147, 2007.

[9] de Moura MFSF and de Morais AB. Equivalent crack based analyses of enf and els tests. *Engineering Fracture Mechanics*, 75(9):2584–2596, 2008.

[10] Blackman BRK, Brunner AJ, and Williams JG. Mode ii fracture testing of composites: a new look at an old problem. *Engineering fracture mechanics*, 73(16):2443–2455, 2006.

[11] de Moura MFSF, Dourado N, Morais JJL, and Pereira FAM. Numerical analysis of the enf and els tests applied to mode ii fracture characterization of cortical bone tissue. *Fatigue & Fracture of Engineering Materials & Structures*, 34(3):149–158, 2011.

[12] El Moustaphaoui A, Chouaf A, and Kimakh K. Experimental and numerical study of the delamination of ceiba plywood under mode i, mode ii and mixed-mode (i+ ii) loading using the dcb, els and mmf tests. *International Journal of Fracture*, 231(1):1–20, 2021.

[13] Blackman BRK, Kinloch AJ, and Paraschi M. The determination of the mode ii adhesive fracture resistance, giic, of structural adhesive joints: an effective crack length approach. *Engineering Fracture Mechanics*, 72(6):877–897, 2005.

[14] Wang H, Vu-Khanh T, and Le VN. Effects of large deflection on mode ii fracture test of composite materials. *Journal of composite materials*, 29(6):833–849, 1995.

[15] Wang H and Vu-Khanh T. Use of end-loaded-split (els) test to study stable fracture behaviour of composites under mode ii loading. *Composite structures*, 36(1-2):71–79, 1996.

[16] Davies P, Blackman BRK, and Brunner AJ. Standard test methods for delamination resistance of composite materials: current status. *Applied composite materials*, 5(6):345–364, 1998.

[17] de Morais AB and de Moura MFSF. Evaluation of initiation criteria used in interlaminar fracture tests. *Engineering fracture mechanics*, 73(16):2264–2276, 2006.

[18] Toolabi M and Blackman BRK. Guidelines for selecting the dimensions of adhesively bonded en-loaded split joints: An approach based on numerical cohesive zone length. *Engineering Fracture Mechanics*, page November, June 2018.

[19] Pérez-Galmés M, Renart J, Sarrado C, and Costa J. Suitable specimen dimensions for the determination of mode II fracture toughness of bonded joints by means of the ELS test. *Engineering Fracture Mechanics*, 202, July 2018.

[20] da Silva LFM, da Silva RAM, Chousal JAG, and Pinto AMG.

[21] Correia DS, Carbas RJC, Marques EAS, das Neves PJC, and da Silva LFM. Experimental study on aluminium to tungsten carbide/polycrystalline diamond (wc/pcd) adhesive bonding for milling tools. *International Journal of Adhesion and Adhesives*, 114:103121, 2022.

[22] Riccio A, Saputo S, Raimondo A, and Sellitto A. Modeling low velocity impact phenomena on composite structures. In *Dynamic Response and Failure of Composite Materials and Structures*, pages 129–158. Elsevier, 2017.

[23] Simulia. *ABAQUS Version 6.6 Documentation.*

B Paper B

Experimental study of an unified specimen for adhesive characterisation

I.D. Costa[1], D.S. Correia[1], R.J.C. Carbas[1], E.A.S. Marques[1], L.F.M. da Silva[2]

1 Instituto de Ciência e Inovação em Engenharia Mecânica e Engenharia Industrial (INEGI), Porto, Portugal
2 Departamento de Engenharia Mecânica, Faculdade de Engenharia (FEUP), Universidade do Porto, Porto, Portugal

Abstract

Adhesive bonding is now seen as a very versatile and efficient joining technique, enabling the construction of multi-material structures with high strength to weight ratio and lower the overall costs. Consequentially, adhesives are now increasingly being employed in multiple industrial applications as a replacement for conventional mechanical joining methods.
These advantages, coupled with an ever increasing range of applications has led to a large demand for characterisation methods that allow to predict the mechanical behaviour of an adhesive, whether in daily use or under extreme or critical loading conditions. These characterisation processes generally feature a wide variety of distinct standards, complex and numerous specimens configurations, and employ data reduction schemes that are currently both extremely time-consuming and expensive. However, their use is indispensable to aid structural engineers in adhesive selection process and the creation of analytical and numerical models.
By suggesting the creation of a new and integrated experimental tool for adhesive characterisation, it will be possible to address this problem in a faster and more integrated manner. In this work, an experimental tool for mode I and II fracture toughness characterisation was developed and validated, being demonstrated that it is possible to obtain such data using a single unified specimen. A code was also developed to automate the data reduction schemes and reduce the amount of computational effort involving this kind of test.

B.1 Introduction

Adhesive bonding processes are replacing and supporting conventional mechanical joining techniques in several industries, supporting new design and construction concepts. Compared to more traditional bonding methods like bolting and riveting, adhesively bonded joints can provide a number of important and unique advantages. Key among these is an even distribution of stress along the bonded area which prevents stress concentrations, enhances load transmission, and increases fatigue resistance. Furthermore, well-designed bonded joints result in weight and cost reductions. The ability of this technique to bond dissimilar materials together and the greater flexibility it provides to a joint designer are further advantages [1].

In order to advance the underlying technology and to ensure accurate optimisation of bonded connection performance, great strides have been made to comprehend the science behind adhesive bonding. A fracture mechanics approach to the failure of adhesive joints has been created in an effort to bring together all the disciplines required for that, namely, surface chemists, polymer chemists and physicists, materials engineers, and mechanical engineers [1, 2].

Fracture mechanics mainly intends to identify fracture criteria, such as G_c, the fracture energy or fracture toughness, which are ideally independent of the geometry of the cracked body and therefore provide a 'material parameter' for characterising the toughness, or crack resistance, of materials, including interfaces and adhesives. A value of the fracture energy of an adhesive, also known as adhesive fracture toughness, G_c, can be defined for either a cohesive failure of the adhesive or for an interfacial failure along the adhesive/substrate interface. These fracture mechanics based procedures have been developed for characterising and predicting the failure of adhesive joints, including flexible laminates [2].

The double cantilever beam (DCB) and tapered double cantilever beam (TDCB) adhesive joint test specimens are the most commonly used test specimens for determining the critical strain energy release rate in mode I (the tensile opening mode), that is, G_{I_c}. The DCB test uses easier, less expensive specimens as opposed to the more complex and expensive ones utilised in TDCB testing. The TDCB has the advantage of displaying a linear change in compliance with crack length, however this only makes them useful in circumstances where it is impractical or undesirable to measure crack lengths while performing the test. However, it is generally preferable to use easy-to-make specimens while performing these tests; as a result, DCB tests are more frequently employed. Such specimens are even more appealing because crack independent data reduction schemes have been developed for DCB tests [3]. Since the 1960s, researchers have studied both of these tests, and their work has resulted in the development of an ASTM D3433 standard . The growing use of fibre-reinforced polymer matrix composites has lately led to the publication of a new international standard, known as ISO 25217 [4].

On the other hand, only composites are currently suitable for standardised tests for pure mode II fracture toughness (G_{II_c}) characterisation during end-notched flexure (ENF) testing, despite being effectively adjusted for adhesive joints. However, the most popular mode II tests still have some limitations. The end-loaded split (ELS) is another method that is suggested for evaluating the fracture toughness in mode II [2, 5].

Due to the flexibility of the adhesive layer, adhesively bonded joints have been observed to have a larger fracture process zone (FPZ) under shear loading compared to mode I or mixed-mode fracture tests and compared to other specimen dimensions. Visual examination of the fracture length is challenging due to the vast FPZ involved and the absence of a crack opening. Approaches based on the J-integral [6] or an effective crack length a_{eq} [3, 7–12] that are independent of the crack have been developed to address this. Other tests have been developed, such as the Tapered ENF (TENF) test, the Stabilised ENF (SENF) test, the Over-Notched Flexure (ONF), the Four-Point ENF (4ENF), or the Inverse ELS test, among others, to achieve stable propagation, since the commonly used End-Notched Flexure (ENF) test has instability problems. Other issues, though, such as difficulties arise with the use of these tests, such as with specimen manufacturing (TENF), the complexity of the test equipment (SENF), or friction-related (4ENF and ONF). Recent research has provided encouraging results for end-loaded split (ELS) tests, which also benefit from simpler manufactured specimens based on DCB specimens. One such benefit is the advantage of stable crack propagation under displacement control in composite joints if the initial crack to span length ratio is higher than 0.55.

According to recent studies, a few requirements must be satisfied in order to ensure stable crack propagation during an ELS test. First, it is necessary to guarantee the formation of the entire FPZ by achieving steady-state crack propagation and, consequently, the plateau of the resistance curve; second, to guarantee the stability of the test under displacement control; third, to prevent significant deflections; and fourth, to prevent adherend failure while testing. To meet these conditions, the ELS specimen geometry's span length, beginning crack length, and, if necessary, specimen total thickness must be altered [13, 14].

In this study, a new experimental unified specimen for combined characterisation of fracture mode I and II is presented, merging a DCB and an ELS specimen in a single specimen and then treating the resulting data by making use of a custom developed code intended to automate the data reduction scheme application. Since the ELS test offers more complexity of boundary conditions, a new setup for this kind of tests was firstly developed and validated and then, adapted to process the test results of the combined specimens.

B.2 Experimental details

B.2.1 Materials

Adhesive

Two alternative adhesives were studied in order to design and validate a new experimental tool for the combined test of mode I and mode II fracture characterisation. To check the applicability of the unified specimen to a variety of mechanical properties, two different adhesives were tested.

The first adhesive under analysis is brittle in nature. It is a two-component, room temperature curing paste adhesive of high strength. According to its datasheet, the adhesive has been formulated to withstand high temperatures and have good chemical resistance when fully cured. This adhesive is fully characterised [15] except for the fracture toughness in mode I and II, G_{I_c} and G_{II_c}, correspondingly, since some manufacturing procedures of the adhesive were changed and these were the main parameters being altered. Both these properties were determined in the scope of this experimental work, the G_{I_c} using a DCB and the G_{II_c} using an ENF, also aiming to compare results with an ELS.

The other adhesive, of ductile behaviour, that has been fully characterised in other works [16], is a one-part epoxy resin that is heat-cured and designed to be compatible with induction curing. It can be used in high stress applications in place of brazing, welding, and riveting. One of its key characteristics is an improved electrical conductivity, resulting from an aluminium filler which is part of its composition.

The properties of each adhesive studied are listed in Table 1 and 2, according to the manufacturer's datasheets.

Table 1: General characteristics of the adhesive used.

Adhesive	**Supplied as**	**Cure type**	**Cure cycle**
Brittle adhesive	Two-parts	Heat	100 °C/5 min
Ductile adhesive	One-part	Heat	150 °C/40 min

Table 2: Mechanical properties of the adhesives.

	Brittle adhesive	**Ductile adhesive**
$E[MPa]$	4890	3880
$\sigma_f[MPa]$	41.00	65.60
G [MPa]	1560	1447
$\tau_f[MPa]$	30.20	41.60
$G_{I_c}[N/mm]$	-	1.27
$G_{II_c}[N/mm]$	-	7.22

Substrates

The substrates were made from the high strength steel DIN 40CrMnMo7. Avoiding plastic deformation during tests is the main purpose behind the selection of this high strength steel, since yielding will generate inaccuracies in the testing results, especially for fracture toughness characterisation processes. Table 3 displays the general characteristics of the substrates.

Table 3: Mechanical properties of the substrates used.

Young's modulus	190-210 GPa
Ultimate tensile strength	965-1030MPa
Yield strength	827-862MPa
Poisson's ratio	0.27-0.3

B.2.2 Specimen manufacturing

DCB specimens

Using CNC-machined high strength steel adherends, DCB specimens, represented in Figure 1, were produced in a proper steel mould [17] in accordance with the applicable standard ASTM D3433-99 [18]. To maximise adhesion, all substrates were grit-blasted and acetone-degreased before the adhesive was applied. A thin, 0.1-mm-thick razor blade positioned in the middle of the bondline caused the initial crack, with length a_0, of 45 mm. Calibrated tapes were used to set an adhesive thickness of 0.2 mm (t). Following the assembly of the specimen, the adhesive was cured under in a hot plate press, following the curing conditions described in Section B.2.1.

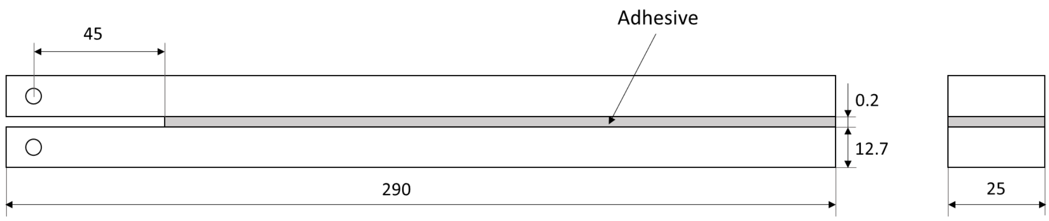

Figure 1: Representation of a DCB specimens' geometry, dimensions in millimeters.

ENF specimens

The specimens used for ENF tests have the same geometry as those used for conventional DCB tests, as shown in Figure 1. Therefore, every step of the production process was the same as for the DCB specimens that were previously described. After curing, the specimen was loaded in mode I until fracture propagation was noticed to create a natural crack. The new initial crack length, a_0, was then directly measured. This procedure was done to promote stable crack propagation and also facilitates the removal of the blade from the bondline.

ELS specimens

For the ELS specimen, the same manufacturing procedure for the ENF specimen was done. This signifies that a specimen with the same features as a DCB specimen, 1, was produced and then, after curing, the specimen was loaded under mode I, to promote a stable crack propagation in mode II testing conditions and to remove the blade introduced in the manufacturing procedure.

Unified specimens

As aforementioned, the combined test merges a DCB with an ELS specimen. Since the ELS specimen is not manufactured differently than the DCB specimen, this unified specimen for combined testing can be understood as an adaptation of a DCB specimen. Being so, the specimen was manufactured in the same way as a DCB, using three CNC machined high strength steel adherends, the smallest one corresponding to the bottom substrate of the unified specimen, as can be seen in Figure 2. In the same way, to guarantee adhesion, all substrates were grit-blasted and acetone-degreased prior to the application of the two layers of adhesive. A 0.1 mm-thick, sharp razor blade placed in the middle of the bondline's thickness induced the initial crack, measured denoted as a_0, to be 45 mm long. Depending on the adhesive that was being used, the adhesive was finally cured under the temperature and pressure settings that were specified in section B.2.1 for the hot plate press cure setup.

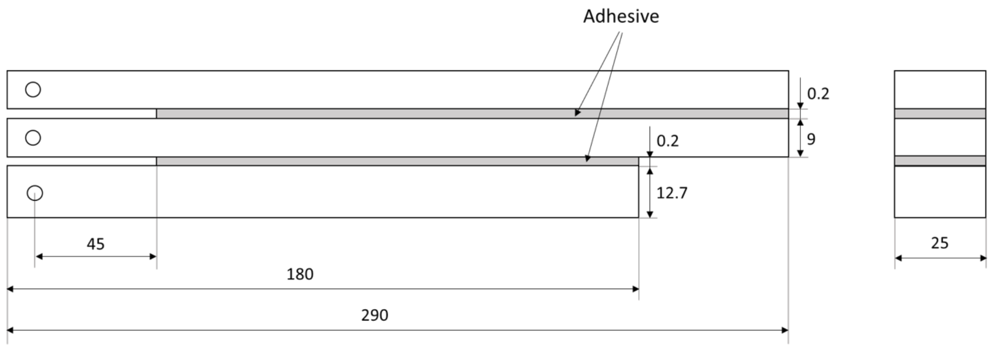

Figure 2: Representation of the unified specimen's geometry, dimensions in millimeters.

After the curing cycle was completed, the specimens were removed from the mould and the excess adhesive was removed using a milling machine. The upper blade of the specimen, related to the ELS part, was also removed. The specimen was then ready to be assembled in the newly designed testing setup for this kind of tests, presented in further detail later in this Section. The specimen designed is presented in Figure 2 and the produced specimen is presented in Figure 3.

Figure 3: Manufactured unified specimen.

B.2.3 Mechanical characterisation test procedures

All tests were performed using a universal testing machine, more specifically an INSTRON ® 3367 whose load cell is capable of measuring up to 30 kN. The tensile and shear strength properties were determined at the loading rate of 1 mm/min. Mode I and II fracture properties were determined for quasi-static conditions, 0.2 mm/min. To ensure accurate displacement extraction data, a DCTH1000A Linear variable differential transformer (LVDT) from RDT Group was used to measure the displacement of both ELS and combined test, since these tests involve larger displacements. Consequently, the same approach was done for mode II related part of the combined test, whilst, for mode I of the same combined test, a digital image correlation (DIC) technique was used for measuring the relative displacement between the DCB upper substrate and the bottom. For that purpose, some areas of the specimen were coated with a white matte paint and speckled with black dots. This allowed the displacement field data to be obtained by analysing the recorded pictures (1 frame per second) using the GOM Correlate software. In order to establish statistical relevance, at least three specimens for each test type were analysed, with their data treated and validated as acceptable.

DCB test

By propagating a crack in mode I up until failure, as illustrated in Figure 4, it was possible to estimate the critical energy release rate in mode I using DCB testing (Figure 5). Unlike the other specimens being tested, for DCBs, there was no need to load the specimens before testing in order to open pre-cracks, since stable crack propagation was consistently obtained. The load-displacement curve was recorded, and then its data was analysed.

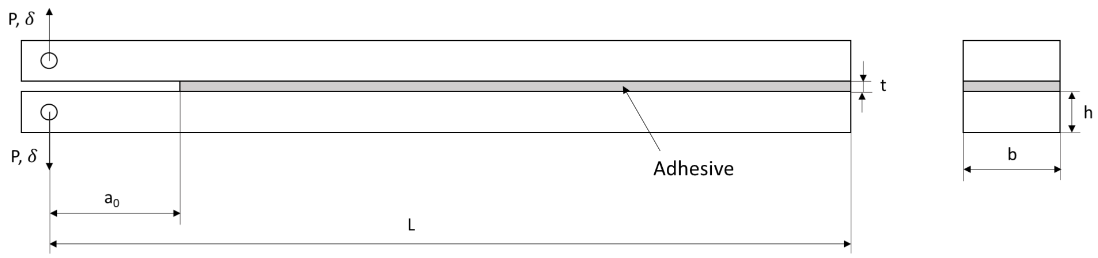

Figure 4: Representation of DCB test.

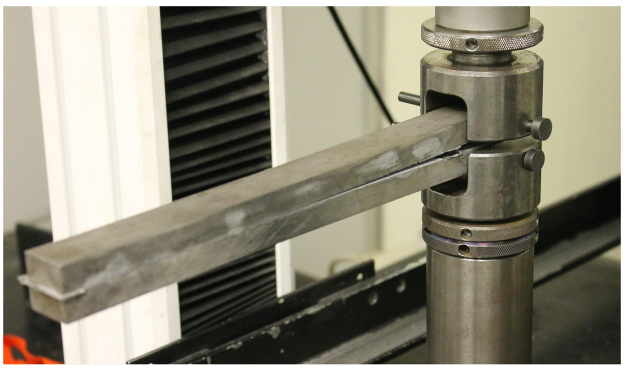

Figure 5: Representation of DCB setup test.

The adhesive's G_{I_c} was determined using the compliance-based beam method (CBBM), a data reduction scheme which is crack independent and thus does not require its direct measurement. Furthermore, it takes into account the fracture process zone [3]. Considering this method, the fracture energy is given by Equation 1 [3]:

$$G_I = \frac{6P^2}{b^2 h}\left(\frac{2a_{eq}^2}{h^2 E_f} + \frac{1}{5G_{13}}\right) \tag{1}$$

where P is the applied load, b is the specimen's width, h is the substrates' thickness, a_{eq} is a crack's equivalent length, G_{13} is the shear modulus, and E_f is the corrected flexural modulus. This approach does not take into account stress concentration and substrate rotation near the fracture tip, hence this final parameter is required.

ENF test

The fracture energy release rate in mode II for the brittle adhesive was determined firstly, using ENF tests, as in Figure 6, once its property was not known prior this work. Besides that, in order to further validate the newly developed setup developed for ELS, it was necessary to have reliable data to compare results with. In the case of the ductile adhesive, its fracture energy release rate in mode II was determined from a previous research work and, therefore, an ENF test was not required for this adhesive.

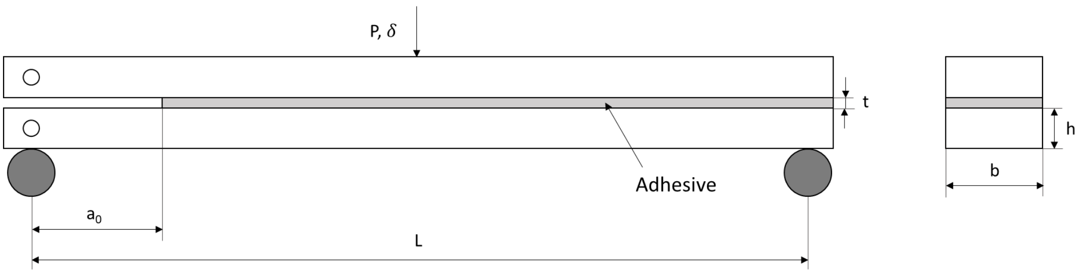

Figure 6: Representation of an ENF test.

In order to avoid friction caused by contact between the upper and lower adherends during testing, a folded Teflon® sheet coated with lubricant was inserted between the adherends in the pre-crack zone (seen in Figure 7 as the green material next to the mode I loading holes). Each test's load and displacement were recorded, and the fracture energy release rate was computed utilising the same data reduction technique as before, the CBBM. The energy release rate, in mode II, is given by Equation 2 [19]:

$$G_{II} = \frac{9P^2 a_{eq}^2}{16b^2 E h^3} \tag{2}$$

being P the load, a_{eq} the length of the equivalent crack, b the specimen width, E the corrected flexural modulus of the substrates and h their thickness.

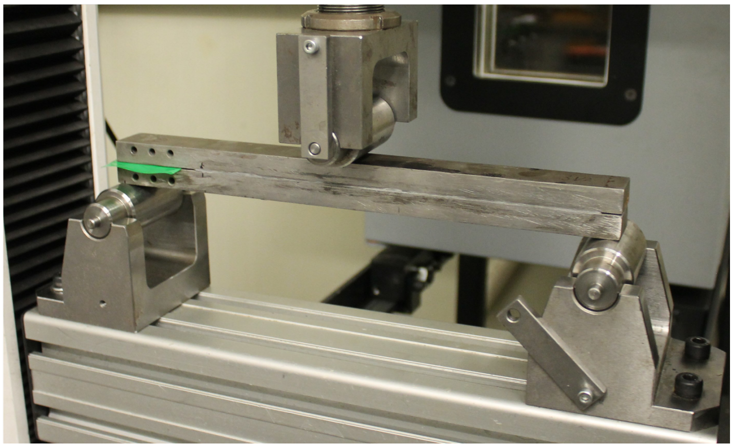

Figure 7: Representation of an ENF test setup.

ELS test

As performed for the ENF test, a folded Teflon® sheet with lubricant was also inserted between the adherends for the ELS test to minimize friction.

A new setup was built accordingly to the boundary conditions presented in Figure 8, where the specimen must allow movement on the horizontal degree of freedom during loading, while the opposite end to where the load is applied must be clamped. The setup was built using a steel base mounted on top of two roller bearings, coupled to a guiding system and, therefore, meeting the requirement of having an horizontal degree of freedom during loading. To address the clamping requirement, a steel block was placed on top of the specimen in one of its ends and then fixed to the steel base with four screws. The setup was assembled in the universal testing machine after the clamping tool was fixed, and the specimen was loaded by a vertical displacement in an ascending movement, precisely replicating the required loading conditions of the ELS test.

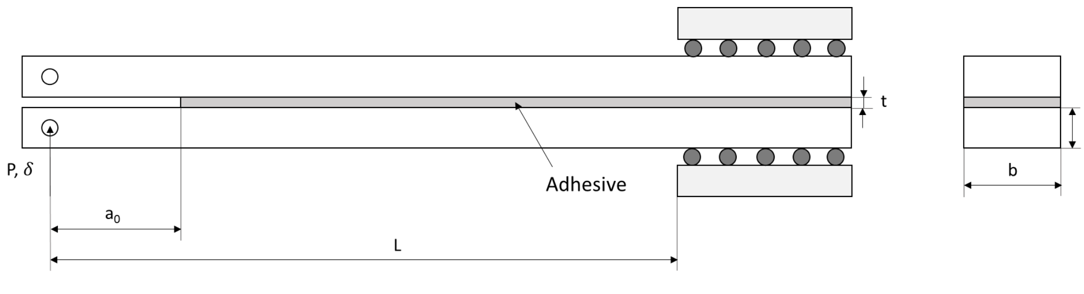

Figure 8: Representation of an ELS test.

The load and displacement for each test were also recorded, and the fracture energy release rate was calculated using the CBBM, following equation The energy release rate, in mode II, is given by Equation 2 [8]:

$$G_{II_c} = \frac{9P^2a_{eq}^2}{4B^2E_1h^3}F_2 \tag{3}$$

being P the load, a_{eq} the length of the equivalent crack, b the specimen width, E_1 is an apparent longitudinal modulus, formulated by the same proposed CBBM model [8] of the substrates, h their thickness, B the specimen width, F_2 is the large displacements correction factor.

Combined test

Being a combination of the DCB and ELS configurations, this test procedure merges the boundary conditions of both tests. A folded Teflon® sheet with lubricant inside was also inserted in between the adherends of the ELS specimen at the pre-crack zone. The specimen is then loaded through the same pin, placed in the hole of the bottom substrate of the ELS specimen and the bottom substrate of the whole unified specimen, corresponding to the DCB part of the test is kept fixed, adding a fixture tool to the designed setup for the ELS test. These boundary conditions are presented in Figure 9.

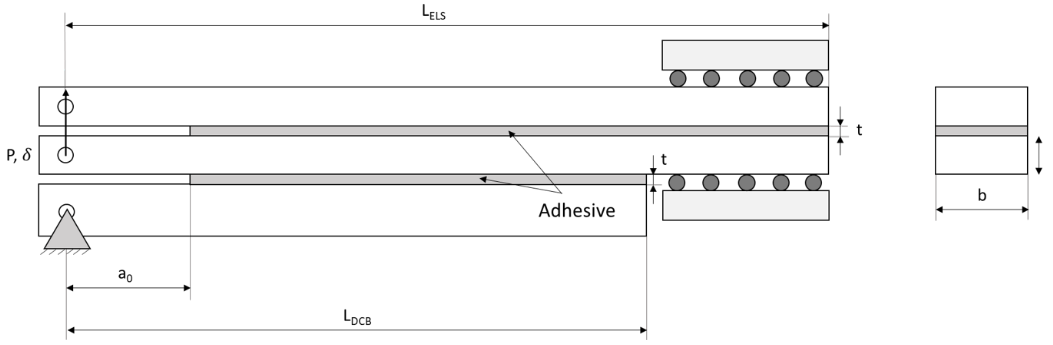

Figure 9: Representation of the combined test.

As described for the other tests, both load and displacement are recorded and, after separating the data related to mode I and mode II, the corresponding fracture energy release rate was computed using CBBM, whether for the DCB or the ELS components. The equations used were 1 and 3.

B.3 Developed code

The first main objective of developing a supporting code was to automate as much as possible the processing of the data reduction schemes and consequently directly obtain mode I and mode II energy release rate G_{I_c} and G_{II_c}. The reason behind the automation of this process is related to the great amount of raw data generated by the data acquisition setup and the considerable amount of mathematical manipulation needed to formulate some data reduction schemes, such as the compliance based beam method (CBBM). For example, for the end-loaded split test, depending on the acquisition rate of the machine, commonly more than 25000 frames of load-displacement are collected, which makes the use of conventional programs such as Excel to process this data needing a bigger computational effort. Furthermore, when using linear variable differential transformer (LVDT), some noise is observed in displacement measurement, so filtering must also be applied to the raw P-δ curve data. Furthermore, the CBBM data reduction scheme for G_{II_c} determination involves at least thirteen equations. The above mentioned reasons sustain the need for a code capable to automate this process. Therefore, a code was developed using Python, in an attempt to meet the previously defined requirements. Next, the functionalities of the developed program will be described.

Firstly when one runs the program, the following window represented in Figure 10 opens and it becomes possible to chose between 'Fracture Tests' and 'Strength tests', depending what kind of test one wants to analyse. A strength platform was also developed to compute strength and shear properties from other specimen configurations, however, for the purpose of this study, only the features related to fracture tests will be exposed.

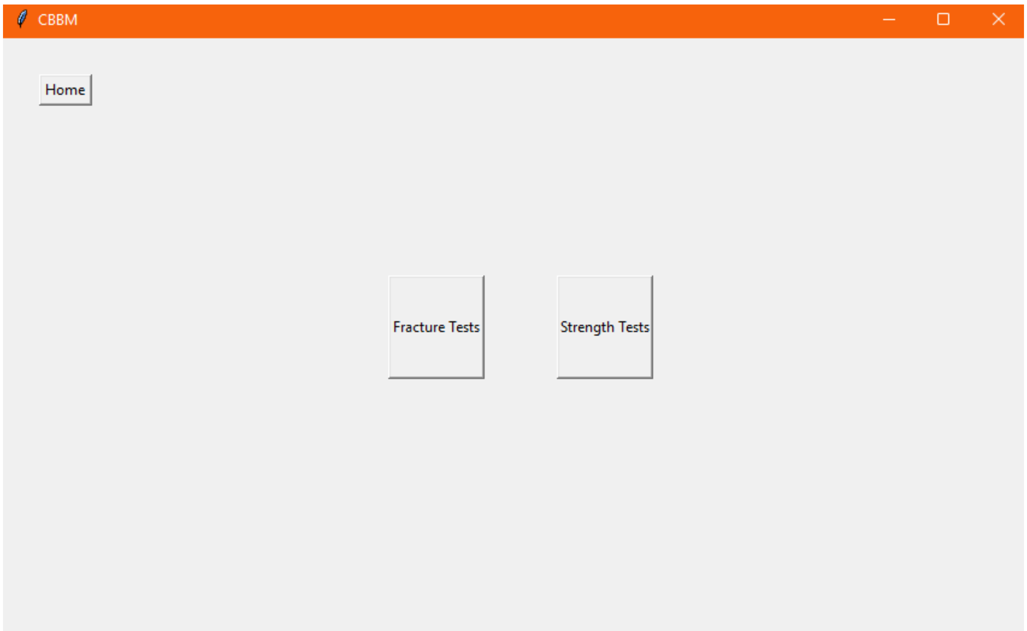

Figure 10: First interface of the program.

If 'Fracture Tests' is clicked, the initial window is close and another one opens, represented in Figure 11, related to the fracture tests.

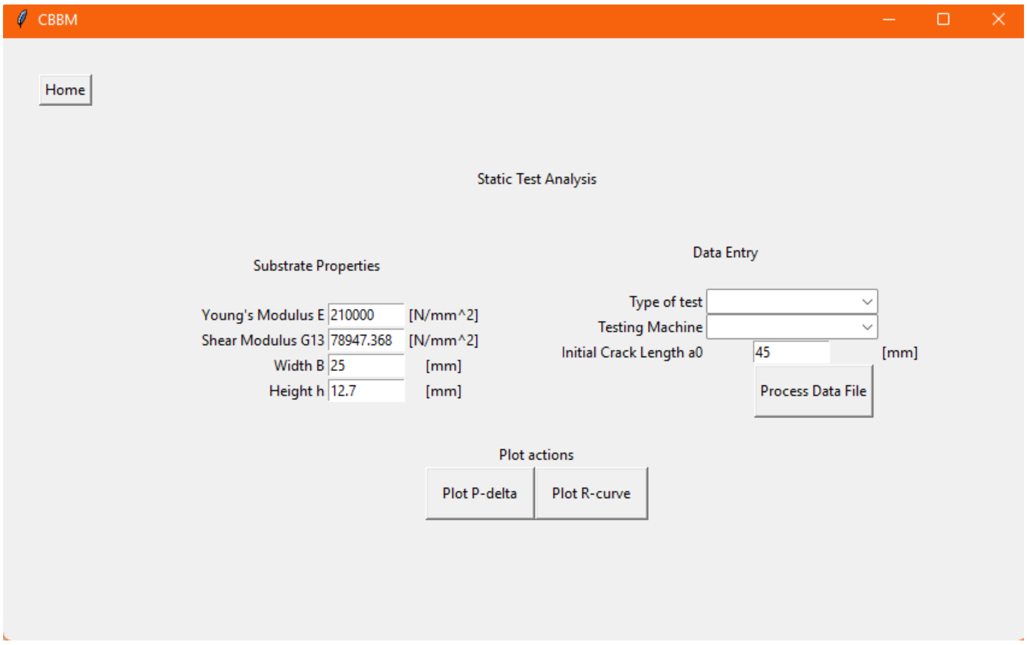

Figure 11: Fracture tests interface of the program.

The substrate properties can be inputted on the left textboxes and the initial crack length, an important parameter to use CBBM, can be introduced to the program via the textbox on the right. If no parameters are inputted by the user, default values are assumed, as can be seen. In 'Type of test' a combobox lets one chose which fracture test is going to be analysed: 'DCB', 'ENF' or 'ELS'. In 'Testing Machine' it is possible to chose between 'Hydraulic' or 'Electro-Mechanical', since the way data will be read in each case is different. The 'Home' button returns to the first window of the program. The next step concerns the processing of the raw data file, achieved by clicking on 'Process Data File', which opens another window as shown in Figure 12.

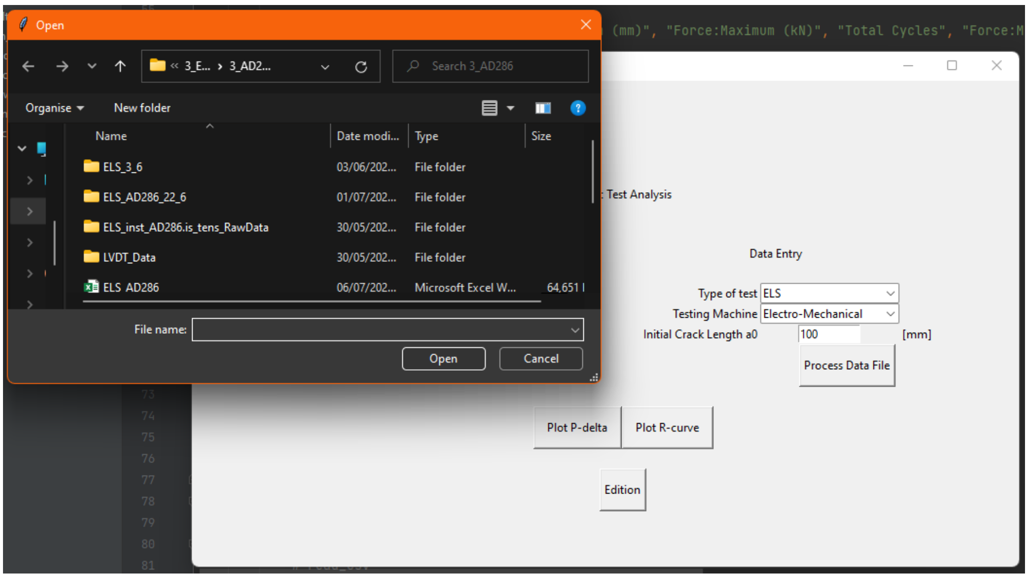

Figure 12: Window to choose the data file to be processed.

The program is prepared to read comma-separated values, commonly denoted as 'csv' files, the most common type of files that data acquisition systems provide. After clicking 'Open', the file is processed and the user can choose to plot the load-displacement curve in 'Plot P-delta'. After plotting the P-δ curve, the user can choose to either plot directly the R-curve or edit the first plot, by clicking 'Plot R-curve' or 'Edition', correspondingly. Figure 13 shows an example where the provided raw data needs some further edition.

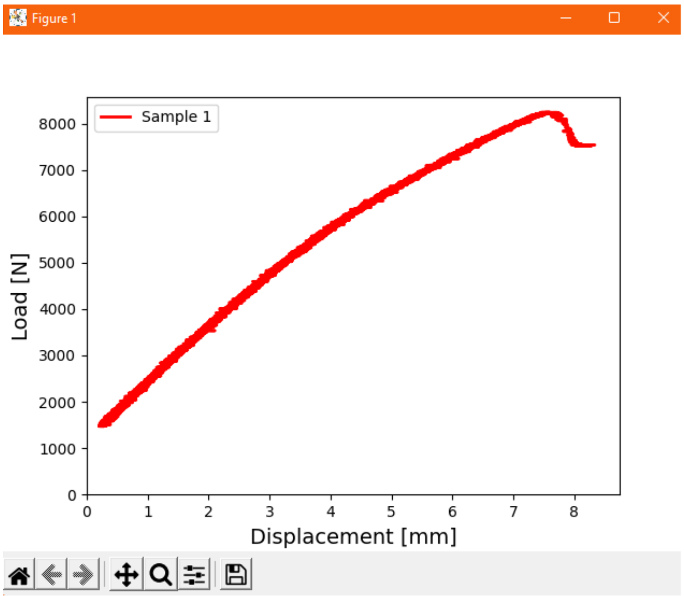

Figure 13: Raw data provided from the load cell.

As it can be seen, the initial slope, related the mechanical adjustments of the machine often does not fit the final slope prior to crack propagation. Accordingly, a linear regression and a displacement offset needs to be performed automatically. In addition, it is noticeable that there is noise related to the measurement of displacement using a LVDT and thus filtering can be applied, if needed.

In Figure 14 the edition page is presented with the features aforementioned.

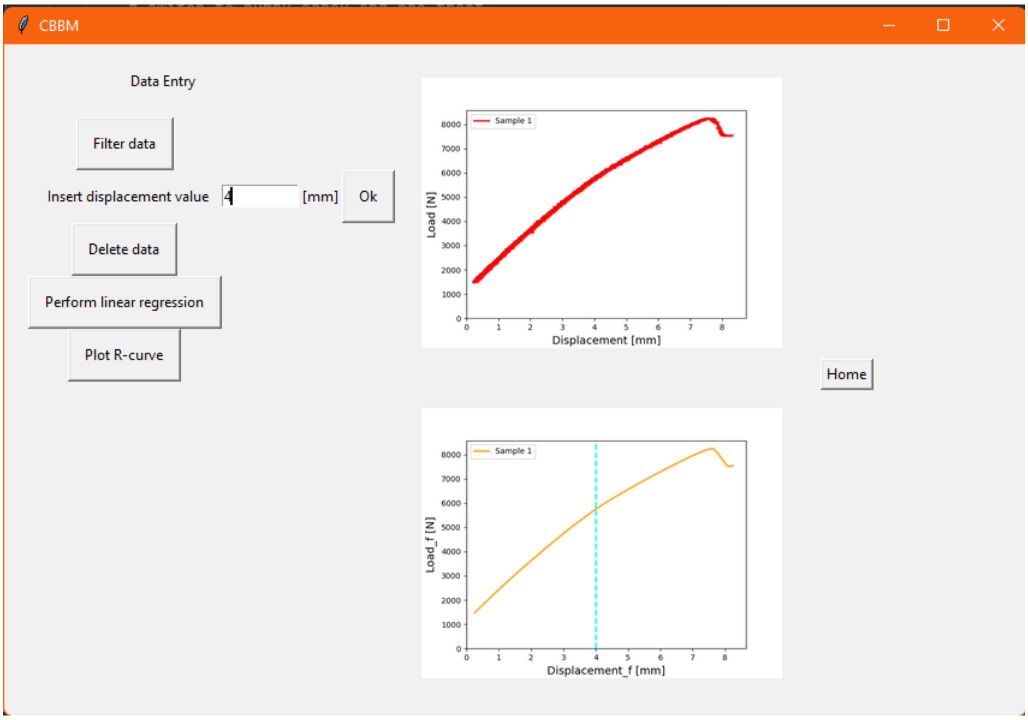

Figure 14: Edition page after applying filters to the raw data.

On the top right corner, the raw P-δ curve presented before in Figure 13 can be seen. Underneath that, the chart presented is already filtered (by clicking in 'Filter data') and a displacement value was inserted, as can be seen by the light blue line in the bottom chart, to request a deletion of the data related to displacements smaller than 4 mm. The filter used was the Savitzky-Golay Filter [20], generally indicated as the most suitable to smooth the inevitable noise present in the raw data.

Next, by clicking in 'Delete data' and 'Perform linear regression' the data related to displacements smaller than the indicated will be removed and a linear regression and positioning of the results to start in the origin of the x and y axes will be done. After that, it is possible to obtain the R-curve by clicking in 'Plot R-curve'. In Figure 15 it is possible to observe the aforementioned changes and the final R-curve on the bottom left corner.

Figure 15: Edition page after treating the raw data.

On the bottom left corner of the window the obtained R-curve is presented. Both the data related to the filtered and cleaned P-δ curve and the obtained R-curve are saved as 'csv' files in the same folder where the raw data is located.

B.4 Experimental results and discussion

In this section the experimental results stemming from the experimental procedures will be presented and analysed.

Firstly, the end-notched flexure test was performed for the brittle adhesive, since its fracture energy release rate in mode II was not yet experimentally characterised. Subsequently, and with both adhesives fully characterised, an end-loaded split test was performed for each of them, in order to validate the experimental setup. Then, since the setup used for the combined tests is the same as the ELS and is validated, the combined tests for mode I and II fracture toughness for both adhesives were carried out.

<u>**DCB test - brittle adhesive**</u>

As mentioned before, it was found necessary to characterise the fracture toughness of the brittle adhesive in mode I. Therefore, double cantilever beam tests were performed and a representative R-curve is presented in Figure 16.

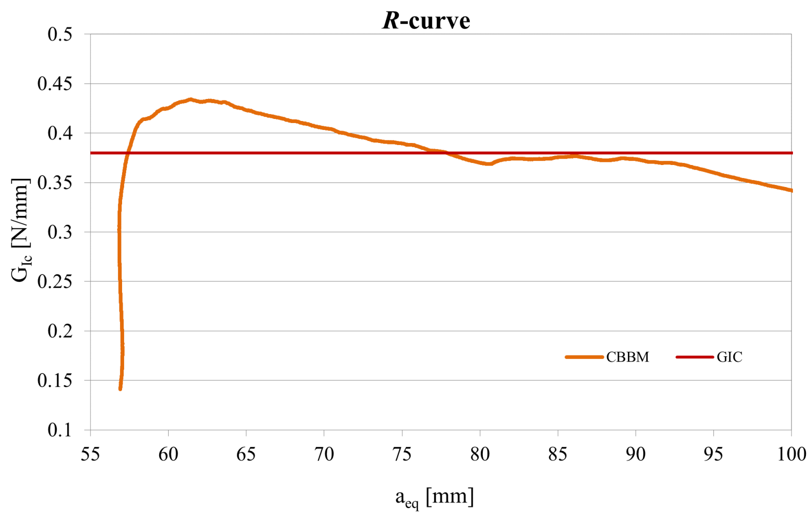

Figure 16: R-curve related to the DCB test of the brittle adhesive.

The obtained energy release rate in mode one was G_{I_c}, of $0.35 \pm 0.08\,\mathrm{N/mm}$.

ENF test - brittle adhesive

After assembling the specimen with the brittle adhesive in the load cell, following the procedures mentioned in section B.2.3, the load-displacement curve was recorded. A representative curve is presented in Figure 17.

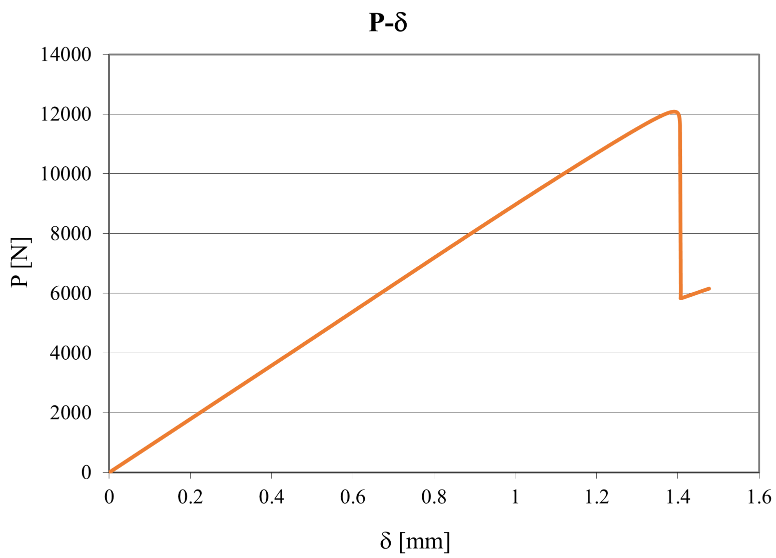

Figure 17: P-δ curve related to the ENF test of the brittle adhesive.

As it can be seen, once the specimen reaches the maximum load around 12 kN, the crack propagation is initiated and it is clear that this material has a brittle behaviour, since there is a sudden decrease in the load, typical of brittle adhesives. This fast and unstable crack propagation process is one of the main disadvantages of ENF tests, leading to a very limited number of data points during this phase. This created difficulties when computing its corresponding R-curve, which is shown in Figure 18.

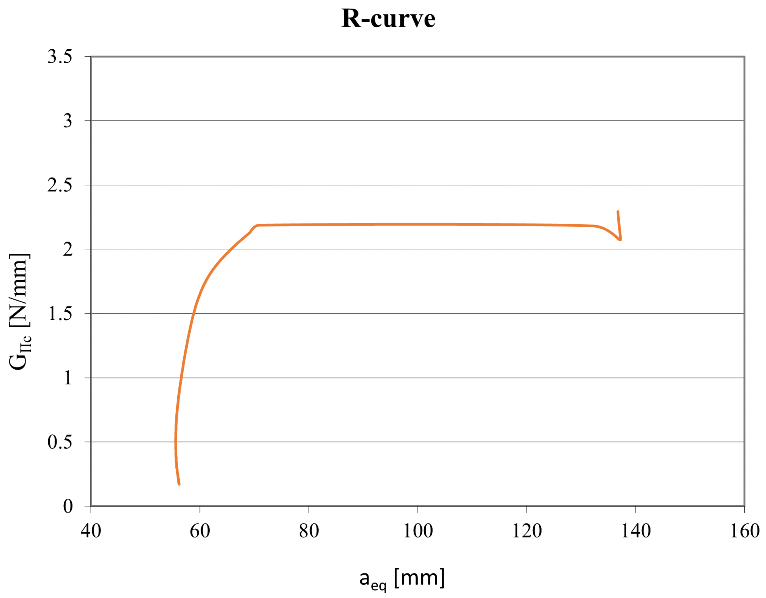

Figure 18: R-curve related to the ENF test of the brittle adhesive.

The flattened plateau is a result of the low number of data points captured during the brittle failure of the adhesive. However, from all the data extracted from the tests, it was possible to obtain a fracture energy release rate in mode II, G_{II_c}, of $2.34 \pm 0.38\,\mathrm{N/mm}$.

ELS test - brittle adhesive

Having characterised the mode II fracture toughness of the brittle adhesive, an ELS test was then performed in order to compare results and validate the developed setup. In Figure 19 is presented a representative P-δ curve of these tests.

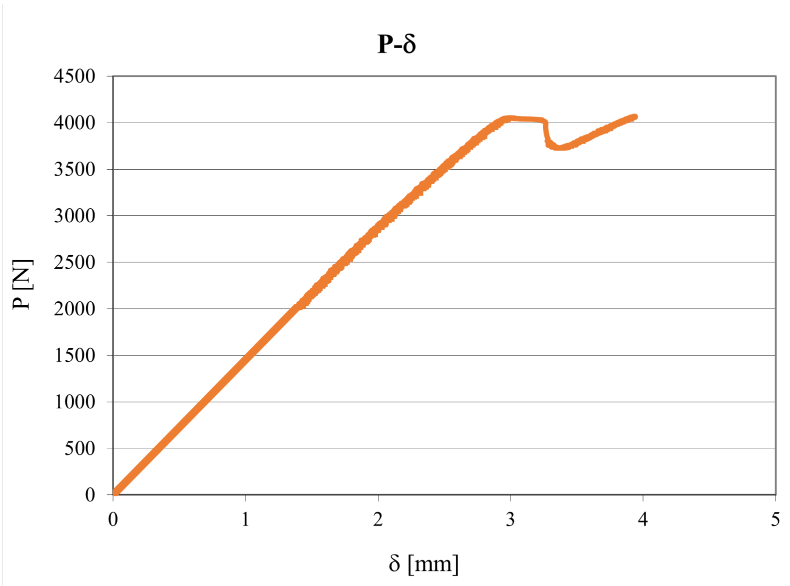

Figure 19: P-δ curve related to the ELS test of the brittle adhesive.

It can be observed that the maximum load that the specimen sustains is approximately one third of the maximum load attained in the ENF. However, when analysing the displacement measured, it can be seen that the displacement needed to reach the maximum load in each test also differs, being the displacement corresponding to the maximum load in the ELS test almost three times larger then what is observable on the ENF test. These differences are mainly a consequence of the loading conditions used for each test, where in the ELS the total length for crack propagation is much larger than the one presented by the ENF test and, therefore, there is a smoother behaviour of the P-δ. In Figure 20 is presented to corresponding R-curve for this test.

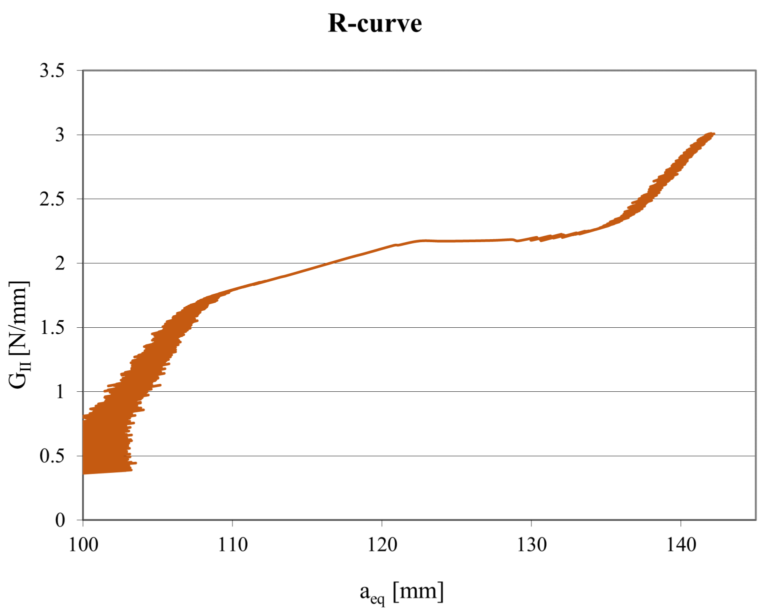

Figure 20: R-curve related to the ELS test of the brittle adhesive.

As it can be seen, there is a pronounced and clear plateau since the number of data points gathered is greater than was the case for the ENF test. However, given the nature of the adhesive, it can be said that the amount of points is still not satisfactory, even with noticeable improvements. From the experimental procedure of this test was possible to achieve a G_{II_c} of 2.35 ± 0.24 N/mm, which presented a good correlation with the results obtained for the ENF test, thus validating the new setup.

ELS test - ductile adhesive

Concerning the ductile adhesive, a reference value was given for G_{II_c} from previous works as presented in Table 2. A representative P-δ curve is presented in Figure 21.

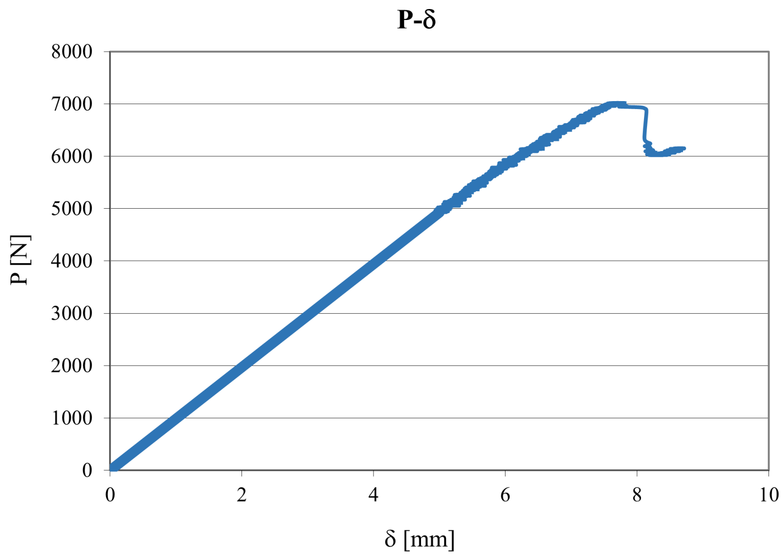

Figure 21: P-δ curve related to the ELS test of the ductile adhesive.

As expected, the maximum load reached and the corresponding displacement were significantly higher than that of the brittle adhesive since the fracture toughness in mode II for the ductile adhesive is greater. By comparing the initial slopes, it can be observed that the brittle adhesive confers a higher stiffness to the specimen, as is expected. It is also important to denote that during the experimental work, some plastic deformation in the substrate was observed. This led to an overestimation of the fracture toughness in mode II for this adhesive, since the substrate also absorbed part of the energy. In Figure 22 the correspondent R-curve is presented.

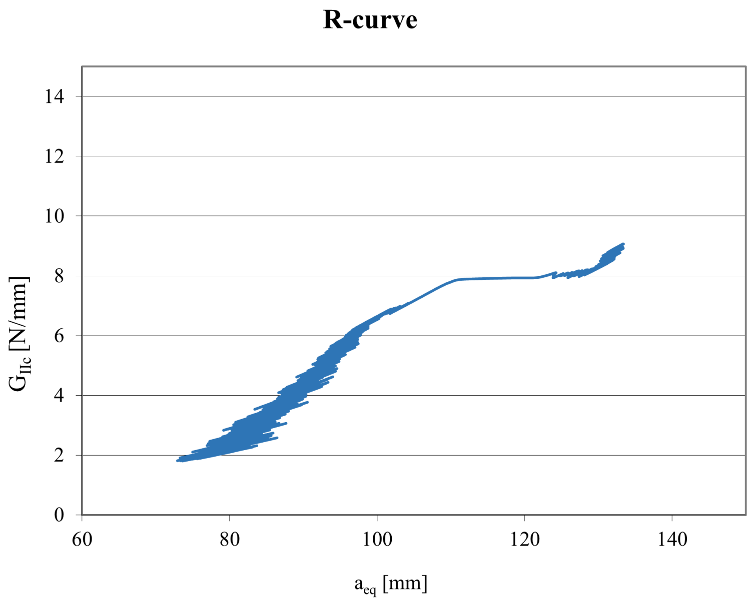

Figure 22: R-curve related to the ELS test of the ductile adhesive.

As stated above, the above curve does not quite represent the energy release rate in mode II of the adhesive as the substrates of the specimen suffered plastic deformation. This implies that the G_{II_c} was overestimated to $7.60 \pm 1.23\,\mathrm{N/mm}$. The solution to this issue lies in the use of steel substrates manufactured from higher strength steel, a process which was not concluded with the time window available for the present work.

Combined mode I and mode II test - brittle adhesive

As previously mentioned, in the combined test, the mode I and II fracture tests, the DCB and ELS, are effectively merged in the same specimen, allowing a faster characterisation of the fracture properties. Both tests are performed sequentially and the load-displacement curve is registered by the load cell, as in Figure 23.

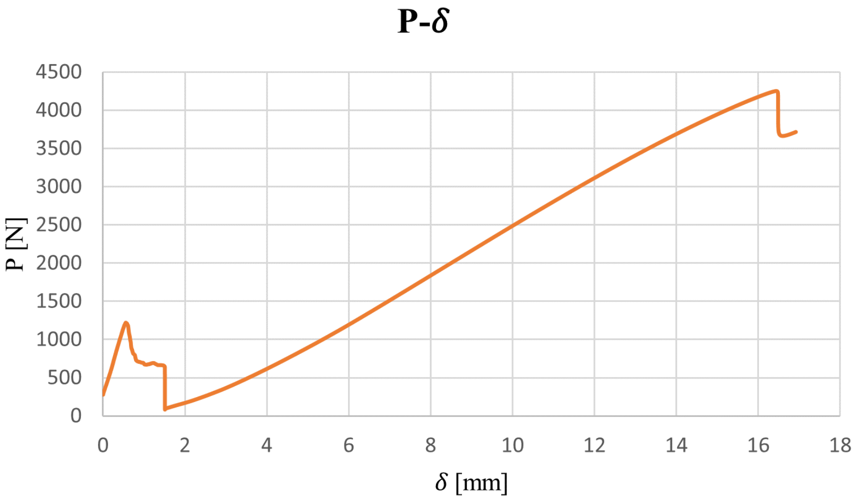

Figure 23: P-δ related to the combined test of the brittle adhesive.

It is possible to denote that the mode I fracture test occurs between 0 and 1.8 mm and the mode II fracture test, the ELS, occurs immediately after that, being possible to observe an adjustment of the initial slope of this test. The displacements shown are from the testing machine crosshead and, therefore, will not be used for the calculations. The resultant testing data was then split into two regions and treated separately, the DCB using DIC technique and the ELS displacement using a LVDT. Firstly, a representative R-curve related to the DCB part of the combined test is presented in Figure 24.

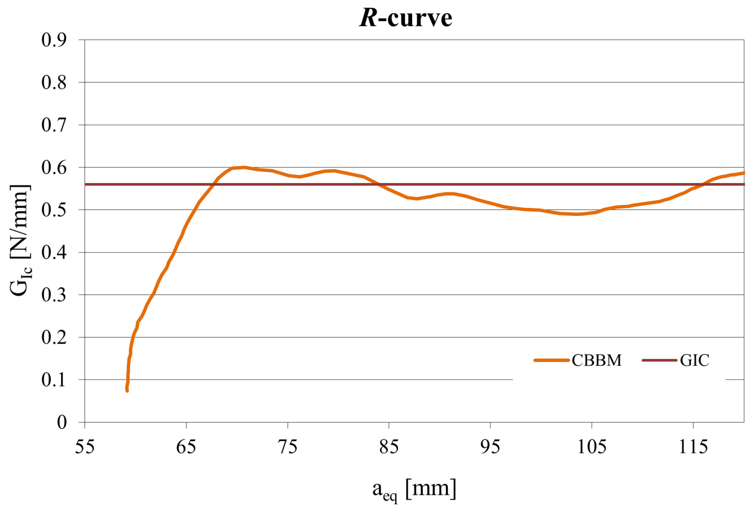

Figure 24: R-curve related to the DCB test of the brittle adhesive.

An overestimation of the fracture energy release rate in mode I, G_{I_c}, was observed for all the tests performed, $0.40 \pm 0.14\,\mathrm{N/mm}$. After looking further in detail to all the processes concerning this combined test, from manufacturing to testing procedure and data analysis, it was detected that, in fact, the type of test being performed is not purely mode I. The bottom and upper substrate of the DCB do not have the same thickness and, when computing the CBBM, a medium thickness of both substrates was used. Being so, the difference between their stiffness was not considered to the model, since the formulation pondered two equal substrates with an average thickness of the two substrates utilised. A difference in stiffness, driven not only because the substrate's thickness but also by the fact that there is an additional adhesive layer in the ELS part of the test, lead to some degree of mode mixity in the mode I test, making it closer in nature to an asymmetric double cantilever beam (ADCB) test. This limitation requires future changes to the data reduction method and possibly a direct tracking of the crack progression [21].

Regarding the part related to fracture energy release rate in mode II, a representative P-δ curve is presented in Figure 25, where the displacement was measured using a LVDT.

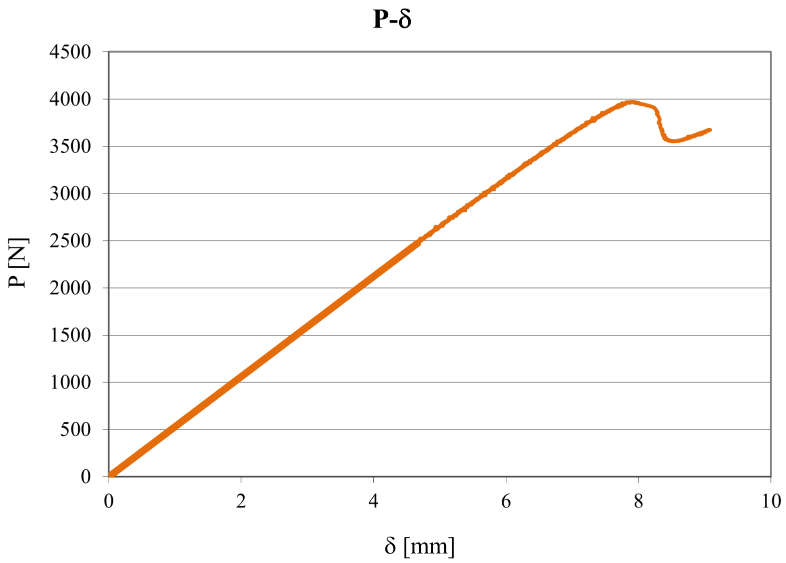

Figure 25: P-δ curve related to the ELS test of the brittle adhesive.

By comparing this P-δ curve with the one in Figure 19, regarding the isolated ELS test for the same adhesive, it is noticeable a large difference between the displacement needed to reach the maximum load, where, for the case of the isolated test, the displacement needed is more than a half than the one needed to attain the same maximum load for the combined test. This is explained by the fact that the ELS specimen of the combined test is less stiff than the isolated one, since the substrate's thickness are smaller and, therefore, the displacement is significantly affected. The large deflection imposed on the specimen will increase, offering instability to the crack propagation, since the specimen gets stiffer due to the bending force [14]. The corresponding R-curve is presented in Figure 26.

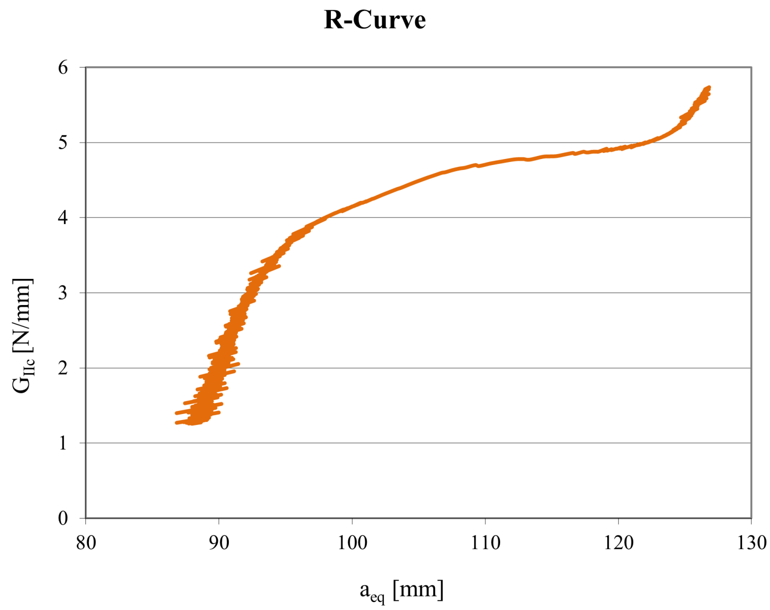

Figure 26: R-curve related to the ELS test of the brittle adhesive.

As expected, the energy release rate in mode II was overestimated and the results obtained were 4.18 ± 0.37 N/mm. Designing a thicker specimen would be a good approach so address this problem, however, further investigation would have to relate the other geometric parameters involved.

Combined mode I and mode II test - ductile adhesive

Similarly to the obtained P-δ curve for the combined test of the brittle adhesive, it is also possible to distinguish both mode I and mode II tests in Figure 27.

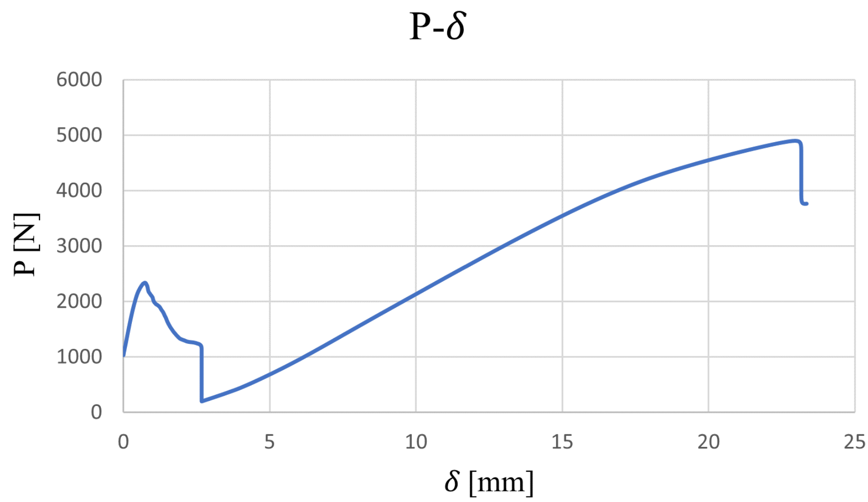

Figure 27: P-δ related to the combined test of the ductile adhesive.

Both tests were then analysed separately, similarly to what was done for the same kind of test for the brittle adhesive. In the following Figure 28.

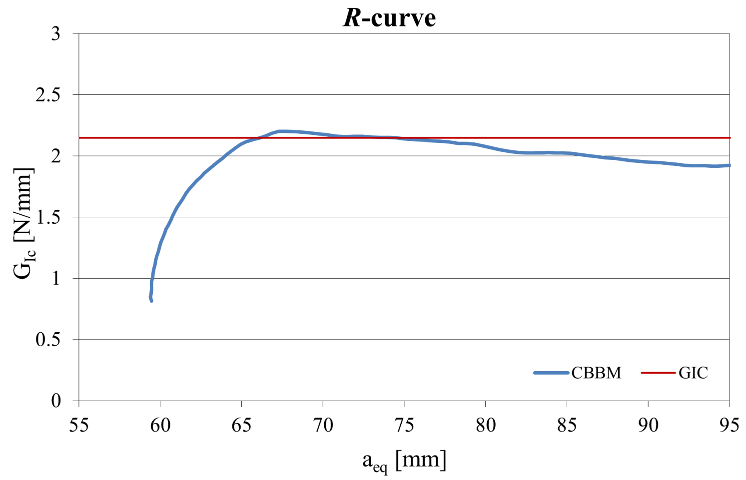

Figure 28: R-curve related to the DCB test of the ductile adhesive.

As expected, the mode I obtained results for this adhesive were also found to be above the tabulated value for G_{I_c}, being $2.35 \pm 0.22\,\text{N/mm}$. Likewise for the brittle adhesive, the mode I data reduction procedure can be improved with the consideration of a data reduction scheme which is suitable for an ADCB type of configuration.

In the next Figure 29, a representative P-δ curve related to the mode II fracture test for the ductile adhesive is presented.

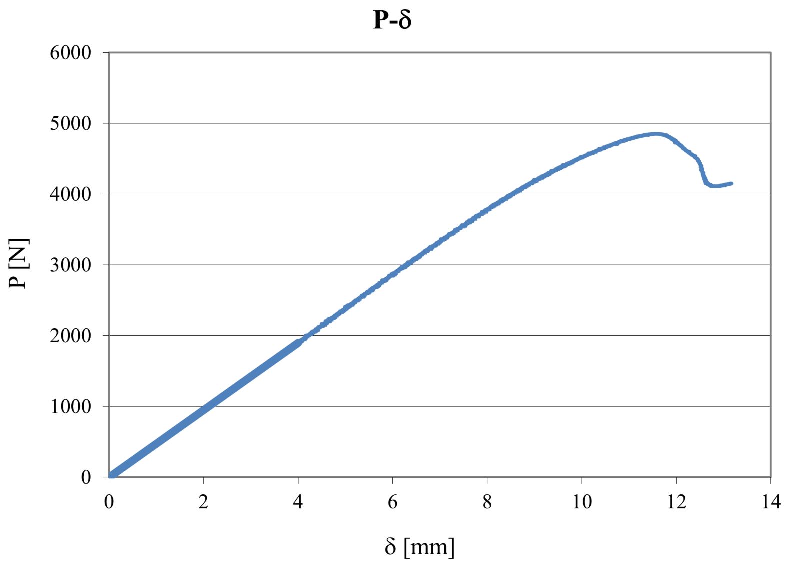

Figure 29: P-δ curve related to the ELS test of the ductile adhesive.

Similarly to what happened for the isolated test for this adhesive, there was plastic deformation of the substrate, promoted and exacerbated by the significantly higher displacement involved in this kind of combined test, as can also be directly observed in the Figure 27. Nevertheless, the corresponding R-curve is presented in Figure 30.

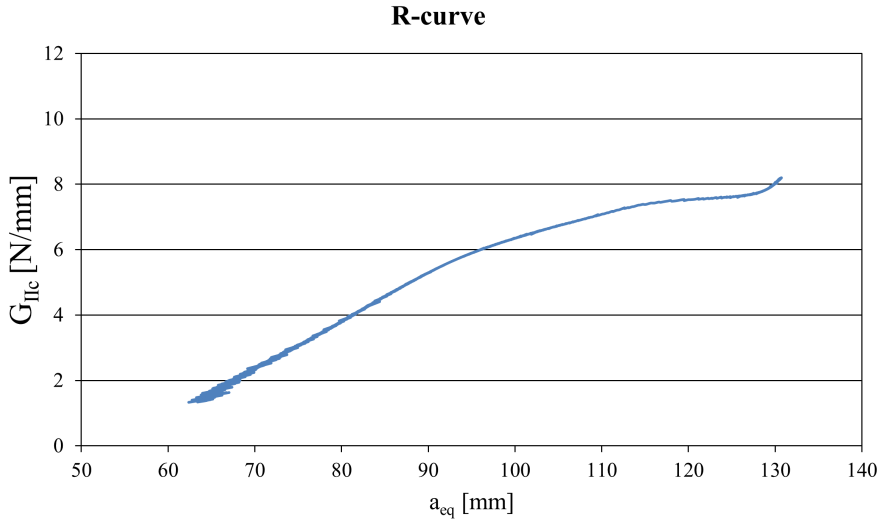

Figure 30: R-curve related to the ELS test of the ductile adhesive.

The G_{II_c} obtained was $10.70 \pm 2.49\,\mathrm{N/mm}$, which was fairly far from the tabulated value. For the same reason, it was not possible to arrange a new and toughened substrate material within the time frame of this work.

B.5 Conclusions

In this experimental study, the ELS test procedure was firstly compared with the ENF test for two different structural adhesives. The ELS procedure was found to offer more stable crack propagation and, therefore, the determination of more consistent plateaus on the R-curves for G_{II_c} extraction. The new apparatus for ELS testing was validated using only the brittle adhesive, since in the ductile adhesive test plastic deformation on the substrates was observed. The second part of the work was devoted to the validation of an unified specimen, intended to be used for mode I and II fracture toughness characterisation of both adhesives. During testing, it was possible to observe the two phases, with two distinct behaviours corresponding to the DCB and ELS tests. However, it was observable that, for both adhesives, the energy release rate in mode I was overestimated by the use of a simplified data reduction scheme. In fact, the ELS specimen introduces a different stiffness to the upper substrate of the double cantilever beam and the assumption of symmetry in the substrates is not entirely accurate, behaving in a manner closer of an asymmetric double cantilever beam. The data reduction scheme related to this last test enables separating the mode mixity into the contributions of mode I and mode II of the test, however, the method is not crack independent and implies that crack propagation of the bottom part of the unified specimen is monitored during the experimental test. Another issue arose with the ELS part of the unified specimen, where, for the brittle adhesive, since the substrate thickness was smaller, the deflection imposed was significantly higher than for the isolated test (with thicker substrates). This larger deflection not only introduced further instability to the test, but also added stiffness to specimen, due to the bending force imposed, resulting in an overestimation of the G_{II_c}. For the case of the ductile adhesive, the specimen underwent plastic deformation when testing, overestimating, again, the fracture energy release rate in mode II of this adhesive. Nonetheless, this initial approach has successfully demonstrated the potential of this concept, which will be modified to account for these findings.

References

[1] da Silva LFM, Öchsner A, and Adams RD. *Handbook of adhesion technology.* Springer, 2018.

[2] Moore DR, Pavan A, and Williams JG. *Fracture Mechanics Testing Methods for Polymers Adhesives and Composites.* ESIS Publication 28, 2006.

[3] de Moura MFSF, Campilho RDSG, and Gonçalves JPM. Crack equivalent concept applied to the fracture characterization of bonded joints under pure mode i loading. *Composites Science and Technology*, 68(10-11):2224–2230, 2008.

[4] da Silva LFM, Dillard DA, Blackman BRK, and Adams RD. *Testing adhesive joints: best practices.* John Wiley & Sons, 2012.

[5] Chaves FJP, da Silva LFM, de Moura MFSF, Dillard DA, and Esteves VHC. Fracture Mechanics Tests in Adhesively Bonded Joints: A Literature Review. *The Journal of Adhesion*, pages 1–39, June 2014.

[6] Pérez-Galmés M, Renart J, Sarrado C, Rodríguez-Bellido A, and Costa J. A data reduction method based on the j-integral to obtain the interlaminar fracture toughness in a mode ii end-loaded split (els) test. *Composites Part A: Applied Science and Manufacturing*, 90:670–677, 2016.

[7] Silva MAL, Morais JJL, de Moura MFSF, and Lousada JL. Mode ii wood fracture characterization using the els test. *Engineering fracture mechanics*, 74(14):2133–2147, 2007.

[8] de Moura MFSF and de Morais AB. Equivalent crack based analyses of enf and els tests. *Engineering Fracture Mechanics*, 75(9):2584–2596, 2008.

[9] Blackman BRK, Brunner AJ, and Williams JG. Mode ii fracture testing of composites: a new look at an old problem. *Engineering fracture mechanics*, 73(16):2443–2455, 2006.

[10] de Moura MFSF, Dourado N, Morais JJL, and Pereira FAM. Numerical analysis of the enf and els tests applied to mode ii fracture characterization of cortical bone tissue. *Fatigue & Fracture of Engineering Materials & Structures*, 34(3):149–158, 2011.

[11] El Moustaphaoui A and Chouaf Aand Kimakh K. Experimental and numerical study of the delamination of ceiba plywood under mode i, mode ii and mixed-mode (i+ ii) loading using the dcb, els and mmf tests. *International Journal of Fracture*, 231(1):1–20, 2021.

[12] Blackman BRK, Kinloch AJ, and Paraschi M. The determination of the mode ii adhesive fracture resistance, giic, of structural adhesive joints: an effective crack length approach. *Engineering Fracture Mechanics*, 72(6):877–897, 2005.

[13] Toolabi M and Blackman BRK. Guidelines for selecting the dimensions of adhesively bonded en-loaded split joints: An approach based on numerical cohesive zone length. *Engineering Fracture Mechanics*, page November, June 2018.

[14] Pérez-Galmés M, Renart J, Sarrado C, and Costa J. Suitable specimen dimensions for the determination of mode II fracture toughness of bonded joints by means of the ELS test. *Engineering Fracture Mechanics*, 202, July 2018.

[15] da Silva LFM, da Silva RAM, Chousal JAG, and Pinto AMG.

[16] Correia DS, Carbas RJC, Marques EAS, das Neves PJC, and da Silva LFM. Experimental study on aluminium to tungsten carbide/polycrystalline diamond (wc/pcd) adhesive bonding for milling tools. *International Journal of Adhesion and Adhesives*, 114:103121, 2022.

[17] Banea MD, da Silva LFM, and Campilho RDSG. Moulds design for adhesive bulk and joint specimens manufacturing. *Assembly Automation*, 2012.

[18] ASTM Standard. D3433-99: Standard test method for fracture strength in cleavage of adhesives in bonded metal joints, astm international, west conshohocken, pa, 2012.

[19] Costa M, Carbas RJC, Benedita M, Marques EAS, Viana G, da Silva LFM, Yokoi E, Nakada S, and Furusawa T. Static assessment of the mixed-mode behaviour of three epoxy adhesives. *Engineering Fracture Mechanics*, 182:552–565, 2017.

[20] Schafer RW. What is a savitzky-golay filter?[lecture notes]. *IEEE Signal processing magazine*, 28(4):111–117, 2011.

[21] Zugliani PA, Banea MD, Budhe S, Carbas RJ, da Silva LFM, Rohem NRF, and de Barros S. Bonded composite repair of metallic pipeline using energy release rate method. *Journal of Adhesion Science and Technology*, 33(19):2141–2156, 2019.

C Developed code using Python

```
import matplotlib
import pandas as pd
from PIL.Image import Resampling
from PIL._imaging import display
from matplotlib import pyplot as plt
import numpy as np
import start as start
from matplotlib import pyplot as plt
import tkinter as tk
from tkinter import ttk
import tkinter.filedialog
from PIL import ImageTk, Image


# basic treatment of results, take P-delta and align with origin
def read_results(test_kind, machine, type_test):
    # input file
    print("Select results file")
    appwindow = tk.Tk().withdraw()
    result_file = tk.filedialog.askopenfilename()
    # print directory for checking
    print(result_file)

    global results
    # read file

    if type_test == "DCB":
        print('This is DCB')
        if machine == "Electro-Mechanical":
            # read_csv
            results = pd.read_csv(result_file, skiprows=3,
            delimiter=',',encoding="utf-8-sig")
        else:
            results = pd.read_csv(result_file, skiprows=0,
            delimiter=',', encoding="utf-8-sig")
        if test_kind == "fatigue":
```

```
        results = results[["Displacement:Maximum (mm)",
        "Force:Maximum (kN)", "Total Cycles",
        "Force:Minimum (kN)"]]
        # switch to numpy array and pre-treat
        results = results.to_numpy()
        results = results.astype(float)
        results[:, 1] = results[:, 1] * 1000
        results[:, 3] = results[:, 3] * 1000

    elif machine == "Hydraulic":

        results = results[["Position (mm)", "Force (kN)"]]

        results = results.to_numpy()
        results = results.astype(float)
        results[:, 1] = results[:, 1] * 1000

    else:

        results = results[["Extension", "Load"]]
        results.drop(labels=None, axis=0, index=0,
        inplace=True)
        print(results)
        results = results.to_numpy()
        results = results.astype(float)
elif type_test == 'ELS':
    print('This is ELS')
    if machine == "Electro-Mechanical":
        # read_csv
        results = pd.read_csv(result_file, skiprows=3,
        delimiter=',', encoding="utf-8-sig")
    else:
        results = pd.read_csv(result_file, skiprows=0,
        delimiter=',', encoding="utf-8-sig")
    if test_kind == "fatigue":

        results = results[["Displacement:Maximum (mm)",
        "Force:Maximum (kN)", "Total Cycles",
        "Force:Minimum (kN)"]]
```

```
        # switch to numpy array and pre-treat
        results = results.to_numpy()
        results = results.astype(float)
        results[:, 1] = results[:, 1] * 1000
        results[:, 3] = results[:, 3] * 1000

    elif machine == "Hydraulic":

        results = results[["Position (mm)", "Force (kN)"]]

        results = results.to_numpy()
        results = results.astype(float)
        results[:, 1] = results[:, 1] * 1000

    else:

        results = results[["Extension", "Load"]]
        results.drop(labels=None, axis=0, index=0,
        inplace=True)
        print(results)
        results = results.to_numpy()
        results = results.astype(float)
elif type_test == 'ENF':
    print('This is ENF')
    if machine == "Electro-Mechanical":
        # read_csv
        results = pd.read_csv(result_file, skiprows=0,
        delimiter=',', encoding="utf-8-sig")
    else:
        results = pd.read_csv(result_file, skiprows=0,
        delimiter=',', encoding="utf-8-sig")
    if test_kind == "fatigue":

        results = results[["Displacement:Maximum (mm)",
        "Force:Maximum (kN)", "Total Cycles",
        "Force:Minimum (kN)"]]
        # switch to numpy array and pre-treat
        results = results.to_numpy()
        results = results.astype(float)
        results[:, 1] = results[:, 1] * 1000
```

```
            results[:, 3] = results[:, 3] * 1000

        elif machine == "Hydraulic":

            results = results[["Position␣(mm)", "Force␣(kN)"]]

            results = results.to_numpy()
            results = results.astype(float)
            results[:, 1] = results[:, 1] * 1000

        else:

            results = results[["Extension", "Load"]]
            results.drop(labels=None, axis=0, index=0,
            inplace=True)
            print(results)
            results = results.to_numpy()
            results = results.astype(float)


        results[:, 0] *= -1
        results[:, 1] *= -1
        print(results)


    pd.options.display.max_columns = 999
    print("Results:␣\n", results)



    return results



# CBBM calculations for GIc

def cbbm(type_test, results, test_kind, a0, machine):
    if type_test == 'DCB':
        crack_length, G, GIc = dcb_cbbm(results, test_kind, a0,
        machine)
```

```
        plotcbbm_dcb(crack_length, G, GIc)
    elif type_test == 'ENF':
        aeq, G, GIIc = enf_cbbm(results, test_kind, a0, machine)
        plotcbbm_enf_els(aeq, G, GIIc)
    elif type_test == 'ELS':
        aeq, G, GIIc = els_cbbm(results, test_kind, a0, machine)
        plotcbbm_enf_els(aeq, G, GIIc)


def dcb_cbbm(results, test_kind, a0, machine, GIc=0):
    global crack_length, G, GIC
    # unchanging values about the specimens
    E1 = 210000
    E2 = 210000
    G13 = E1 / (2 * (1 + 0.33))
    width = 25
    B = 25
    L = 290
    height1 = 12.7
    # height2 = 12.7
    heightmed = height1  # (height1 + height2)/2



    # calculate compliance and reference compliance
    (graph minimum)
    compliance = np.divide(results[:, 0], results[:, 1])
    print("compliance")
    print(compliance)

    if machine == "Electro-Mechanical":

        reference_compliance = min(compliance[300:15000])
    else:

        reference_compliance = min(compliance[3000:70000])

    # calculating a few constants
    T = 1.18 * np.sqrt(E1 * E2) / G13
    D3 = height1 * np.sqrt(E1 / 11 / G13 *
    (3 - 2 * (T / (1 + T))) * 2)
```

```
Ef = (reference_compliance - 12 * (a0 + abs(D3)) /
(5 * B * heightmed * G13)) ** (-1) * 8 * (a0 + abs(D3))
** 3 / (B * heightmed ** 3)

a = 8 / (B * heightmed ** 3 * Ef)
b = 12 / (5 * B * heightmed * G13)

# a few more values from the compliance
g = -compliance
A = ((-108 * g + 12 * np.sqrt(3 * (4 * b ** 3 + 27 * a
* g ** 2) / a)) * a ** 2) ** (1 / 3)

# calculate crack length
crack_length = A / (6 * a) - 2 * b / A

# clean some values
crack_length[np.isnan(crack_length)] = 0
crack_length[np.isinf(crack_length)] = 0

load = results[:, 1]

# calculate G
G = np.multiply(6 * np.power(load, 2) / (B ** 2 * heightmed),
(2 * np.power(crack_length, 2) / (heightmed ** 2 * Ef) + 1 /
(5 * G13)))

if test_kind != "fatigue":

    # np.savetxt("crack.csv", G, delimiter=",")
    # set crack length limits for calculation of GIC,

    then calculate

    if machine == "Electro-Mechanical":
        start = np.where(crack_length.astype(int)
        == 95)[0][0]
        end = np.where(crack_length.astype(int)
        == 120)[0][0]
```

```
        else:
            start = np.where(crack_length.astype(int)[5000:]
            == 95)[0][0] + 5000
            end = np.where(crack_length.astype(int)[5000:]
            == 120)[0][0] + 5000

        print("start: \n", start, "\n End: \n", end)
        GIC = np.mean(G[start:end])
        print("GIC: ", GIC)

    return [crack_length, G, GIC]


# CBBM calculations for GIIc (ENF + ELS)

def enf_cbbm(results, test_kind, a0, machine, GIIc=0):
    global aeq, G
    # unchanging values about the specimens
    E1 = 210000
    E2 = 210000
    G13 = E1 / (2 * (1 + 0.33))
    width = 25
    L = 130
    B = 25
    height1 = 12.7
    # height2 = 12.7
    heightmed = height1  # (height1 + height2)/2



    # calculate compliance and reference compliance
    (graph minimum)

    compliance = np.divide(results[:, 0], results[:, 1])

    if machine == "Electro-Mechanical":

        reference_compliance = min(compliance[300:15000])
    else:
```

```
        reference_compliance = min(compliance[3000:70000])

    # calculating a few constants
    I = B * ((2 * heightmed) ** 3) / 12
    print('I = ' + str(I))

    Ef = (3 * a0 ** 3 + 2 * L ** 3) / (12 * I) *

    np.power((reference_compliance - (3 * L) /
    (5 * G13 * B * heightmed)), -1)

    Cc = compliance - 3 * L / (5 * G13 * B * heightmed)
    C0c = reference_compliance - 3 * L /
    (5 * G13 * B * heightmed)
    aeq = np.power((np.divide(Cc, C0c) * (a0 ** 3) + 2 / 3 *
    (L ** 3) * (np.divide(Cc, C0c) - 1)), (1 / 3))

    # clean some values
    aeq[np.isnan(aeq)] = 0
    aeq[np.isinf(aeq)] = 0

    load = results[:, 1]

    # calculate G
    G = 9 * np.power(load, 2) * np.power(aeq, 2) /
    (16 * Ef * (B ** 2) * heightmed ** 3)

    print("GIIc: ", GIIc)

    return [aeq, G, GIIc]


def els_cbbm(results, test_kind, a0, machine, GIIc=0):
    global aeq, G
    # unchanging values about the specimens
    E1 = 210000
    E2 = 210000
    L = 220
    G13 = E1 / (2 * (1 + 0.33))
    width = 25
```

```
B = 25
height1 = 12.7
# height2 = 12.7
heightmed = height1  # (height1 + height2)/2

print('This is cbbm for ELS')
#input initial crack length

# displacement
displacement = results[:, 0]
print('results 0')
print(results[:, 0])
print('results 1')
print(results[:, 1])
# calculate compliance and reference compliance
(graph minimum)

compliance = np.divide(results[:, 0], results[:, 1])

if machine == "Electro-Mechanical":
    reference_compliance = min(compliance[300:15000])
else:
    reference_compliance = min(compliance[3000:70000])

# calculating a few constants



N2_1st = 1
Cc_1st = np.divide(compliance, N2_1st) - 3 * L /
(5 * G13 * B * heightmed)
C0c = np.divide(reference_compliance, N2_1st) -
3 * L / (5 * G13 * B * heightmed)
Ef = (3 * a0 ** 3 + L ** 3) /
((2 * B * heightmed ** 3 * C0c) - 1)



help = np.multiply(Ef * B * heightmed ** 3, Cc_1st)
aeq_1st = np.power((2 / 3) * help, (1 / 3))
a_L = np.divide(aeq_1st, L)
fi_5 = 36 / 35 * ((1 + (7 / 8 * np.power(a_L, 3))
```

```
    * (35 + 182 * np.power(a_L, 2) + 367 * np.power(a_L, 4)))
    / np.power((1 + np.power(a_L, 3)), 3))
    fi_1 = 3 / 20 * np.divide((15 + 50 * np.power(a_L, 2)
    + 63 * np.power(a_L, 4)),
    np.power((1 + 3 * np.power(a_L, 3)), 2))
    N2 = 1 - np.multiply(fi_5, np.power(np.divide
    (displacement, L), 2))
    F2 = 1 - np.multiply(fi_1,
    np.power(displacement / L, 2))
    Cc = np.divide(compliance, N2) - 3 * L /
    (5 * G13 * B * heightmed)
    help_2 = np.divide(compliance, C0c)
    aeq = np.power((help_2 * (a0 ** 3) + 1 / 3 * (L ** 3)
    * (np.divide(Cc, C0c) - 1)), (1 / 3))

    # clean some values
    aeq[np.isnan(aeq)] = 0
    aeq[np.isinf(aeq)] = 0

    load = results[:, 1]

    # calculate G
    G = 9 * np.power(load, 2) * np.power(aeq, 2) /
    (4 * (B ** 2) * Ef * heightmed ** 3) * F2

    if test_kind != "fatigue":

        np.savetxt("crack.csv", G, delimiter=",")
        # set aeq limits for calculation of GIIC, then calculate

        print("GIIc: ", GIIc)

    print('GIIc = ' + str(GIIc))
    return [aeq, G, GIIc]


# ----------------------------------------------------------------
# ---------------- Plotting-Only Functions ----------------
```

```
# ----------------------------------------------------------------

# plot P delta
def pdeltaplot(results):


    fig1 = plt.figure()
    ax = fig1.add_subplot(1, 1, 1)

    colors = ['blue', 'red', 'cyan', 'orange', 'green']
    legend = ['Sample 1', 'Sample 2', 'Sample 3', 'Sample 4',
    'Sample 5']


    x = results[:, 0]
    y = results[:, 1]

    plt.plot(x, y, color=colors[1], linewidth=2,
    label=legend[0])

    plt.legend()
    ax.set_xlim(xmin=0)
    ax.set_ylim(ymin=0)
    ax.set_xlabel('Displacement [mm]', loc='center',
    rotation=0, labelpad=5, size='14')
    ax.set_ylabel('Load [N]', loc='center', rotation=90,
    labelpad=5, size='14')


    fig = plt.gcf()
    plt.show()

    fig.savefig('raw_data.png')

    return (results)


def filter(results, x_clean):
    import plotly
    import plotly.graph_objects as go
```

```
import numpy as np
import pandas as pd
import scipy
from scipy import signal

print('what I read was')
print(x_clean)
# np.random.seed(1)

x = results[:, 0]
y = results[:, 1]

dispsmooth_x = signal.savgol_filter(x, 200, 1)

dispsmooth_y = signal.savgol_filter(y, 200, 1)

x = dispsmooth_x
y = dispsmooth_y

print('new x')
print(x)
print('new y')
print(y)

results[:, 0] = x
results[:, 1] = y

print('filtered results!')
print(results)


pd.DataFrame(results).to_csv('Filtered_data')
fig_f = plt.figure()
ax = fig_f.add_subplot(1, 1, 1)

colors = ['blue', 'red', 'cyan', 'orange', 'green']
legend = ['Sample 1', 'Sample 2', 'Sample 3', 'Sample 4',
'Sample 5']

plt.plot(results[:, 0], results[:, 1], color=colors[3],
```

```
    linewidth=2, label=legend[0])
    matplotlib.pyplot.axvline(x_clean, color = colors[2],

    linewidth=2, linestyle="--")
    plt.legend()
    ax.set_xlim(xmin=0)
    ax.set_ylim(ymin=0)
    ax.set_xlabel('Displacement_f␣[mm]', loc='center',

    rotation=0, labelpad=5, size='14')
    ax.set_ylabel('Load_f␣[N]', loc='center', rotation=90,
    labelpad=5, size='14')

    print('done')


    plt.savefig('plot_filtered')

    return (results)



def plotcbbm_dcb(crack_length, G, GIc):
    fig1 = plt.figure()
    ax = fig1.add_subplot(1, 1, 1)

    print('plot␣dcbcbbm')

    plt.plot(crack_length, G, color='black', linewidth=2,

    label="Sample␣1")
    plt.plot([0, 200], [GIc, GIc], color='red', linewidth=2,
    linestyle="--")

    plt.legend()
    ax.set_xlim(xmin=0)
    ax.set_ylim(ymin=0)
    ax.set_xlabel(r'$a_{eq}␣␣$␣␣[mm]', loc='center',

    rotation=0, labelpad=5, size='14')
```

```python
    ax.set_ylabel(r'$G_{IC}  $  [N/mm]', loc='center',

    rotation=90, labelpad=5, size='14')
    ax.text(0.75, 0.1, r'$G_{IC} = $%s' % (round(GIc, 2)),
    transform=ax.transAxes, bbox=dict(facecolor='none',
    edgecolor='black'))

    plt.xlim(50, 150)
    plt.show()

def plotcbbm_enf_els(aeq, G, GIIc):
    fig1 = plt.figure()
    ax = fig1.add_subplot(1, 1, 1)

    plt.plot(aeq, G, color='black', linewidth=2,
    label="Sample 1")
    plt.plot([0, 200], [GIIc, GIIc], color='red', linewidth=2,
    linestyle="--")

    plt.legend()
    ax.set_xlim(xmin=0)
    ax.set_ylim(ymin=0)
    ax.set_xlabel(r'$a_{eq}  $  [mm]', loc='center',
    rotation=0, labelpad=5, size='14')
    ax.set_ylabel(r'$G_{IIC}  $  [N/mm]', loc='center',
    rotation=90, labelpad=5, size='14')
    ax.text(0.75, 0.1, r'$G_{IIC} = $%s' % (round(GIIc, 2)),
    transform=ax.transAxes, bbox=dict(facecolor='none',
    edgecolor='black'))

    plt.xlim(100, 150)
    plt.ylim(5, 17)
    plt.savefig('r_curve.png')


# ------------------------------------------
# --------------GUI code--------------
# ------------------------------------------
```

```
# define each page layout and their objects

def homepage(window):
    page = tk.Frame(window)
    page.grid()

    # changes to static test window
    button_static = tk.Button(window, text="Static Test",
    command=lambda: changepage(1))
    button_static.config(height=5, width=10)
    button_home = tk.Button(window, text="Home",

    command=lambda: changepage(0))

    spacelabel = tk.Label(window, text="")
    spacelabel.grid(row=1, column=1, padx=90, pady=30)

    button_home.grid(row=0, column=0, padx=30, pady=30)
    button_static.grid(row=2, column=2, padx=30, pady=30)
    # button_fatigue.grid(row=2, column=4, padx=30, pady=30)


def staticpage(window):

    page = tk.Frame(window)
    page.grid(row=1, column=1)

    button_home = tk.Button(window, text="Home",
    command=lambda: changepage(0))

    button_home.grid(row=0, column=0, padx=30, pady=30)

    pagetitle = tk.Label(page, text="Static Test Analysis")
    pagetitle.grid(row=0, column=0, columnspan=2, pady=20)


    # properties insertion frame
    properties = tk.Frame(page)
    properties.grid(row=1, column=0, padx=20)
    propertiestitle = tk.Label(properties,
```

```
text="Substrate Properties")
propertiestitle.grid(row=0, column=0, columnspan=3,
pady=20)

Elabel = tk.Label(properties, text="Young's Modulus E",
anchor="e", width=20)
Ebox = tk.Entry(properties, width=10)
Ebox.insert(0, 210000)
Eunits = tk.Label(properties, text="[N/mm^2]")

Elabel.grid(row=1, column=0)
Ebox.grid(row=1, column=1)
Eunits.grid(row=1, column=2)

G13label = tk.Label(properties, text="Shear Modulus G13",
anchor="e", width=20)
G13box = tk.Entry(properties, width=10)
G13box.insert(0, 78947.368)
G13units = tk.Label(properties, text="[N/mm^2]")

G13label.grid(row=2, column=0)
G13box.grid(row=2, column=1)
G13units.grid(row=2, column=2)

Blabel = tk.Label(properties, text="Width B",
anchor="e", width=20)
Bbox = tk.Entry(properties, width=10)
Bbox.insert(0, 25)
Bunits = tk.Label(properties, text="[mm]")

Blabel.grid(row=3, column=0)
Bbox.grid(row=3, column=1)
Bunits.grid(row=3, column=2)

hlabel = tk.Label(properties, text="Height h",
anchor="e", width=20)
hbox = tk.Entry(properties, width=10)
hbox.insert(0, 12.7)
hunits = tk.Label(properties, text="[mm]")
```

```
hlabel.grid(row=4, column=0)
hbox.grid(row=4, column=1)
hunits.grid(row=4, column=2)

# data insertion frame
dataentry = tk.Frame(page)
dataentry.grid(row=1, column=1, padx=20)
datatitle = tk.Label(dataentry, text="Data Entry")
datatitle.grid(row=0, column=0, columnspan=3, pady=20)

testlabel = tk.Label(dataentry, text="Type of test",
anchor="e", width=20)
type_test = tk.StringVar()
testbox = ttk.Combobox(dataentry, width=20,
textvariable=type_test)
testbox['values'] = ('DCB', 'ENF', 'ELS')

testlabel.grid(row=1, column=0)
testbox.grid(row=1, column=1)

machlabel = tk.Label(dataentry, text="Testing Machine",
anchor="e", width=20)
machine = tk.StringVar()
machbox = ttk.Combobox(dataentry, width=20,
textvariable=machine)
machbox['values'] = ('Electro-Mechanical', 'Hydraulic')

machlabel.grid(row=2, column=0)
machbox.grid(row=2, column=1)

a0label = tk.Label(dataentry, text=
"Initial Crack Length a0", anchor="e", width=20)
a0box = tk.Entry(dataentry, width=10)
a0box.insert(0, 45)
a0units = tk.Label(dataentry, text="[mm]")

a0label.grid(row=3, column=0)
a0box.grid(row=3, column=1)
a0units.grid(row=3, column=2)
```

```
# Data entry button calls the read file method
(#read up on partial objects and wrapper methods)
filebutton = tk.Button(dataentry, text="Process Data File",
pady=10, command=lambda: (read_results("static",
machbox.get(),      testbox.get()), get_variables()))
filebutton.grid(row=4, column=1, columnspan=3)

# changes to edition window
button_edition = tk.Button(window, text="Edition", pady=10,
command=lambda: (changepage(5), plt.close()))
button_edition.grid(row=3, column=1, columnspan = 3)

# actions frame

actions = tk.Frame(page)
actions.grid(row=2, column=0, columnspan=2, pady=20)


pdelta_plot = tk.Button(actions, text="Plot P-delta",
pady=10, padx=10, command=lambda: pdeltaplot(results))

pdelta_plot.grid(row=1, column=0)


# plot R-curve button
rcurve_plot = tk.Button(actions, text="Plot R-curve",
pady=10, padx=10, command=lambda: cbbm(testbox.get(), results,
"static", int(a0box.get()), machbox.get()))
rcurve_plot.grid(row=1, column=1)

def get_variables():
    global test_static
    global a0_static
    global machine_static
    a0_static = a0box.get()
    test_static = testbox.get()
    machine_static = machbox.get()
    print('Aqui sim')
    print(a0_static)
    print(test_static)
```

```python
        print(machine_static)
        return a0_static, test_static, machine_static


    a0_static, test_static, machine_static = get_variables()

    return test_static, a0_static, machine_static

def editionpage(window):
    from PIL import ImageTk, Image

    page = tk.Frame(window)
    page.grid()

    print('saved variables')
    print(a0_static)
    print(test_static)
    print(machine_static)

    image = Image.open("raw_data.png")

    resized_image = image.resize((300,225), Resampling.LANCZOS)
    render = ImageTk.PhotoImage(resized_image)

    raw_data_title = tk.Label(page, text="Raw P-delta curve",

    image= render)
    raw_data_title.image = render
    raw_data_title.grid(row=1, column=20, columnspan=3, pady=20)

    button_home = tk.Button(window, text="Home", command=lambda:
    changepage(1))
    button_home.grid(row=0, column=8, padx=30, pady=30)

    # data insertion frame
    dataentry_edition = tk.Frame(page)
    dataentry_edition.grid(row=1, column=2, padx=20)
    datatitle = tk.Label(dataentry_edition, text="Data Entry")
    datatitle.grid(row=0, column=2, columnspan=3, pady=20)
```

```
# develop here
x_input_label = tk.Label(dataentry_edition, text=
"Insert␣displacement␣value", anchor="e", width=20)
x_input_box = tk.Entry(dataentry_edition, width=10)
x_input_box.insert(0, 0)
x_input_units = tk.Label(dataentry_edition, text="[mm]")

x_input_label.grid(row=8, column=3)
x_input_box.grid(row=8, column=4)
x_input_units.grid(row=8, column=5)

# Ok button
ok_button = tk.Button(dataentry_edition, text="Ok",
pady=10, padx=10, command = lambda:
(print(str(x_input_box.get())), delete_data(
x_input_box.get(),
results),filter(results, int(x_input_box.get())),
plot_filter()))
ok_button.grid(row=8, column=6)

# Filter_plot button
filter_plot = tk.Button(dataentry_edition, text=
"Filter␣data",
pady=10, padx=10, command=lambda: (filter(results,
int(x_input_box.get())),plot_filter()))
filter_plot.grid(row=3, column=3)

#Delete_data button
delete_data_call = tk.Button(dataentry_edition, text=
"Delete␣data", pady=10, padx=10, command=lambda:
(delete_data(int(x_input_box.get()),results),
filter(delete_data(int(x_input_box.get()), results), 0),
plot_filter()))

delete_data_call.grid(row=12, column=3)

#linear_reg button
linear_reg = tk.Button(dataentry_edition, text=
"Perform␣linear␣regression", pady=10, padx=10,
command=lambda:
```

```
(linear_regression(delete_data(int(x_input_box.get()),
results)),
plot_lin_reg()))

linear_reg.grid(row=16, column=3)

def plot_filter():
    plot = Image.open("plot_filtered.png")

    resized_plot = plot.resize((300, 225),
    Resampling.LANCZOS)
    render_plot = ImageTk.PhotoImage(resized_plot)

    plot_filter_title = tk.Label(page,
    text="Filtered P-delta curve", image=render_plot)
    plot_filter_title.image = render_plot
    plot_filter_title.grid(row=10, column=20,
    columnspan=3, pady=20)

def plot_lin_reg():
    plot = Image.open("lin_reg.png")

    resized_plot = plot.resize((300, 225), Resampling.LANCZOS)
    render_plot = ImageTk.PhotoImage(resized_plot)

    plot_filter_title = tk.Label(page, text=
    "Filtered P-delta curve", image=render_plot)
    plot_filter_title.image = render_plot
    plot_filter_title.grid(row=10, column=20,
    columnspan=3, pady=20)


# plot R-curve button
rcurve_plot = tk.Button(dataentry_edition, text=
"Plot R-curve", pady=10, padx=10,
command=lambda: (cbbm(test_static, results_new,
"static", int(a0_static), machine_static),
plot_r_curve()))
rcurve_plot.grid(row=20, column=3)
```

```
    def plot_r_curve():
        plot_r = Image.open('r_curve.png')
        resized_plot_r = plot_r.resize((300, 225),
        Resampling.LANCZOS)
        render_plot_r = ImageTk.PhotoImage(resized_plot_r)

        plot_filter_title = tk.Label(page, text="R-curve",
        image=render_plot_r)
        plot_filter_title.image = render_plot_r
        plot_filter_title.grid(row=10, column=2,
        columnspan=3, pady=20)

    return x_input_box

def delete_data(x_input, results):
    print(results)
    print('This the x input: ')
    print(x_input)
    print(results[:,0])
    first_column = results[:,0]
    print(first_column)
    difference = lambda first_column:
    abs(first_column - int(x_input))
    res = min(first_column, key=difference)
    print(res)

    index = np.where(results[:,0] == res)
    print(index)
    print(index[0])
    results = results[int(index[0]):, :]

    print(results)

    return results

def linear_regression(results):
    global results_new
    # take first 200 values for linear regression
    start_values = results[0:199, [0, 1]]
    # perform regression
```

```
lin_reg = np.polyfit(start_values[:, 0],
start_values[:, 1], 1)
# find x intercept, subtract from displacement and
add 0,0 to data
xintercept = -lin_reg[1] / lin_reg[0]
results[:, 0] -= xintercept
print('xintercept: \n', xintercept)

print('see here!_plot')
print(results)

#adjust data
results = np.insert(results, 0, [0, 0], axis=0)

print('insert 0')
print(results)

results_new = results

fig2 = plt.figure()
ax = fig2.add_subplot(1, 1, 1)

colors = ['blue', 'red', 'cyan', 'orange', 'green']
legend = ['Sample 1', 'Sample 2', 'Sample 3',
'Sample 4', 'Sample 5']


x = results_new[:, 0]
y = results_new[:, 1]

plt.plot(x, y, color=colors[1], linewidth=2,
label=legend[0])

plt.legend()
ax.set_xlim(xmin=0)
ax.set_ylim(ymin=0)
ax.set_xlabel('Displacement [mm]', loc='center',
rotation=0, labelpad=5, size='14')
ax.set_ylabel('Load [N]', loc='center', rotation=90,
labelpad=5, size='14')
```

```
    fig = plt.gcf()

    fig.savefig('lin_reg.png')

    return results_new


# page changing function
def changepage(pagenum):
    # remove all widgets
    for widget in window.winfo_children():
        widget.destroy()

    # change to new page

    if pagenum == 0:
        homepage(window)

    if pagenum == 1:
        staticpage(window)

    if pagenum == 3:
        staticpage(window)

    if pagenum == 4:
        staticpage(window)

    if pagenum == 5:
        editionpage(window)



window = tk.Tk()
window.geometry("850x500")
window.title("CBBM")
homepage(window)
window.mainloop()
```